5-2006

Molecular classification and prediction of metastatic potential in early malignant melanoma: improvement of prognostic accuracy by quantitative in situ proteomic analysis

Aaron J. Berger
Yale University.

Molecular Classification and Prediction of Metastatic Potential in Early Malignant Melanoma:
Improvement of Prognostic Accuracy by
Quantitative *in situ* Proteomic Analysis

A Dissertation
Presented to the Faculty of the Graduate School
of
Yale University
in Candidacy for the Degree of
Doctor of Philosophy

By
Aaron J. Berger

Dissertation Advisor: David L. Rimm, M.D., Ph.D.

May 2006

Abstract

Molecular Classification and Prediction of Metastatic Potential in Early Malignant Melanoma:
Improvement of Prognostic Accuracy by
Quantitative *in situ* Proteomic Analysis

Aaron J. Berger

2006

The incidence of cutaneous malignant melanoma continues to increase every year, and remains the leading cause of skin cancer death in industrialized countries. In spite of the aggressive nature of advanced melanoma, there are no standard biological assays in clinical usage that can predict metastasis. This may be due, in part, to the inadequacy of reproducible assessment of protein expression using traditional immunohistochemistry. This dissertation will discuss the use of tissue microarrays combined with quantitative *in situ* molecular analysis of protein expression to allow prediction of melanoma metastasis. Through the identification and validation of novel prognostic biomarkers, we seek to identify subsets of patients that are at high or low risk for melanoma recurrence or melanoma-related death. Some of these biomarkers may also serve as potential targets for future biologic therapy in melanoma, a disease for which no effective medical treatment is currently available. We demonstrate that quantitative assessment of a small number of markers is predictive of metastasis and outcome, augmenting the current system of prognosis.

The dissertation begins with a brief introduction on the current state of melanoma diagnosis, staging, and treatment, as well as a review of current efforts to understand the biology of melanoma progression and metastasis. The fundamentals of tissue microarray technology are then described. Critical aspects of quantitative immunohistochemistry,

including a description of the Automated Quantitative Analysis (AQUA) system developed in our laboratory, are also addressed. The second chapter demonstrates the use of tissue microarray technology to examine melanoma specimens by the current field standard, with a study of activating transcription factor 2 (ATF2); an example of semi-quantitative immunohistochemical analysis of protein expression. The third chapter provides validation of the AQUA technology on melanoma tissue by evaluation of the human homologue of murine double minute 2 protein (HDM2). Chapter four demonstrates an example of the critical--and beneficial--aspect of subcellular compartmentalization that the AQUA system provides, demonstrating that the ratio of cytoplasmic-to-nuclear expression of activator protein 2 (AP-2) predicts outcome in melanoma patients. The last chapter draws these concepts together and presents results from the analysis of 50 protein biomarkers in melanoma. It also introduces the use of a number of statistical methods (traditional and novel) employed to develop an optimal biomarker set for future analyses.

This dissertation is dedicated to the memory of my friend Marco Palma. If he were alive, I think he'd be doing this type of work. I miss him with each day that passes.

Acknowledgements

First and foremost, I would like to thank my mentor, David Rimm, M.D., Ph.D. I was drawn to him and his lab based on his deep interest in translational research, as well as his remarkable ability to describe extremely complicated concepts scientists, clinicians, and laypeople. I initially 'discovered' David as he was a guest lecturer in a seminar course, and then again as a section leader for the medical school Pathology course. After almost committing myself to another laboratory, I cam back from six months of medical school clerkships with a strong desire to work in David's lab on clinically relevant problems in cancer research. The type of work we do in his lab will hopefully change the face of oncology care in our society. The tools developed and refined in our lab are unique and exciting. David is an outstanding mentor; he always puts his students first. His creativity, intellectual curiosity, and courage to pursue the answers to complex, almost 'unanswerable' questions are admirable traits that I hope I have acquired. In addition, his enthusiasm is infectious.

The second person I would like to thank is Robert (Bob) Camp, M.D., Ph.D. Bob is probably one of the smartest people I know, and among the best dressed. Without Bob's mind, 'vision' and programming skills, none of this work would be possible. He is an asset to this lab, the department, the world in general; a true genius.

All members of the Rimm lab deserve recognition in terms of the assistance they have provided me on this journey. In particular, I would like to thank the graduate students (past and present) who have provided guidance and support (intellectual and emotional) throughout this process: Elayne Provost, Ph.D., Derek Pappas, Ph.D., Marisa Dolled-Filhart, Ph.D., Jena Giltnane, and Sharon Pozner. THANK YOU! Other

individuals who have provided tremendous assistance include Kyle DiVito and Melissa Cregger, who took many of my projects into their own hands. Additionally, Sophya Rodov and Harriet Kluger, M.D. were quite helpful. Jay Cowan, Maciej Zerkowski, Tom D'Aquila, Mark Gustavson, Ph.D., Summar Siddiqui, Malini Harigopal, M.D., Gina Chung, M.D., Amanda Psyrri, M.D., and Carola Zalles, M.D. all became my friends and made graduate student life more palatable. The Tissue Microarray Facility, run by Lori Charette and Joanna Graham, deserves special mention. Without your hardwork and help, the puzzle ends up missing pieces.

Critical collaborators on my projects include Dr. Stephan Ariyan, M.D. and his assistant Carolyn Truini, Michael Krauthammer, M.D., Ph.D. (Bioinformatics) and Antonio Subtil, M.D. (Dermatopathology).

People who have made the Department of Pathology a truly hospitable and fun place to be include JoAnn Falato, Dagmar Moore, the business office crew (Janice, Rachel, and Beth), and JoAnn D'Agostino.

In terms of my personal life, I am grateful to all of my friends, but especially Lee Sylvestre for keeping everything in perspective.

I would like to express thanks to my Dissertation Committee (Michael Kashgarian, M.D., Ruth Halaban, Ph.D., and Jeffrey Sklar, M.D., Ph.D.) for their feedback and suggestions, as well as their acceptance of this project as a meaningful endeavor.

I also owe a debt of gratitude to the MD/PhD Program (Jim Jamieson, M.D., Ph.D. and Sue Sansone) for the support that they have provided (and continue to provide) in my attempt to become a physician-scientist.

Table of Contents

Table of Figures

List of Tables

Chapter 1: Introduction

Current Understanding and Treatment of Melanoma

Malignant melanoma is currently the most rapidly increasing malignancy in the United States.[1] It is currently the sixth most common cancer in the US; for 2005, 59,580 new cases will be diagnosed and the disease will be responsible for approximately 7,770 deaths.[2] Melanoma is also the most common fatal malignancy among young adults.[3] Among cancers, its mortality rate is surpassed only by lung cancer.[4] Current estimates predict that 1 in 71 individuals will develop melanoma during their lifetime, up from an initial estimate of 1 in 600 in 1960 and 1 in 150 in 1985.[1] There is no clear explanation for this increase in incidence, though a combination of increased recreational sun exposure and global ozone depletion have been held partly responsible.[5] However, the relationship between sun exposure and melanoma remains complex.

The cell of origin is the melanocyte, and melanoma can arise in normal-appearing skin, solar lentigo, or atypical, benign melanocytic lesions.[4] Studies on familial, as well as sporadic, melanoma have demonstrated that there are clear genetic underpinnings to the evolution of this disease.[6-14] It appears that the genetic pathways of melanoma involve many genes with probable links to ultraviolet light exposure.[12] The definitive diagnosis of melanoma is often quite complicated and uncertain even in the hands of the most skilled dermatopathologists. In addition, while a number of clinical and pathologic factors have been described and established as markers of prognosis, there is room for significant improvement in terms of accuracy. There are currently no accepted histopathological, molecular, or immunohistochemical markers to define subsets of this neoplasm.[15]

Regarding prognosis, early detection and treatment are critical and result in improved patient survival rates. Surgical excision remains the mainstay of treatment but many new promising therapies are being investigated.[16] However, non-surgical treatment of advanced disease has been largely unsuccessful.[17] The literature regarding effective adjuvant therapy for melanoma is questionable at best, and experts tend to recommend that patients with advanced disease enroll in a clinical trial.[18]

The prognosis of isolated, primary cutaneous melanoma remains favorable, with a 5-year overall survival rate above 90%. However, the discovery of metastatic disease dramatically affects outcome. The presence of regional lymph node metastases reduces 5-year overall survival rates to 10-46%.[19] Although the use of sentinel lymph node biopsy has improved the staging of melanoma, there is a critical need to determine the metastatic potential of melanoma early in disease progression. It is not uncommon to have widely disseminated disease at the time of initial diagnosis. The fact that patients with local or nodal recurrences fare as poorly as those with overt distant metastases implies that the former events are predictors of subclinical systemic disease.[20] A more precise staging system is needed; one which will take into account the aggressive nature of the disease.

The histopathologic progression of melanoma is thought to progress through a series of defined stages, yet melanoma has been shown to arise spontaneously in the context of normal-appearing skin. Normal skin typically has an even distribution of melanocytes at the basal layer of the epidermis, with one melanocyte found for every 4 or 5 basal cells.[21] The compound nevus, a benign proliferation of melanocytes, is defined by uniform nests of melanocytes. The dysplastic nevus demonstrates irregular and

bridging nests of atypical melanocytes. *In situ* melanoma remains confined to the epidermis. Early melanoma development is characterized by the radial growth pattern. A vertical growth phase can follow, which is thought to indicate the transition to a more aggressive and lethal condition, characterized by tumor invasion into the underlying dermis and subcutis, and often presages metastasis to distant sites. While melanoma tends to spread to nonvisceral sites such as skin or lymph nodes, it is notorious for its ability to metastasize to practically any organ, including lung, liver, brain, bone, and small intestine.[22]

Initial management of the primary lesion is by surgery. A wide local excision removes the tumor along with a margin of normal appearing skin. Current clinical guidelines dictate that the margin of excision be proportional to the depth of tumor invasion into the skin. If the tumor depth is $\leq$ 1 mm, a 1 cm margin is recommended, while a depth of 1-2 mm suggests a 1-2 cm margin. When the tumor depth exceeds 2 mm, guidelines recommend a 2 cm margin of normal skin.[23, 24] The surgical treatment of melanoma, in particular, can range from a marginal biopsy to wide local excision with regional lymphadenectomy, and advance in some cases to include extraction of distant metastases.

Adjuvant therapy for melanoma is limited at best. Over the past 20 years, numerous agents have been evaluated in a series of both nonrandomized and randomized adjuvant therapy trials in melanoma patients. While many of these clinical trials suffered from serious methodological problems such as inadequate statistical power, use of inappropriate controls, and/or lack of stratification for known prognostic factors, the major obstacle to the success of adjuvant therapy of melanoma has been the lack of active

agents. Popular agents that have demonstrated little or no benefit include: BCG, levamisole, interferon gamma, interleukin-2, retinoids, dacarbazine, and megestrol acetate.[25]

High-dose interferon (IFN) alpha-2b is the only FDA-approved agent for the adjuvant treatment of melanoma in the US. This treatment is used predominantly for high-risk, stage III (i.e., lymph node disease) patients with cutaneous primaries; these patients have a 50-85% risk of further metastasis.[19] However, the benefit of this treatment is controversial. The initial multicenter study, in 1995, reported improved long-term and disease-free survival in melanoma patients.[26] However, more recent clinical trials have demonstrated that while there is an approximate 10% reduction in risk of recurrence, there is no effect on overall survival. In addition, despite 20 years of study, the mechanisms of IFN's antitumor activities remain unknown. Studies speculate that its efficacy may lie in its immunomodulatory functions, its antiangiogenic activities, or it may have direct antiproliferative effects on melanoma.[27] Without understanding its mechanism of action, surrogate markers of response/remission cannot be used to guide dose selection and duration of therapy.

The absence of effective medical treatment for melanoma leads many patients with advanced disease to enroll in clinical trials. Current experimental treatments for melanoma are based on immunotherapy, through immune-boosting cytokines (e.g., IL-2 or GM-CSF) and/or vaccines against melanoma-specific antigens, or molecularly-targeted therapy with specific inhibitors.

Prognostic Indicators in Melanoma

Prognosis in melanoma is currently determined by a number of factors unique to the primary lesion, as well as the presence of loco-regional (lymph node and in-transit metastases) and distant metastatic disease. Over the past 30 years, a number of models have been developed to predict patient outcome for cutaneous melanoma based on characteristics unique to the primary lesion. The information gleaned from these studies, through both univariate and multivariate analyses, has been incorporated into the most recent Melanoma Staging System of the American Joint Committee on Cancer (AJCC).

The first published reports of variables to predict survival in primary melanoma came with publications from A Breslow[28, 29] and WH Clark[29] in the 1970s. The models they described have changed little and remain the most powerful and reliable predictors of survival based on characteristics of the primary cutaneous lesion. The figure below demonstrates how each of these criteria are measured:[22]

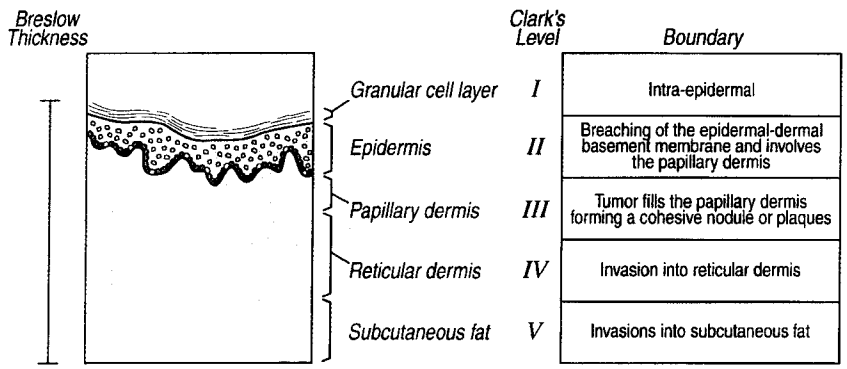

Figure 1 (adapted from Chin et al.[22]). Cross-section of skin demonstrating the methods for measurement of Breslow depth and Clark level.

Wallace Clark first described the phenomenon of the 'early radial' and 'late vertical' growth phases in primary cutaneous melanoma. He also demonstrated that the

radial growth phase is only rarely associated with the development of metastases, while the vertical growth phase is more commonly associated with subsequent metastatic disease. From these observations, he developed a classification system for staging primary cutaneous melanomas, in which the depth of tumor invasion is measured relative to the anatomical layers of the skin. Alexander Breslow's classification suggests that incidence of metastasis in primary cutaneous melanoma is proportional to maximal tumor thickness; it is based on the direct measurement (depth in millimeters) of invasion from the lowest level of the epidermis to the deepest level of invasion.

Clark's measurement is an indirect measure of tumor thickness and is not as accurate as Breslow's in predicting metastases because of the marked variation in thickness within each level[30], which can also vary depending on anatomical location. The marked variability in skin layers and the difficulty in discriminating those layers from each other leads to a great deal of interobserver variability amongst pathologists. For these reasons, the Breslow depth remains a stronger and more reliable predictor of metastatic potential.

The current AJCC Staging Sytem for *local disease* is based on the following criteria: tumor thickness (Breslow thickness), ulceration, and—in the case of very thin lesions—level of invasion (Clark level).[19] However, there are a number of other factors that have shown significant prognostic value in melanoma.[31] Among the clinical prognostic factors are: age[32-36] (older age is unfavorable); gender[35-37] (females have improved survival over men); and anatomical location [35, 38-40] (head, neck and axial melanomas fare worse than melanoma on the extremities).

In addition to Breslow measurement and Clark level, a number of other histopathological characteristics in melanoma have been observed to correlate with disease outcome. Other strong histological predictors of outcome include: lesion ulceration[35, 41-46], mitotic rate[47], and microscopic satellitosis (discrete nests of tumor cells separated from the main body of the tumor by normal subcutaneous tissue). Less powerful histopathological factors include: histologic subtype (i.e., superficial spreading, nodular, lentigo maligna, acral lentiginous, desmoplastic; acral and nodular melanomas may be more aggressive than other types[4]), angiogenesis[48], vascular invasion, regression, and tumor infiltrating lymphocytes. Of all clinical and pathological criteria, the majority of studies demonstrate that tumor thickness (Breslow) is the most reliable independent prognostic factor in cutaneous melanoma.[28, 35, 39, 40, 42, 43, 49-54]

Current methods of prognosis in cutaneous melanoma are far from precise, and, aside from minor adjustments, have not changed much over the past 30 years. It should be noted that the mortality rate from melanoma is decreasing but this has been associated with earlier clinical recognition (on the part of patients and their physicians) and expedited surgical treatment. It is important to note that the histopathologic characteristics of the primary tumor may not necessarily be indicative of tumor aggressiveness. There are a surprisingly large number of cases of melanoma in which tumor thickness does not predict outcome; cases in which thin melanoma turns out to be aggressive[36, 38, 44, 54-76] or thick melanoma indolent[77-80].

Regarding *loco-regional or metastatic disease*, the "up"-staging of melanoma has become dependent upon sentinel lymph node (SLN) biopsy. It is imperative to determine if a patient has metastatic disease—regional or distant—at the time of initial diagnosis for

proper staging. Originally developed to aid in the prognosis and treatment of penile carcinoma, it has become common practice in the diagnostic evaluation of a number of cancers, particularly melanoma.[81] The procedure for SLN biopsy involves the injection of a colored dye, as well as a radiotracer, to determine the lymphatic drainage of a primary tumor and identify the first lymph nodes in a regional group. The SLN serves as a guide to the status of the rest of the nodes in the respective lymph node basin. If the SLN is negative for disease, it can be assumed that rest of the regional nodes are also negative. If this is the result, the patient will be spared an "unnecessary", invasive and debilitating procedure.

Techniques in surgery and nuclear medicine have advanced so rapidly that SLN biopsy is now a well-established standard procedure in many countries.[82] It is a relatively accurate mechanism for predicting the pathologic status of regional lymph nodes, and, in turn, aiding in the prediction of patient outcome.[83] Shown to be the most important prognostic factor in determining survival in melanoma[84], it has become an essential component of the AJCC TNM classification of melanoma.[19]

The decision to perform a sentinel lymph node biopsy (in the absence of clinically apparent LN disease) is typically based upon the Breslow depth of the primary lesion. The criteria necessary to go forth with this procedure varies from surgeon to surgeon. It is often based on the surgeon's discretion. Generally, the threshold for performing a sentinel lymph node biopsy in the absence of clinical lymph node involvement is a primary lesion around 1 mm thick[85], and the procedure is quickly becoming the standard of care for patients with primary melanoma greater than 1 mm in thickness.[86] The true

benefit of this procedure lies in its ability to aid in the accurate staging of patients for prognostic purposes.

The degree of sentinel lymph node disease, in which the lymph node disease ranges from only detectable at the molecular level (i.e., through RT-PCR analysis for melanoma-specific markers) to grossly apparent (i.e., large pigmented deposits in lymph nodes), and its relevance to prognosis is under investigation by a number of groups. Because of the precision afforded by SLNB, the AJCC revised its staging system for melanoma.[19] Nodal involvement is distinguished first on the basis of the number of nodes with disease, and then on micro- versus macro-scopic involvement. It should be noted that IHC increases detection rate in SLN by at least 10% over H&E alone.[87] The staging system is demonstrated by the tables below:

Table 1. Melanoma TNM Classification (adapted from Balch et al.)[19]

T classification	Thickness	Ulceration Status
T1	≤ 1.0 mm	a: without ulceration b: with ulceration or Clark level > III
T2	1.01-2.0 mm	a: without ulceration b: with ulceration
T3	2.01-4.0 mm	a: without ulceration b: with ulceration
T4	> 4.0 mm	a: without ulceration b: with ulceration
N classification	**No. of Nodes**	**Nodal Metastatic Mass**
N1	1 node	a: only detected by pathology b: clinically detectable
N2	2-3 nodes	a: only detected by pathology b: clinically detectable c: in transit mets without nodal disease
N3	≥ 4 nodes	
M classification	**Site**	**Serum LDH**
M1a	Distant skin, subcutaneous, or nodal mets	Normal
M1b	Lung metastases	Normal
M1c	All other visceral metastases	Normal
	Any distant metastases	Elevated

Table 2. Stage Grouping for Cutaneous Melanoma (adapted from Balch et al)[19]

Stage	T	N	M
0	T_{is}	N0	M0
IA	T1a	N0	M0
IB	T1b T2a	N0	M0
IIA	T2b T3a	N0 N0	M0 M0
IIB	T3b T4a	N0 N0	M0 M0
IIC	T4b	N0	M0
III	Any T	N1 or N2 or N3	M0
IV	Any T	Any N	Any M1

The following graph demonstrates Kaplan-Meier survival curves for 17,600 melanoma patients, grouped by the new staging system. The AJCC staging system for melanoma appears to be quite reliable for predicting survival based on primary tumor characteristics and nodal/metastatic status.[19]

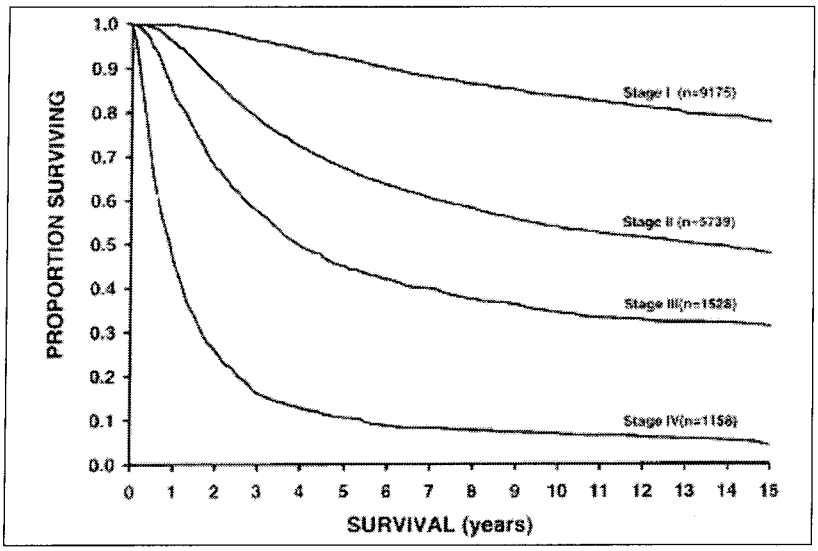

Figure 2 (adapted from Balch et al.[19]). Fifteen-year survival curves comparing localized melanoma (stages II and I), regional metastases (stage III), and distant metastases (stage IV). The numbers in parentheses are patients from the AJCC melanoma staging database used to calculate the survival rates. The differences between the curves are significant ($P < .0001$).

To date, there have not been any widely accepted immunohistochemical—or other molecular—markers to predict patient outcome or guide therapy in melanoma. There is a need for a more precise diagnosis of melanoma through molecular staging, similar to the use of HER2 in breast cancer. One of the major impediments to the development of useful molecular assays for melanoma is the absence of any molecularly-targeted therapy for the disease. In fact, there are no effective biological, chemotherapeutic, or biochemotherapeutic treatments for melanoma. There have been

some attempts to develop molecularly targeted therapies for melanoma but success, at even the level of cell culture, is rare; translation to the clinical setting is rarer still.

There have been a number of studies that have evaluated markers on an individual basis and on a relatively small number of patients.[88, 89] In addition, none of these studies have made use of automated quantitative analysis. Differences in expression levels in the tissues have been based on those that are perceptible only by the human eye. Those molecular markers that have not shown statistical significance may not have been evaluated on a large enough patient cohort.

The advent of high-throughput genomic technologies has made it possible to survey the expression of a large number of genes simultaneously in cancer tissue. Additionally, the availability of quantitative analysis introduces the ability to more accurately discriminate expression levels within tumors and relate those to recurrence, survival, and response to therapy.

While a number of clinical and pathologic factors have been established as markers of prognosis, no marker, molecular or morphologic, can exceed the predictive strength of assessment of metastasis to lymph nodes. The presence of metastasis to lymph node metastases reduces 5-year overall survival rates by between 10 and 30%, for any given stage of the disease.[90]

The use of sentinel lymph node biopsy has significantly improved the staging of melanoma, but this procedure is both morbid and imperfect. In a recent series by our collaborator, Dr. Stephan Ariyan, only 11% of 263 patients showed metastasis in the sentinel node. Although this rate is somewhat lower than other larger series[91], highest numbers from other studies are near 25% and related to the depth of the primary tumor.

Overall, between 75% and 90% of the procedures are done unnecessarily. Furthermore, of the 10% of the patients in the Yale study that developed local recurrence or distant metastasis, only about half were predicted by positive sentinel nodes. In other studies as many as 25% of negative nodes will ultimately develop recurrent disease.[92] Thus, there is a critical need to predict which patients will have nodal disease, or more importantly, which patients have a disease subclass that will progress compared to those that will not.

This clinical problem is compounded by the fact that the amount of tissue available for making this determination is often very small. It has, historically, been difficult to look at low stage melanomas since the material is nearly completely exhausted at diagnosis. A number of new developments that have been advanced in the last few years can now be combined to address this issue.

Molecular Classification of Melanoma

While the morphological biology of melanoma progression is well described, the genetic changes that take place as lesions invade deeper and ultimately become metastatic are not well understood. Work is under way in a number of laboratories to describe these changes and use them for their prognostic potential (to help predict aggressive potential) and ultimately develop therapies that target these changes. No single marker has distinguished itself in a manner that it has been broadly accepted, but many markers have shown promise in small, single institution studies or in basic cell biological studies. These efforts provide a good starting place for our goal of predicting metastatic potential. We aim to take advantage of these efforts to select markers whose expression is likely to be correlated with metastasis, based on the historic, basic and translational work related to each marker. Data from cDNA array studies suggest numerous markers will be

required for disease classification or prediction of metastasis. We believe this will also be true of protein markers, although we believe substantially fewer markers are required.

A number of studies have been performed identifying gene expression profiles unique to melanoma relative to normal melanocytes or nevi. In addition, a number of relatively small-scale immunohistochemical and *in situ* mRNA-DNA hybridization studies have been published over the past few years. Additionally, it has been demonstrated that previously unrecognized gradations of melanoma can be distinguished by gene expression profiling.[15]

We seek to discover a set of molecular markers that can be used as an independent predictor of survival, to be used on a regular basis to aid in patient prognosis. Assessing a small battery of markers at the time of initial diagnosis will aid clinicians in the prognosis of their patient's disease, and may, in some cases, provide therapeutic guidance. Though the current aim of this project is to define aggressive melanoma from 'benign—less aggressive' melanoma, a number of molecular targets will be defined that may have therapeutic potential.

Table 3. Previous IHC Studies demonstrating markers with prognostic potential:

Author/Date	Markers	Patient/Sample Number	Correlation with Survival
Eliopoulos, P. *MR* 2002[93]	• HER-2	51 lesions ≥ 10 mm / 11 lesions ≤ 1 mm	• HER-2 overexpressed in 29.4% of thick lesions; none in thin. • No prognostic significance in this study.
Ferrier, CM. *BJC* 2000[94]	• tPA • uPA • PAI-1 • PAI-2 • uPAR	214 primary melanomas (only local disease at time of acquisition)	• High tPA expression correlates with good outcome.
Florenes, VA. *J Path* 2001[95]	• Cyclin A • Ki-67	172 primary (110 sup + 62 nod) / 73 mets / 10 nevi	• Cyclin A independent predictor of survival (p=0.0003) in SSM. • Cyclin A & Ki67 correlate with depth in SSM.
Florenes, VA. *CCR* 2000[96]	• Cyclin D1 • Cyclin D3	172 primary (110 sup + 62 nod) / 73 mets / 10 nevi	• Cyclin D1 expression correlates with SSM relapse (p<0.001) and early death (p=0.009)
Florenes, VA. *AJP* 1998[97]	• p27	113 primary / 45 metastases (36 distant) / 4 nevi	• Inverse correlation with DFS (stronger in nodular than SSM).
Gradilone,[98] A. *JCO* 2003	• Survivin • bcl-2 • bax • bcl-X	36 SLN's evaluated by RT-PCR (and IHC in some cases)	• Survivin expression correlates with survival, but not bcl-2, bax, or bcl-X.
Hieken, TJ. *Cancer* 1999[99]	• p53 • β1 integrin • β3 integrin	111 intermediate-thickness primary melanomas	• p53: no association with survival. • β1 integrin: correlates with survival (p=0.0004) • β3 integrin: correlates with survival (p=0.0001)
Kageshita, T. *BJD* 2001[100]	• β-catenin	91 primary / 50 mets / 50 nevi	• Loss of β-cat expression associated with disease progression. Thickness inversely correlates with B-cat.
Karjalainen, JM. *AJP* 2000[101]	• CD44 • Hyaluronan	292 stage I melanomas	• Reduced cell surface CD44 and HA levels associate with poor prognosis.
Kunz, M. *ADV* 2002[102]	• Thombospondin2 • Desmoglein 2	Tbsp2: 5 primary and 5 mets Dsmg2: 20 primary and 20 mets	• Neither antibody stained well in primaries, but all mets showed expression of Thrombospondin 2 and Desmoglein 2.
Massi, D. *Hum Path* 1999[103]	• Osteonectin	188 thin primaries	• Osteonectin overexpression correlates with progression and betastasis.
Miranda, E. *JSO* 2003[104]	• Apo D	32 invasive / 8 *in situ* / 10 benign lesions	• Apo D expression higher in nodular (p=0.011). • Signifcant corr with Clark (p=0.046)
Morgan, MB. *AJDP* 1999[105]	• p27 (kip1)	21 melanomas / 21 Spitz nevi / 21 compound nevi	• No difference in staining between groups. • Not useful in distinguishing between lesions.
Niezabitowski, A. *JSO* 1999[106]	• Ki-67 • PCNA • p53 • Vimentin • S100 • HMB45 (gp100) • Vimentin	93 patients	• Ki-67, PCNA, & HMB45 overexpression correlate with decreased survival.
Ostmeier, H. *Cancer* 1999[107]	• VLA-2 • HLA-ABC • HLA-DR • NKI-beteb • Mel 14 • ICAM-1 • K-1-2 • G-7-E2 • H-2-4-7	> 500 primary melanomas	• None of these markers improved the prognostic model that included Breslow, localization, or mitoses.
Ostmeier, H. *BJD* 2001[108]	• Ki-67 • HLA-DQ • HLA-DP • Muc 18 • A-10-33 • Transferrin receptor • H-2-8-10	Biopsies from 688 patients	• Ki-67 (n=399) and HLA-DQ (n=452) retain prognostic significance in multivariate analyses.
Polsky D. *JNCI* 2002[109]	• HDM2 • p53 • Ki-67	134 patients	• HDM2 overexpression correlates with survival.
Salti, GI. *CR* 2000[110]	• MiTF	63 intermediate thickness (1-4mm) melanomas	• Increased MiTF expression correlates with improved survival.
Sparrow, LE. *AJDP* 1998[111]	• MIB-1	11 thin that later metastasized / 11 thin control tumors (nonprogressors) 25 benign and 70 malignant melanomas	• Strong correlation with Clark (r=0.71)and Breslow (r=0.77)
Straume, O. *AJP* 2002[112]	• VEGF-C • FLT-4 • bFGF • FGFR-1 • IL-8 • Ephrin-A1 • EphA2	202 VGP melanoma cases / 68 mets from 58 pt's	• Ephrin-A1 correlated directly with Breslow (p=0.017), Clark (p=0.004), & ulceration (p=0.006)
Straume, O. *CCR* 2000*	• p16 • Ki-67 • p53	Same as above	• loss of nuclear p16 = increased Ki-67 and poor prognosis • absence of p53 correlates with improved survival
Straume, O. *AJP* 2001*[113]	• VEGF • Flt-1, kdr • Tsp-1		
Straume, O. *IJC* 1997[114]	• p16 • p53	102 nodular melanomas	• Loss of p16 expression correlates with reduced survival & recurrent disease (p=0.013) • p53 was not prognostically important.
Vaisanen, A. *J Path* 1998[115]	• MMP-2	50 primary skin melanomas	• High MMP-2 expression indicates an unfavorable prognosis.

Although some of the studies listed above have demonstrated that the levels of melanoma-associated proteins can serve as markers to predict disease outcome, there are

a multitude of genes and gene products with prognostic potential in patients with localized melanoma. The expression of thousands of genes in melanoma tumors and cell lines can be surveyed using cDNA microarrays. It has been proposed for various cancers that a discrete and previously unrecognizable cancer taxonomy can be identified by assessing the systemized data acquired from gene expression experiments.[15] Most gene expression studies reported thus far have been based on cell lines, which may not be entirely representative of *in vivo* tumor biology. The data acquired must be validated on *in vivo* models and patient samples.

Differential expression of genes discovered by cDNA microarray analysis

Melanoma is an unpredictable cancer. It is not clear what genetic changes take place in melanoma progression. Through comparative gene expression studies, a number of investigators are intensively trying to understand the molecular pathogenesis of melanoma. As this cancer remains refractory to virtually every pharmacologic treatment, and has an incredible potential for aggressive growth, it is not surprising that many melanoma patients submit themselves to toxic and experimental therapies.[116] The products from cDNA microarray analyses not only provide validation of previously identified biomarkers, but also offer new genes that might be useful in molecular diagnosis, pathogenesis studies, and possible molecular targets for therapeutic interventions.

In collaboration with Dr. Ruth Halaban, we have participated in a study which sought to profile genome-wide changes in melanoma.[117] Using cDNA microarrays, global expression changes were assessed in melanomas compared to normal melanocytes (harvested from newborn foreskins). Affymetrix and spotted oligonucleotide microarrays

were used to assess global differential gene expression comparing normal human melanocytes with six independent melanoma cell strains from advanced lesions. The data, validated at the protein level for selected genes, confirmed the overexpression in melanoma cells relative to normal melanocytes of several genes in the growth factor/receptor family that confer growth advantage and metastasis. In addition, novel pathways and patterns of associated expression in melanoma cells not reported before emerged, including the following: (*a*) activation of the NOTCH pathway; (*b*) increased Twist expression and altered expression of additional transcriptional regulators implicated in embryonic development and epidermal/mesenchymal transition; (*c*) coordinated activation of cancer/testis antigens; (*d*) coordinated down-regulation of several immune modulation genes, in particular in the IFN pathways; (*e*) down-regulation of several genes implicated in membrane trafficking events; and (*f*) down-regulation of growth suppressors, such as the Prader-Willi gene *NECDIN*, whose function was confirmed by overexpression of ectopic Flag-necdin. Validation of differential expression using melanoma tissue microarrays showed that reduced ubiquitin carboxy-terminal esterase L1 in primary melanoma is associated with worse outcome and that increased expression of the basic helix-loop-helix protein Twist is associated with worse outcome. Some differentially expressed genes reside on chromosomal regions displaying common loss or gain in melanomas or are known to be regulated by CpG promoter methylation. These results provide a comprehensive view of changes in advanced melanoma relative to normal melanocytes and reveal new targets that can be used in assessing prognosis, staging, and therapy of melanoma patients.

In summary, the data demonstrate that changes take place in previously recognized melanoma-activated pathways (e.g., upregulation of transcriptional proteins, activation of cancer/testis antigens, downreguation of immunomodulatory gene expression and growth suppressor expression), as well as some novel associations (e.g., upregulation of the NOTCH pathway). The figure below demonstrates unsupervised hierarchical clustering of gene expression profiles in these melanoma cell lines and normal melanocytes.

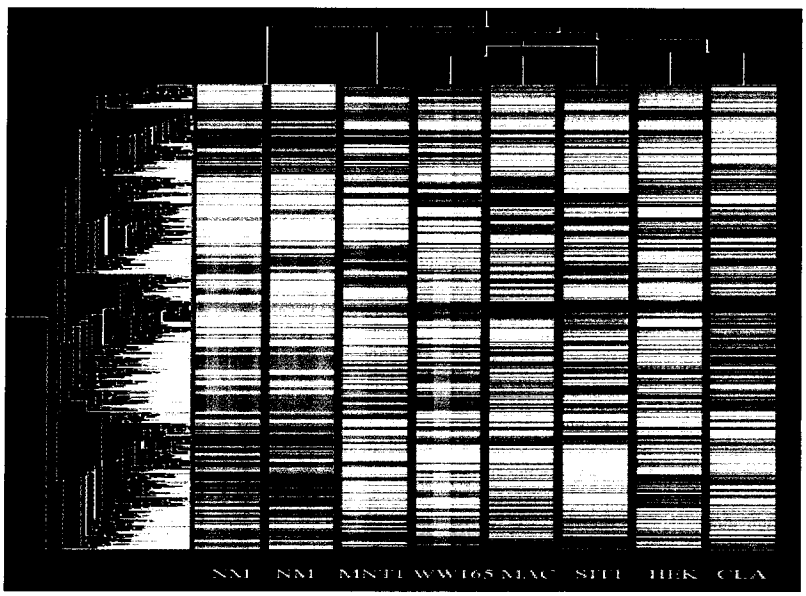

Figure 3 (adapted from Hoek et al.[117]). Hierarchical Clustering. Cluster map and phylogenetic tree resulting from a hierarchical cluster analysis of normalized intensity data across two control (melanocytes; NM) and six sample (melanoma, as indicated) data sets. Genes were selected for clustering according to a fold change and signal intensity cutoff protocol described in the text. Clustering was performed using GeneSpring 6.0 (Silicon Genetics, Inc.).

Bittner et al.[15] examined the expression profiles for 31 melanomas—biopsies and cell lines—relative to 7 control cell lines. Using a matrix of Pearson correlation coefficients from complete pair-wise comparison of all experiments, the authors developed a hierarchical clustering dendrogram as well as a three-dimensional

multidimensional scaling (MDS) plot. The MDS plot displays the position of each tumor sample in relative Euclidean space; the distance between them represents their approximate degree of correlation.[118] With this plot, the authors were able to distinguish a gene expression profile unique to 19 of the melanomas. The figures below display the dendrogram and MDS plot showing the major cluster of 19 samples (within the cylinder) and the relative expression of the top 22 genes used to discriminate this cluster. Their analysis is by no means complete, and they state that "the extent to which melanoma samples can be clinically subdivided by expression patterns remains to be elucidated." The information their 'weighted' list of genes provides should allow for the dissection of other clinically relevant subsets for melanoma.

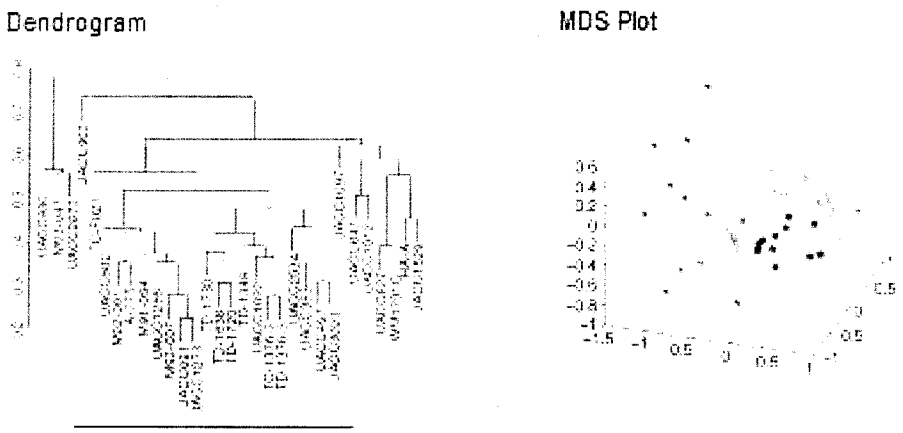

Figure 4 (adapted from Bittner et al.[15]). **[Left]** Hierarchical clustering dendrogram demonstrating a unique cluster of 19 melanomas at the centre. **[Right]** MDS three-dimensional plot of all 31 cutaneous melanoma samples showing major cluster of 19 samples (blue, within cylinder).

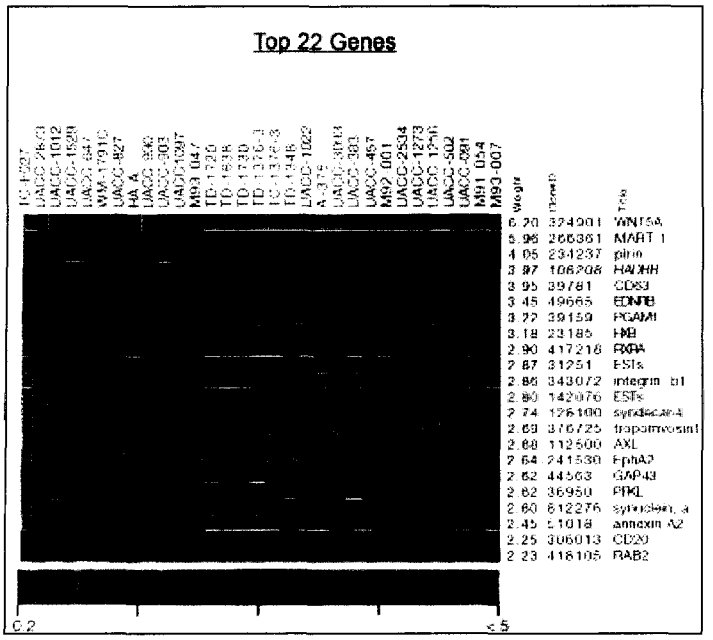

Figure 5 (adapted from Bittner et al.[15]). After MDS analysis, ranking genes according to their impact on minimizing cluster volume and maximizing centre-to-centre inter-cluster distance, this clustergram demonstrates the top 22 genes obtained by these criteria listed in order of decreasing weight.

Based on the results of the above study, Weeraratna *et al.* investigated the role of WNT5A in melanoma further. In transfected cell lines, they demonstrated that WNT5A expression correlates with increased cell motility and invasiveness. They were also able to show that WNT5A expression in human melanoma biopsies correlates directly with increasing tumor grade, and inversely with patient survival.[119]

Valéry et al.[120] identified the target genes of ultraviolet (UV) stress response by culturing normal human melanocytes in the presence of UV irradiation. Out of the ~9000 genes on their cDNA microarray, they noted that 198 were found to be modulated ≥1.9 times over the non-irradiated cells. The majority of the genes they identified are involved in DNA or RNA binding/synthesis/modification or ribosomal proteins. Others included transcription factors, receptors, tumor suppressors and oncogenes. Although they did not perform any cluster analyses, they did compare their results with those of the Bittner[15]

study (Table 4). Although the identified genes are not necessarily melanoma-specific, they are potential markers of disease, capable of being used in the development of new molecular-based strategies for risk prediction in melanoma patients.

Table 4. Comparison of genes between Valery et al. and Bittner et al. studies.

Clones	Valéry *et al.*	Bittner *et al.*
Concordant Up-Regulation		
Actin-related protein 2/3 complex, subunit 1B (41 kDa)	+	+
Actin, gamma 1	+	+
Adenine phosphoribosyltransferase	+	+
Adenylate cyclase 9	+	+
Aquaporin 4	+	+
ATP synthase, H+ transporting, mitochondrial F0 complex, subunit c (9) isoform 3	+	+
ATP synthase, H+ transporting, mitochondrial F1 complex, a-subunit, isoform 1, cardiac muscle	+	+
Receptor (calcitonin) activity modifying protein 1	+	+
Guanylate kinase 1	+	+
Human clone 23815 mRNA sequence	+	+
Mannosidase, alpha, class 2B, member 1	+	+
NADH dehydrogenase (ubiquinone) 1 beta subcomplex, 7 (18 kDa, B18)	+	+
Phosphofructokinase, liver	+	+
Protein tyrosine phosphatase, receptor type, c polypeptide-associated protein	+	+
Ribose 5-phosphate isomerase A (ribose 5-phosphate epimerase)	+	+
Ribosomal protein L10	+	+
Ribosomal protein L19	+	+
Ribosomal protein S14	+	+
Syndecan 4 (amphiglycan, ryudocan)	+	+
Concordant Down-Regulation		
Apoptosis inhibitor hiap-1	-	-
DEAD/H (Asp-Glu-Ala-Asp/His) box polypeptide 15	-	-
DEAD/H (Asp-Glu-Ala-Asp/His) box polypeptide 5 (RNA helicase 68 kDa)	-	-
E74-like factor 1 (ets domain transcription factor)	-	-
Fibronectin 1	-	-
Hypoxia-inducible factor 1, alpha subunit (basic helix−loop−helix transcription factor)	-	-
Interferon regulatory factor 2	-	-
Mitogen-activated protein kinase kinase kinase 7	-	-
Multimerin	-	-
Protein tyrosine phosphatase, nonreceptor type 12	-	-
Ribosomal protein S6 kinase, 90 kDa, polypeptide 3	-	-
Solute carrier family 12 (sodium/chloride transporters), member 3	-	-
SON DNA binding protein	-	-
Translin-associated factor X	-	-
Zinc finger protein 184 (Kruppel-like)	-	-
Zinc finger protein 38 (KOX 25)	-	-
Discordance		
arsA (bacterial) arsenite transporter, ATP-binding, homolog 1	+	-
C3H-type zinc finger protein; similar to D, melanogaster muscleblind B protein	-	+
Chromodomain helicase DNA binding protein 1	-	+
Coatomer protein complex, subunit beta	-	+
Hypothetical protein P1 p373c6	-	+
Interferon, gamma-inducible protein 16	-	+
Kinesin family member 5B	-	+
Laminin receptor 1 (67 kDa, ribosomal protein SA)	+	-
Leucine-rich repeat (in FLII) interacting protein 1	-	+
Major histocompatibility complex, class I, C	+	-

Clones	Valéry *et al.*	Bittner *et al.*
Myosin, light polypeptide 1, alkali; skeletal, fast	+	-
Myosin, light polypeptide 6, alkali, smooth muscle and nonmuscle	+	-
Pre-B-cell colony-enhancing factor	-	+
Proteasome (prosome, macropain) subunit, beta type, 6	+	-
RAN binding protein 2 like 1	-	+ and -
Ras-GTPase-activating protein SH3-domain-binding protein	-	+
Ribosomal protein L28	+	-
Ribosomal protein S23	+	-
Serum/glucocorticoid regulated kinase	-	+
Solute carrier family 24 (sodium/potassium/calcium exchanger), member 1	-	+
Suppression of tumorigenicity 16 (melanoma differentiation, ST16)	-	+
Transducin-like enhancer of split 4, homolog of Drosophila E(sp1)	+	-
UDP-glucose ceramide glucosyltransferase	-	+
v-yes-1 Yamaguchi sarcoma viral related oncogene homolog	-	+
Zinc finger protein 7 (KOX 4, clone HF.16)	-	+
+ = overexpressed; - = underexpressed		

Seykora et al.[121] demonstrated differences in gene expression between nevi and melanomas. Nevi mRNA was pooled from four benign melanocytic lesions, while melanoma mRNA was collected from two nodular primaries and two metastatic lesions. It is not clear how pooling samples from different locations (and possibly different patients) may have affected the results of their experiments, but they do provide a chart demonstrating genes that can be used to classify nevi and melanoma.

Table 5. Differentially expressed genes in Seykora et al. study.

		Ratio of Expression in Melanoma Relative to Nevi
Expressed similarly in melanoma and nevi	GADPH	0.9
	HLA Class I	1.3
	Matrix metalloproteinase 14 precursor	0.9
	Fibroblast growth factor 8	1.0
	Glia-derive neurite-promoting factor	1.1
Expressed preferentially in melanoma	Cdc2-related protein kinase	3.5
	Cyclin D1	2.7
	PCNA	1.3
	c-Jun N-terminal protein	3.3
	c-Myc binding protein MM1	13.5
	Notch 2	4.3
	CD59	10.25
	β4 integrin	3.7
	Matrix metalloproteinase 17	3.3
	Nucleoside diphosphate kinase B	3.5
	Early growth response protein 1	5.2
	Pleiotrophin	33
	40S ribosomal protein	3.5
Expressed preferentially in nevi	Growth factor receptor bound protein 2	0.8
	Glutathione-S-transferase homolog	0.8
	Fibronectin	0.6
	α3 integrin	0.7

Using the DermArray® DNA microarray, Dooley et al.[122] investigated novel markers of human melanocytes in two experiments. The DermArray DNA microarray contains over 26,000 unique human cDNAs, with a number of them (important in dermatology research) spotted in triplicate to aid in statistical analyses. In their first experiment, they compared normal melanocyte cells to keratinocytes and fibroblasts. In the second experiment, they compared normal melanocytes to two melanoma cell lines; one primary (MS7) and one metastatic (SKMel-28).

Clark et al.[123] devised a clever study to identify novel genes specific for melanoma metastases. Starting with weakly metastatic parental cell lines (mouse and human melanomas), they performed an *in vivo* serial selection scheme in mice to derive a robust metastatic cell line. The gene expression profiles of subsequent metastatic

pulmonary tumors were compared to the primary tumors. The table below demonstrates the thirty-two out of approximately 7000 genes with enhanced expression levels (>2.5 fold) in the metastatic tumors.

Table 6. (adopted from Clark et. al[123]). Enhanced gene expression in metastatic melanomas

	Human A375			Mouse B16		
Gene Name	Pulm. Met #1	Pulm. Met #2	Pulm. Met #3	Pulm. Met #1	Pulm. Met #2	Pulm. Met #3
Fibronectin	10.1	3.2	4.0	2.8	2.8	2.8
RhoC	4.7	3.1	4.0	2.9	4.9	2.5
Thymosin β4	3.3	3.6	3.5	4.1	3.5	3.5
t-PA	5.2	9.6	5.2			
Angiopoietin 1	4.3	9.4	3.3			
IEX-1/Glu96	9.1	3.3	4.5	0.4	0.6	0.5
RTP/NDR1	8.6	5.4	4.7	A	0.7	1.5
Fibromodulin	8.3	4.7	8.2	2.0	2.0	1.1
Hsp70	7.8	4.2	5.0	2.1	1.8	1.8
IL13 Receptor	7.6	2.9	3.1			
Sec61β	3.8	4.7	3.3			
snRNP, polypep C	3.8	5.3	3.2			
Collagen Iα2	2.5	3.6	3.6	3.1	2.3	3.7
UBE21	3.6	3.4	3.4			
TGFβ superfamily	3.4	3.4	3.0			
Surfactant protein C				32	12	16
Lysozyme M				20	10	22
KIAA0156	3.6	3.4	3.4			
Matrix Gla protein	3.2	4.4	1.1	12	11	5.4
Tsa-1				9.7	6.1	7.2
Collagen IIIα1				8.2	5.6	5.5
Biglycan		3.7	3.7	3.8	4.4	6.9
α-catenin	1.3	1.0	1.9	3.4	3.0	5.7
Valosin-cont. protein				3.0	3.9	5.9
ERK-1				2.6	2.6	3.0
α-actinin 1				3.6	3.3	7.3
calmodulin				4.8	6.7	5.5
EIF4γ				4.7	3.2	2.6
α-centractin				2.9	3.8	3.6
IQGAP1				3.6	3.5	3.2
cathepsin S				2.8	2.8	3.1
EF2				2.6	2.5	2.9

The most interesting genes expressed in the highly invasive tumors included genes involved in cytoskeletal organization and cell migration (an observation also observed in Bittner et al.). Three of the genes identified by Clark *et al.* — those encoding fibronectin, thymosin β4 and RhoC — showed increased expression in all of the human

and mouse melanoma-derived metastases. Anne Ridley suggests in a *News and Views* article that these genes operate in a coordinated fashion to attain metastatic status.[124]

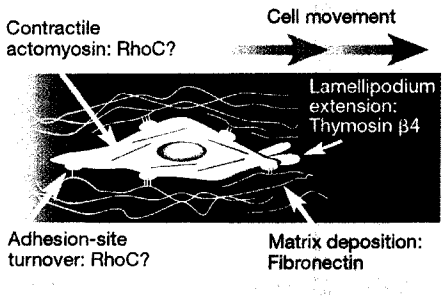

Figure 6.[124] Molecular model for melanoma invasion and metastasis. Cell migration involves protrusion of the plasma membrane (lamellipodium extension) at the leading edge of the cell; the formation of new sites of adhesion to the extracellular matrix at the front; the release of old adhesion sites at the back; and contraction of actomyosin-based cytoskeletal filaments in the cell body to move the bulk of the cell forward. Rho proteins regulate actomyosin-based contractility and adhesion turnover, implicating it in these steps of cell migration. Thymosin beta4 buffers monomeric actin in cells, and could act to provide actin monomers for rapid polymerization into actomyosin filaments in lamellipodia. Fibronectin is an extracellular matrix protein, and deposition of fibronectin by the cell could promote migration by signalling through specific receptors on the cell surface.

A recent study published in *Cell* by McGill et al.[125] used cDNA microarrays to identify the transcriptional targets of the micropthamia gene, Mitf, a transcription factor essential for melanocyte development. Mitf also appears to be a highly sensitive and specific histopathological melanocyte marker for melanoma.[126, 127] In their article, McGill et al. demonstrate that Bcl-2, an antiapoptotic factor, is one of the major targets of Mitf, and is critical for melanocyte and melanoma survival. A number of histopathologic studies have evaluated the relevance of Bcl-2 expression in melanomas, and although its association with aggressive potential is unclear[128-143], it has been targeted in clinical trials using Bcl-2 antisense oligonucleotides[144].

Another recent study be de Wit et al.[145] used the Affymetrix Hu6800 and Hu35K array set to identify genes associated with metastasis by comparing the mRNA expression of two human melanoma cell lines with different metastatic behavior; 1F6 is poorly

metastatic, leading to metastases in only 4% of mice, while Mel57 leads to metastases in all injected mice. Among known genes (~5000 on the Hu6800), 29 were up-regulated and 62 were down-regulated, using a 3.5-fold cutoff. Of the 35,000 EST sequences on the other array, 94 were up-regulated and 133 were down-regulated. Based on the results of this study, it appears that a relatively small number of genes are responsible for the differences between these two cell lines. They were able to validate most of their results in the cell lines, by Northern blot or RT-PCR analysis, but could not always show the same correlations in human tissue. Regarding *in vivo* melanocytic tumor progression they were able to validate the array results for five selected genes: **APOCII, TGFβ,** and **PACE4** show up-regulation, whereas **hCDC10** and **DYRK1A** are down-regulated. The graph below displays the up- and down-regulated genes categorized by cellular function.

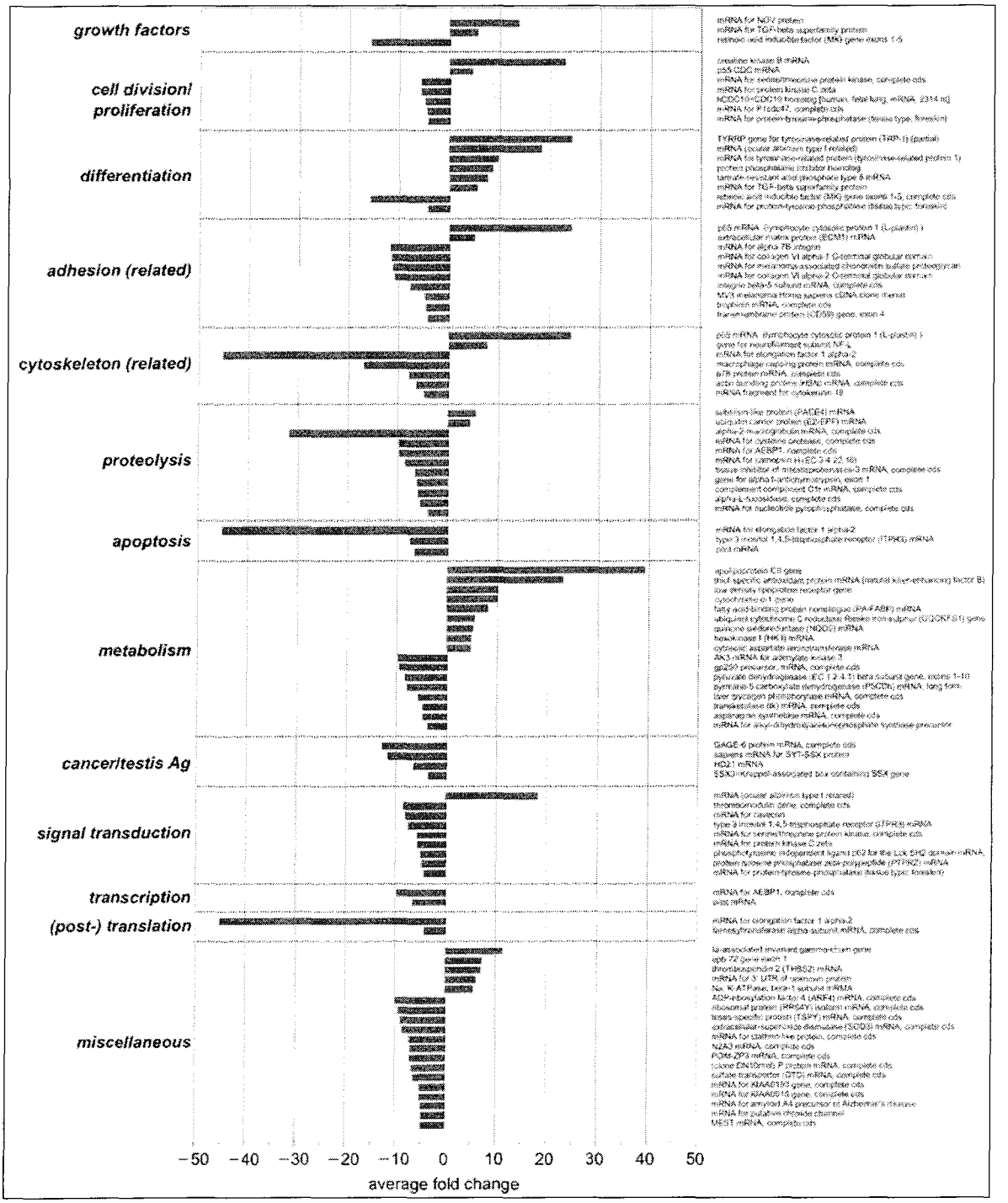

Figure 7.[145] Categorization of differentially expressed genes. Genes showing differential expression in 1F6 and Mel57, identified with the Affymetrix Hu6800 array, were subdivided into categories representing particular cellular processes or specific function of proteins. A positive average fold change correlates with upregulation in Mel57, and a negative average fold change with downregulation.

Brem et al.[146] performed an experiment very similar to that described above. They compared the expression profile of metastatic (NMCL-1) versus non-metastatic (530) melanoma cells. They used the Affymetrix HuGene FL array, containing 6800 genes. They found that genes involved in a multitude of processes (e.g., transcriptional control, cell cycle regulation, proteolysis, cell adhesion, immune response, and signaling) were differentially expressed. They especially note that genes involved in MHC-interactions and cell adhesion were down regulated.

Somewhat unrelated to the scope of this project, as it focuses on treatment response prediction, Wang et al.[147] utilized gene expression profiling in melanoma to search for molecular predictors of treatment outcome. The authors compared the gene expression profiles of subcutaneous melanoma metastases before and after various immunotherapy treatments. They were unable to demonstrate subsets of melanoma predictive of clinical outcome, based on gene expression profiles. It seems that the extent of immune responsiveness may be predetermined and not dependent on the level of immune response elicited by a particular therapy. They did show that melanoma metastases express a heterogeneous array of cytokines, growth factors, and metalloproteinases; a number of which have chemotactic properties (e.g., BLC, eotaxin, IL-1, IL-8, IL-16, lymphotactin, MCP-1, MCP-3, MCP-4, RANTES) or inflammatory action (e.g., IL-6, MIP-1α, MIP-1β, MIP-2α, TNF-γ).

Time and testing will reveal the accuracy and clinical relevance of these various genes in melanoma progression. These experiments are yielding new insights into the molecular genetics of this truly unpredictable disease. The results will be important for a

complete understanding of melanoma, and equally important for the development of new treatments.[116]

It is unfortunate that most cDNA microarray studies have been performed on cell lines instead of fresh human melanocytic tumor lesions. However, it is difficult to run cDNA array analyses on these tissues because the amount of mRNA required for these studies would be inadequate in most cases. In addition, even with the specificity of laser capture microdissection, it is difficult to distinguish expression in the stroma versus tumor tissue. This is a major problem with all forms molecular biological analysis that require homogenization of tissue.

The findings from these studies provide 'potential' biomarkers. They must be validated by another method (i.e., quantitative RT-PCR or Northern blots at the RNA level, and immunodetection by ELISA or Western blots). In addition, further evaluation must be performed to determine their clinical significance on human tissues. This is the place for TMAs, allowing one to screen hundreds of markers on hundreds of tissues.

Although DNA microarray technology is becoming omnipresent in research laboratories, the results require rigorous evaluation by competent biologists, with expertise in molecular biology, cell biology, biochemistry, genetics, and bioinformatics. In this 'post-genomic' era, it is important to avoid over-interpretation of the significance of data obtained through DNA microarray experiments. However, these tools still remain a valuable tool for identifiying the genes altered in the metastatic progression of tumor cells.

Selection of markers from cDNA microarray expression profiles incorporated the known biological significance of genes and their products, as well as cross-validation of

multiple studies. Comparison of *"Melanoma vs. Normal Nevus"* and *"Benign Melanoma vs. Aggressive Melanoma"*, as well as a marker type *stratification system* was developed. DNA microarray studies, such at those detailed above and our own work led by Dr. Halaban[117], have identified numerous very promising markers which are just beginning to be validated. From these lists, as well as recommendations from experts in the melanoma field[148] and functional studies on individual genes and gene products, a series of approximately 50 markers were selected based on the availability of good antibodies and their performance in validation studies.

Tissue Microarray Technology

Tissue microarray (TMA) technology was first described by Kononen and Kallioniemi in 1997.[149] Consisting of an ordered array of tissue cores—up to 2,000—on a single glass slide, tissue microarrays provide a mechanism for the maximal use of scarce tissue resources.[149] Most tissue microarrays are currently constructed from pathology tissue block archives, and the coordinate clinical data can be correlated with experiments performed on these tissues. TMAs allow for the validation of new concepts in cell and molecular biology on human tissue.[150, 151] They are the ultimate step in the association of gene expression information with human tissues and human disease.

Tissue microarrays supply a mechanism for conservation of tissue, while providing the ability to evaluate hundreds of archival tissue specimens on one microscope slide. As illustrated in the figure below, tissue microarrays are constructed from formalin-fixed, paraffin-embedded tissues. Under the guidance of a pathologist, the target tissues are core-biopsied with a 0.6 mm diameter needle, and the cores are placed in a 'recipient' paraffin block. The maximum number of specimens one block can hold varies from 600 to 2000 (with new smaller diameter needles). The block containing the array is sectioned in an identical fashion to any paraffin tissue block. The maximum number of sections a block can provide ranges from 100 to 200, depending on the size of the original tumors and the skill of the histotechnologist.[149-151]

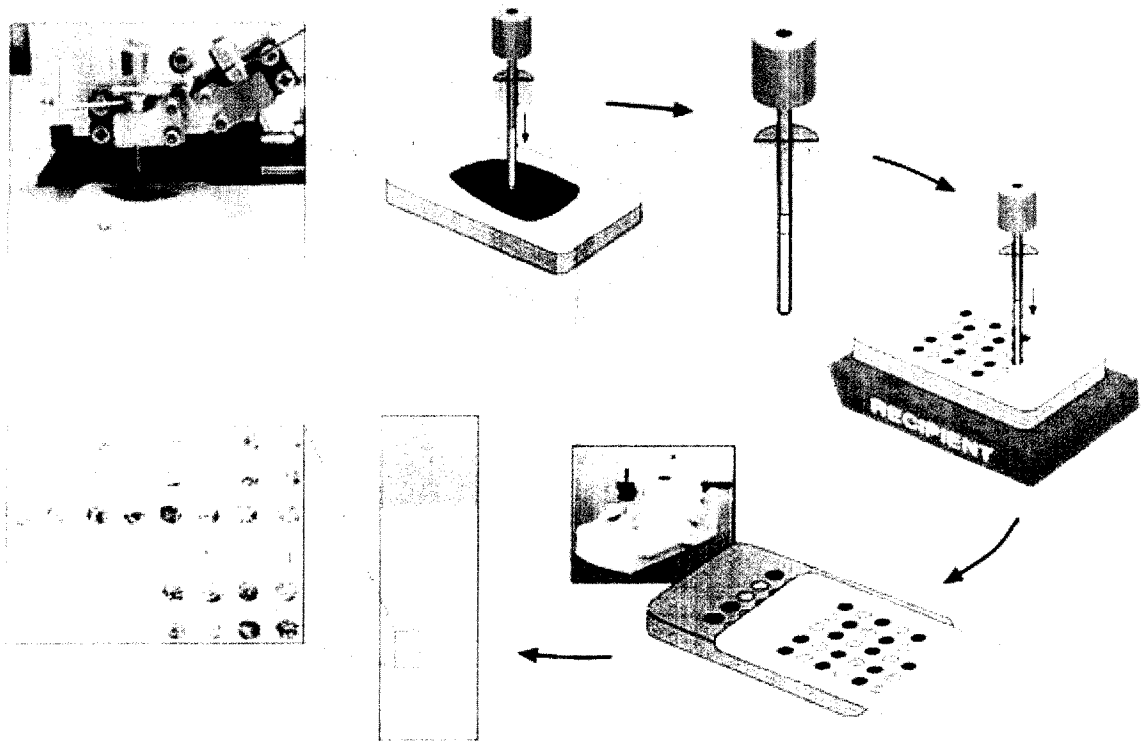

Figure 8.[152] Tissue microarrray construction. Cores are removed from paraffin-embedded tissue "donor" blocks, and placed into a "recipient" block. A grid format is created, and the position of each "donor" specimen is recorded for later analyses. The recipient block is then sliced at a thickness of 5um on a digital microtome, and transferred onto a slide. A sample of a stained tissue microarray is shown in the inset.

In addition to providing a means of preserving human tissues, which are always in limited supply, the ability to examine many histological specimens on a single slide is of great value. By exposing all tissues to precisely the same conditions, the slide-to-slide variability inherent to immunohistochemistry and *in situ* hybridization is minimized.

Unlike DNA microarrays, where each microscopic spot represents a unique cloned cDNA or oligonucleotide, the spots on tissue microarrays are larger and contain histologic tissue sections from unique patients or tumors. This technology reverses the typical array paradigm. Instead of testing one sample for expression of thousands of

genes, tissue microarrays allow testing of one gene (or more typically a protein) on hundreds or thousands of samples (patients).

It is estimated that there are over 30,000 genes within the human genome, encoding over 100,000 proteins. Researchers are currently beset with the task of filtering through the vast number of gene and protein targets to identify those with clinical relevance and diagnostic/prognostic/therapeutic potential. Target validation is a critical step in sifting through such targets. Traditionally, target validation was done with static assays such as Northern blot analysis, RT-PCR, macroarray, microarray, and gene chips. These technologies simply provide evidence of differential expression of specific genes and only rudimentary clinical information is obtained. For most techniques in molecular biology, tissue is homogenized to isolate RNA or protein for expression analysis. Unfortunately, the tissue obtained is not necessarily composed solely of the cells of interest. The tissue homogenate can contain normal cells, tumor cells, blood cells, muscle cells, and other cell types that may result in misleading information. Critical spatial information is lost in these studies, convoluting the results and making truly well-informed mechanistic explanations nearly impossible. Tissue microarrays provide an optimal venue for establishing the clinical importance of various gene products.

A key criticism of tissue microarrays is that the small tissue disk is not representative of the entire tumor. This is particularly problematic when the tumors are highly heterogeneous, on both a morphological and a molecular level. To evaluate this issue, numerous studies have compared IHC findings on TMAs with their corresponding traditional whole tissue sections[153-172], with the vast majority revealing a high level of concordance.[154-166, 168, 169, 171] Most of these studies used multiple cores from donor

blocks in order to determine how many samples are needed to obtain results on TMAs that are concordant with whole tissue sections. It has been generally found that two to three samples are needed to achieve a good concordance level. However, this number is highly dependent on the tumor type and the design of the study. In our effort on breast cancer, Camp et al. analyzed estrogen and progesterone receptors and HER2 on 2-10 cores per breast cancer donor block. It was found that analysis of two cores was sufficient to obtain identical results as compared with the corresponding whole tissue sections in 95% of cases; four cores yield a concordance of 99%.[161] It is important to recognize that these studies are based on the assumption that traditional whole tissue sections, the current gold standard for molecular tumor tissue analysis, are representative of an entire tumor.[173] A section from a tumor that measures 3 x 2 cm in diameter, cut 3 μm thick, has a volume of 0.0018 cm^3. This volume is only 1/19,000 of a tumor with a diameter of 4 cm or 1/150,000 of a tumor with a diameter of 8 cm. A TMA sample measuring 0.6 mm in diameter represents a tumor volume of 0.00000108 cm^3, which is 1/1600 of a 3 cm x 2 cm x 3 μm whole section tissue slice. Based on these numbers, the representivity problem is about 100-times greater between the entire tumor and a traditional large section than comparing results obtained on large sections and TMA sections.[173] In addition, it should be noted that the tissues on the TMA are carefully selected to be representative of tumor on the whole tissue section.

Quantitative Immunohistochemistry

Oxidation and Storage

Tissue microarrays have facilitated the evaluation of large cohort studies with the use of formalin-fixed, paraffin-embedded tissues that can sometimes be almost a century old. The current method of archival storage of tissues—formalin fixation followed by paraffin embedding—is a remarkably resilient method of specimen and antigen preservation. However, once the samples from such blocks are cut into 5 micron sections and deparaffinized, the tissue is exposed to ambient air and the potential effects of oxidation. Several studies have demonstrated the detrimental effects of storing pre-cut tissue slides under ambient conditions.[174-178] For some proteins (i.e., estrogen receptor), pre-cut slides stored in room air lose all detectable antigenicity in one month, with a statistically significant difference from fresh cut seen by 6 days[179]; demonstrated in Figure 9. Unfortunately, there is not a universally accepted method for storing slides that reduces the loss of antigencity. Cold storage of slides at 4°C has shown some promise, but still results in significant loss of antigenicity.[176, 177] One method of antigen preservation that has demonstrated moderate success is paraffin coating of pre-cut slides.[176] Non-formalin-based fixatives have been tested and have some benefits, but they do not reduce the loss of antigenicity due to oxidation.[180-185] While these fixatives show great promise in overcoming some of the deleterious effects of formalin-based fixation, they are not useful for retrospective studies on paraffin-embedded archival tissues, the vast majority of which are formalin-fixed.

The advent of tissue microarrays as a tool for the study of immunohistochemical stains has renewed interest in finding methods for cut-slide preservation. To avoid

repeatedly facing the paraffin block containing a TMA, serial sections are typically cut at one time and stored as individual slides. While this procedure increases the quantity of high quality slides that can be cut from a particular TMA block, it necessitates rigorous slide storage techniques that will ensure antigen preservation. Our laboratory has developed a reliable method for the long-term storage of TMA slides that entails paraffin-coating of slides followed by (long-term) storage in a nitrogen dessication chamber.[179] This method of cut-slide storage maintains tissue antigenicity comparable to fresh-cut slide for up to 3 months.

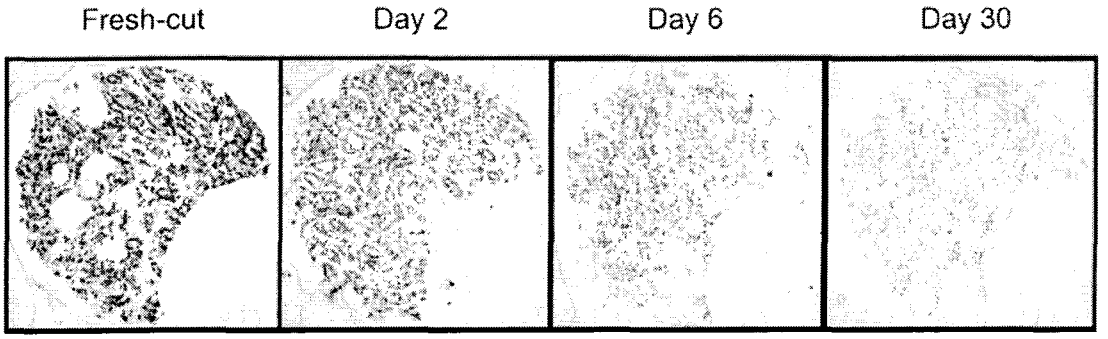

Figure 9.[186] Effects of oxidation on tissue antigenicity. Estrogen receptor immunohistochemistry is abrogated by storage under ambient air conditions. Matched histospot of breast cancer from freshly-cut slide, as well as slides stored for 2, 6, and 30 days in ambient air. Slides were stained for ER and visualized with DAB. Staining is localized to the tumor nuclei when assayed under high power.

Fixation and Antigen Retrieval

For over 100 years, pathologists have relied upon formalin—a 37% solution of formaldehyde gas in water—for fixation of tissue specimens.[187] Formalin has several advantages over alcohol and other precipitative (non-cross-linking) fixatives, in that it maintains excellent preservation of morphologic detail. Quick and effective fixation of fresh tissue is necessary to fix antigens *in situ*, prior to the onset of autolytic changes. Although the biochemical mechanisms of the fixation process are not entirely understood,

it is clear that formaldehyde-based fixation involves the formation of cross-links of amino groups[188-190], among other reactions, recently summarized by Shi et al.[191] These formalin-induced protein cross-linkages can result in partial or complete loss of immunoreactivity of various antigens, either through intramolecular crosslinks within the epitope region of the target antigen, or cross-linking of unrelated proteins to the epitope.

Although formalin fixation will allow some epitopes to emerge unchanged (formalin-resistant), others will undergo substantial changes (formalin-sensitive). Despite the loss of immunoreactivity by many antigens as a result of formalin fixation, formalin-fixed paraffin-embedded (FFPE) tissue remains the medium of choice for clinical and research studies because of the superior preservation of morphology.

Various alternatives to formalin have been tested, and it is likely that an ideal fixative will never be found.[192, 193] To counteract, or 'reverse', the effects of formalin fixation—to improve the immunoreactivity of FFPE tissues—a number of unmasking techniques, such as enzymatic digestion and heat-induced antigen retrieval, were introduced. The first attempts to 'improve' IHC involved the use of tryptic digestion prior to immunofluorescent staining.[194] Other proteolytic enzymes (e.g., bromelain, chymotrypsin, ficin, pepsin, pronase) were tried for restoration of immunoreactivity to tissue antigens with varying degrees of success.[195] Proteolytic digestion compensates for the impermeable nature of the non-coagulant fixatives by "etching" the tissue and allowing hidden determinants to be exposed. Use of these enzymes may however also entail the risk of destroying some epitopes.

Currently, the principle of antigen retrieval is based upon the application of heat for varying lengths of time to FFPE tissue sections in an aqueous medium. The

technique, initially developed by Shi et al. in 1991, is a high-temperature heating method to recover the antigenicity of tissue sections that has been masked by formalin fixation.[196] A number of modalities for heat generation have been tested, including microwave oven, pressure cooker, steamer and autoclave. The advantages and disadvantages of various heating modalities and retrieval solutions are the subject of ongoing experiments.[191] Alternate terminology used for "antigen retrieval" includes epitope retrieval, heat-induced epitope retrieval, target retrieval and target unmasking. The latter two versions have more generic appeal and have also been applied to the retrieval of nucleic acid targets for in situ hybridization. In general, antigen retrieval refers to a technique, used widely in pathology and other fields of morphology, which improves IHC staining on archival FFPE tissue sections by reducing detection thresholds of immunostaining (increases sensitivity) and retrieval of some antigens (e.g., Ki-67, ER-1D5, androgen receptor, many CD markers) that are otherwise negative in IHC. Antigen retrieval serves as a pre-treatment amplification step, in contrast to amplification in the phases of detection (e.g., multistep or polymeric detection systems) or post-detection (i.e., enchanced substrated such as DAB using metal, imidazole, CARD, anti-end product, gold-silver enhancement).[197]

Although the molecular mechanism of antigen retrieval is not entirely clear at this time, it is apparently influenced by the pH of the antigen retrieval solution as well as temperature and time of heating.[191] A number of hypotheses have been proposed, including: loosening or breaking of the formalin-induced cross-links[198, 199]; protein denaturation[200]; hydrolysis of Schiff bases[201]; chelation of cage-like calcium complexes, which may develop during formalin fixation[202, 203]; heat-induced reversal of chemical

modification to protein structure that occurs during formalin fixation[199]. This topic has been most recently characterized by the Mason group in a series of papers that look at the biophysical effects of formalin on RNAse.[204, 205]

The technique of antigen retrieval, a heat-induced remodification of formalin-induced modification of protein conformation, may contribute to standardization of IHC staining of FFPE tissue by equalizing the intensity of IHC staining under variable conditions of fixation and processing.[197] While the molecular mechanisms of antigen retrieval are the subject of intense investigation, the main concern is that the procedure works and provides reproducible results. Importantly, antigen retrieval has become increasingly more useful in research and diagnostic pathology, as it provides increased sensitivity for the demonstration of molecular markers not previously demonstrable in standard tissue sections. A number of different antigen retrieval techniques are in development, and it is essential that scientists and pathologists focus on standardization of antigen retrieval, which will likely entail optimization for individual antigens.[206]

Standardization of Immunohistochemistry

The Biological Stain Commission (BSC) was founded in 1944 as a nonprofit organization to address the problem of standardization of chemical stains in pathology.[207] The BSC was able to achieve considerable success with regard to biological dyes, but the introduction of immunohistochemistry brought new challenges. The origins of immunohistochemistry date back to 1941, when Coons et al. established an immunofluorescence technique for detection of bacteria.[208] It was many years before it became a common part of diagnostic pathology. In 1977, the National Cancer Institute held a workshop to address the standardization of immuno-reagents in diagnostic

pathology.[209] From its inception and until recently, the use of IHC was limited to qualitative assessments of expression. The major application of the method in pathology was in the detection of cellular lineage markers to diagnose poorly differentiated malignancies. Interpretation of results was a matter of positive or negative, present or absent. Little attempt was made to distinguish degrees of staining, or differences in intensity.[210]

The introduction of immunoperoxidase methods and increasingly sensitive detection systems in the mid-1970s provided the ability for broad application of IHC on routine FFPE tissues. With the promise of unparalleled specificity, IHC transformed histopathology from something resembling an art into something more closely resembling a science.[211] The application of IHC to routinely processed tissues represented a new era for the demonstration of antigens in situ, allowing pathologists to correlate immunologic findings directly with traditional cytologic and histologic criteria.[212]

Immunohistochemistry typically follows a series of universal steps. A) Pretreatment (antigen retrieval), often with pressure-cooking of tissue in citrate buffer to unmask antigens hidden by formalin cross-links or other fixation. Other agents used for antigen retrieval include proteases, such as pepsin, trypsin, bromelain. B) Application of primary antibody; antibody binds to antigens of interest. C) Wash off excess primary antibody. D) Application of labeled anti-IgG antibody (secondary antibody), which binds to the primary antibody. The secondary antibody is typically conjugated to biotin or horseradish peroxidase. E) Application of detection chemicals, including a chromagen (color changing reagent), usually 3, 3' diaminobenzidine (DAB). It is necessary add an

avidin-biotin-peroxidase complex prior to DAB in the case of biotinylated antibodies. The slide is then counterstained with hematoxylin to identify all nuclei. This is the standard method for the 'brown stain'.

While immunohistochemistry has become an established method in research and clinical pathology, a surprising lack of standardization and reproducibility exists among different laboratories. Enormous variability has developed in terms of the reagents available, the detection methods used, and, most importantly, the interpretation and reporting of immunohistochemical findings.[213] Although efforts have been made to standardize immunohistochemistry, difficulties remain.

Recently, the need for IHC standardization has expanded due to the inception of bio-specific therapies that are approved with partner pharmco-diagnostics. Quantitative (or at least semiquantitative) IHC is likely to become more critical as pathologists are required to accurately distinguish expression levels of markers to determine whether or not a patient is a candidate for a specific therapeutic. The classic example is the evaluation of HER2-2/neu expression to aid in prognosis of breast cancer. Although this marker is an "easy one", there has still been considerable literature on the inaccuracy of of the pathologist-based test. More recently, market forces have resulted in standardized test kits, such as the HerceptTest (DAKO, Carpinteria, CA) and INFORM DNA probe test (Ventana Medical Systems, Tucson, AZ), that have been approved by the FDA. None-the-less, the accuracy and comparability of these methods is somewhat controversial.[214]

Efforts to standardize immunohistochemistry have focused on three areas: (1) antibodies and reagents, (2) technical procedures, and (3) interpretation of IHC findings

for research and diagnostic uses. There has been recommendation for a Total Test Approach to standardization of IHC[213], requiring that the pathologist pay close attention to each and every step of the procedure: from excision of the biopsy, including the type and duration of fixation, through the antigen retrieval method and detection procedure, as well as interpretation of the resulting stain. Much of the variability in staining is introduced by differences in fixatives or fixation times[215], and these can be reduced, if not eliminated by the use of an optimized antigen retrieval protocol[210]. In addition to optimization of antigen retrieval, the authors suggest simplification of IHC staining method, and the implementation of quantitative IHC.

Quantitative Immunohistochemistry

Although the current gold standard for diagnosis amongst pathologists relies upon morphological criteria, histochemistry—immunohistochemistry in particular—has provided a more accurate mechanism for diagnosis, as well as the ability to assess molecular interactions *in situ*. The primary usage has been as an ancillary test to assist in classifying tumors or in making a diagnosis. But there is now a trend toward increased usage of this test as a mechanism to predict response to therapy. This trend, as well as advances in computation power, is driving numerous efforts toward quantitative assessment of expression. The critical information that makes techniques such as immunohistochemistry and *in situ* hybridization so valuable is that they provide molecular information within the architectural context of tissues. This information, including architectural and subcellular localization, can be critical for classifying tumors, or providing prognostic or predictive information. This information needs to be maintained as a unique part of the molecular information package that now includes

various molecular-based techniques, which typically rely on suspensions or extracts of cells or tissues, such as PCR, DNA sequencing, FACS and ELISA assays.

Quantitative immunohistochemistry (QIHC) is composed of two general methodologies, manual and automated analysis. Pathologists typically perform the manual method of QIHC. After identifying the region of interest within a tissue section (i.e., tumor or other diseased tissue), estimation of intensity or percentage of IHC staining is determined. This method is presently more commonly used, and is well recognized in the literature. However, this approach is relatively subjective, based on visual estimation of the intensity and percentage of positive staining of IHC. The immunoreactive grading system provides a visual aggregate of intensity/percentage, denoted by "0, 1+, 2+, 3+", representing negative, weak, moderate, and strong staining, respectively. Semi-quantitative systems have been invented and some have seen extensive usage, including the H-score system[216] and the Allred system.[217] Both are based on the product of staining intensity and the percentage of positive cells. Though widely used, the manual system of QIHC is imperfect, based on human fallibility, which suffers from a high degree of inter- and intra-observer variability.[218, 219]

Automated systems for QIHC begin with acquisition and storage of digital images, followed by image correction and enhancement, segmentation of objects within the images, and ultimately image measurement.[220] Several commercial systems are currently available for image analysis of brown stain IHC slides. Among these systems, the CAS system, originally invented by James Bacus[221], was perhaps the most popular as judged by the number of units sold, although now it is outdated. The CAS 200 system, and its successor, the BLISS system, is designed for quantitative analysis of "brown"

stained IHC material. The optical density of the reaction product is determined through conversion of the light transmission, or gray level, and the relative area of the staining reaction is also determined. Other systems with similar functionality are listed below.

Table 7. Commercially Available Automated Analysis Systems

System	Source	
Bliss	Bacus Laboratories, Inc.	http://www.bacuslabs.com
Chromavision ACIS®	Clarient	http://www.chromavision.com
IVision and GenoMx™	Biogenex	http://www.biogenex.com
Scanscope® Systems	Dako Cytomation	http://www.aperio.com
Ariol SL-50	Applied Imaging	http://www.aicorp.com
PATHIAM	Bioimagene, Inc.	http://www.bioimagene.com
Discovery	Molecular Devices	http://www.moleculardevices.com
TissueAnalytics	Tissue Informatics, Inc.	http://www.tissueinformatics.com
LSC	CompuCyte Corporation	http://www.compucyte.com
AQUA™	HistoRx	http://www.historx.com

These systems generally cost between $200,000 and $300,000. In addition, some investigators have developed analysis systems on their own[222, 223] or using commercially available software.[224, 225]

Because these systems are designed to analyze brown stain IHC, they rely upon absorbance (i.e., optical density) to compute an intensity score. In spectrophotometry, Beer's Law ($A = \varepsilon l c$) states that the absorbance (**A**) of a species at a particular wavelength of electromagnetic radiation, is proportional to the concentration (**c**) of the

absorbing species and to the length of the path (**l**) of the electromagnetic radiation through the sample containing the absorbing species. The extinction coefficient (ε), also known molar absorptivity, is dependent upon the wavelength of the light and is related to the probability that the species will absorb light of a given wavelength. When A equals zero, no photons are absorbed; when A equals 1.0, 90% of photons are absorbed, i.e., 10% detected; when A equals 2.0, 99% of photons are absorbed, i.e., 1% detected. Most brown stains are optimized by eye for signal to noise such that the absorbance of a 'positive' case is over 1.0 and often over 2.0. Thus, only a tiny percentage of the light is detected, which decreases the dynamic range of the assay and makes co-localization more challenging. Fluorescence-based imaging could circumvent these problems, but that imaging modality has other problems. As a result, very few companies have developed quantitative analysis on the basis of this platform.

Fluorescence-based Platforms for Quantitative Analysis

Although fluorescence-based methods have numerous advantages with respect to dynamic range and co-localization, they have not been broadly used for numerous reasons. Firstly, formalin fixed tissue generally has a substantial amount of auto-fluorescence, especially in the wavelengths of the most common fluorophores. Red cells are a particular problem. A second issue is the higher cost and limited accessibility of epifluorescent microscopy equipment. Perhaps the greatest barrier is the inability of the pathologist to judge the surrounding tissue and architectural context. This can be seen as a huge disadvantage, or, arguably, an advantage if the goal is to reduce subjectivity. In flow cytometry, pathologists do not see any cells, but that is not seen as a disadvantage. Furthermore, recent studies suggest that pathologists tend to select non-representative

regions when they select an area to score (Gann et al, personal communication). This can decrease the overall accuracy of assessment of protein expression levels.

A small number of laboratories have now begun developing analysis systems for fluorescence-based quantification. The following paragraphs describe our lab's efforts in this area.[226] The assembly consists largely of off-the-shelf microscopy equipment based on an Olympus AX51 automated microscope, with a Cooke digital camera, and computerized image acquisition based on the IP Lab software (v3.54, Scanalytics, Inc.). The imaging system captures stacks of images that are then analyzed on custom software developed in our laboratory, written by Robert Camp called AQUA (Automated Quantitative Analysis, Figure 3). The underlying principle behind the software is that spatial information is maintained, but that all localization is based on molecular information, rather than feature identification or morphology. Thus, the steps for analysis of each image include identification of a mask to separate tumor from non-tumor, followed by definition of compartments on the basis of other molecular interactions. For example, keratin may be used as a mask (for cells of epithelial origin) and DAPI to define a nuclear compartment. Then, the target of interest is measured (for example estrogen receptor) in a quantitative fashion only in the pixels that are within the mask and compartment defined by the previous markers. The intensity then divided by the area of the compartment to define a normalized value that is directly proportional to the protein concentration of the target. The following is a detailed description of the process.

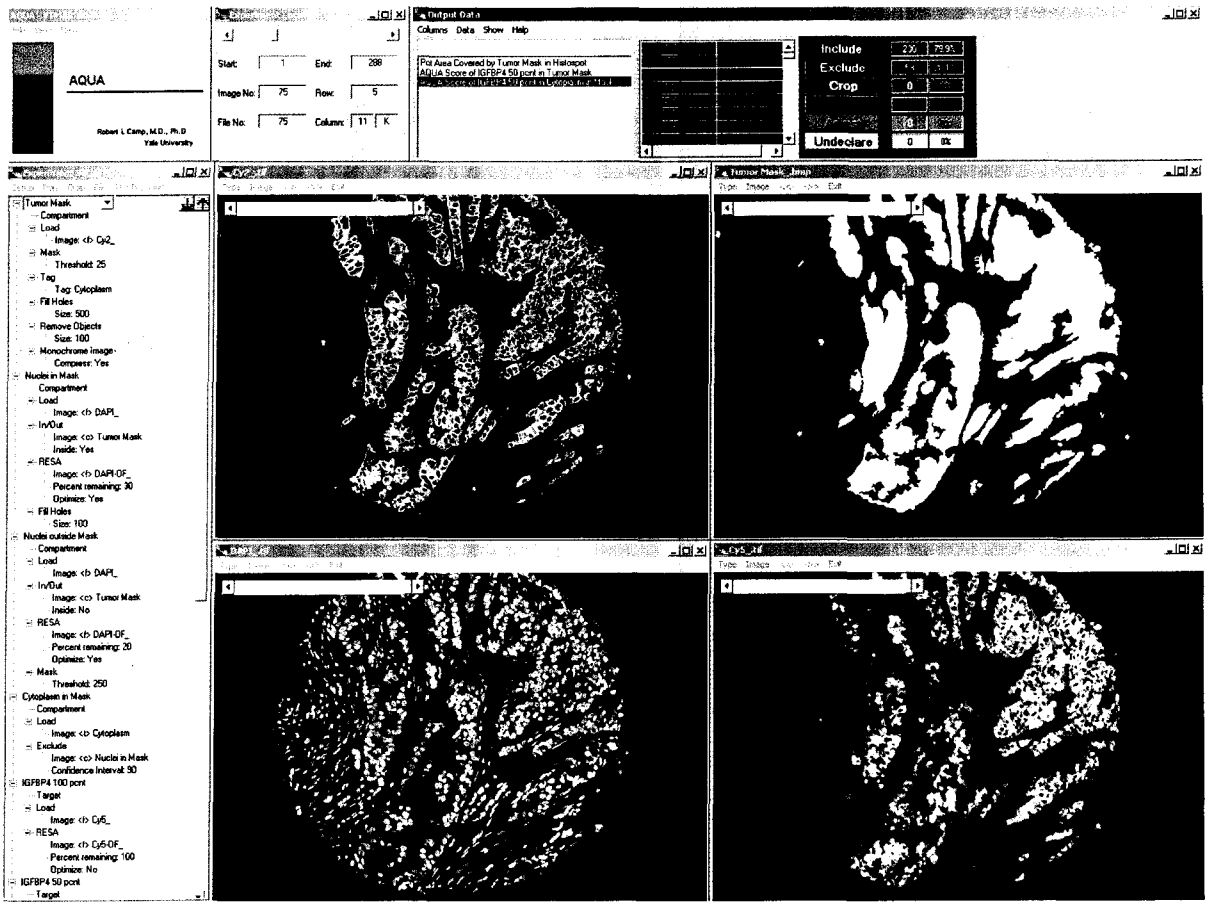

Figure 10. AQUA software. The windows of the AQUA software are shown including the algorithm description window, the settings window, score window and 4 image windows for the images of different raw images or processed images. For example the upper left image is the keratin immunofluorescence image from which the upper right mask image was constructed.

Image acquisition: Images of microarrays are obtained using an Olympus Motorized Reflected Fluorescence System and software (IP lab v3.54, Scanalytics, Inc.), with an attached Cooke Sensicam QE High Performance camera through an Olympus BX51 microscope with automated *x*, *y*, *z* stage movement. Low power images of microarrays are stitched together using multiple low-resolution images of the microarray (64 x 64 pixel) at approximately 7-micron resolution.

Histospots are identified using a custom written spotfinder algorithm (written by Robert Camp) based on the signal from DAPI or other tags. This signal is gated (i.e., a threshold of pixel intensity is set) to create a binary image of the microarray. Histospots

are identified using size criteria. Rows and columns of histospots are then identified, and missing histospots filled in, allowing each histospot to be identified based on its row/column grid position. The coordinates of each histospot are then recorded.

Subsequently, monochromatic, high-resolution (1024 x 1024 pixel, 0.5-micron resolution) images are obtained of each histospot, both in the plane of focus and 8 microns below it, and recorded in an image stack as bitmaps. This depth, slightly below the bottom of the tissue, was determined to be optimal for 5-micron histologic sections. A resolution of 0.5 microns is suitable for distinguishing between large subcellular compartments such as the cell membrane and nuclei. Efforts are underway to accommodate smaller subcellular compartments (for example, mitochondria, nucleoli) using high power objectives. Images are obtained using a pixel intensity dynamic range of 0–255.

RESA/PLACE algorithmic analysis of images: Through the use of two algorithms, RESA (rapid exponential subtraction algorithm) and PLACE (pixel-based locale assignment for compartmentalization of expression), AQUA carries out the following functions:

- Identification of the tumor locale within the histospot ("tumor mask")
- Identification of subcellular compartments (nuclei, membranes, cytoplasm, etc.)
- Defines the localization and intensity of the "target"

First, a tumor-specific mask is generated by thresholding the image of a marker that differentiates tumor from surrounding stroma and other non-tumor material. This

creates a binary mask (each pixel is either 'on' or 'off'). Keratin is the most common mask used for epithelial neoplasms and S100 protein is used for melanocytic lesions. As formalin-fixed tissues can exhibit autofluorescence, analysis may give multiple background peaks. The RESA/PLACE algorithms determine which of these peaks is predominant and sets a binary mask threshold at a slightly higher intensity level. This provides an adaptive (unique to each histospot) thresholding system that ensures that only the target signal from the tumor and not the surrounding elements is analyzed. Thresholding levels are verified by spotchecking a few images and then automated for the remaining images. This binary mask can be modified using standard image manipulations. In most cases this involves filling holes of a particular size (for example, less than 500 pixels, to fill in tumor nuclei that do not stain for S100) and removing extraneous single pixels. Once set, these image manipulations are performed automatically on all images. All subsequent image manipulations involve only image information from the masked area.

Next, two images (one in-focus, one slightly deeper) are taken of the compartment-specific tags and the target marker. A percentage of the out-of-focus image is subtracted from the in-focus image, based on a pixel-by-pixel analysis of the two images. This percentage is determined according to the ratio of the highest/lowest intensity pixels in the in-focus image – representing the signal-to-noise ratio of the image. By using an exponential scale, this allows RESA to subtract low intensity pixels in images with a low signal-to-noise ratio less heavily than low intensity pixels from images with a high signal-to-noise ratio. The overall degree of subtraction is based on a user-defined percentage for each subcellular compartment. For most applications this is

empirically set to 40% of the total signal, and remains constant for images from an entire microarray. RESA thus eliminates nearly all of the out-of-focus information. The algorithm has the added benefit of enhancing the interface between areas of higher intensity staining and adjacent areas of lower intensity staining, allowing more accurate assignment of pixels of adjacent compartments. In contrast to the compartment-specific tags, the RESA subtraction of the target signal is uniform and not based on overall intensity of the image intensity. This ensures that the same amount of subtraction occurs with the target signal from all specimens.

Finally, the PLACE algorithm assigns each pixel in the image to a specific subcellular compartment. Pixels that cannot be accurately assigned to a compartment to within a user-defined degree of confidence (usually 95%) are discarded. This is accomplished iteratively by determining the ratio of signal from two compartment-specific markers that minimizes the spillover of marker from one compartment into another. Once each pixel is assigned to a subcellular compartment (or excluded as described above), the signal in each location is added up. This data is saved and can subsequently be expressed either as a percentage of total signal or as the average signal intensity per compartment area. The score is expressed on a scale of 1 to 1000 as the total intensity divided by the area of the compartment to 3 significant figures. A step by step illustration of this process is illustrated in the schematic in figure 4. These algorithms are described in further detail in a patent of this technology owned by Yale University.

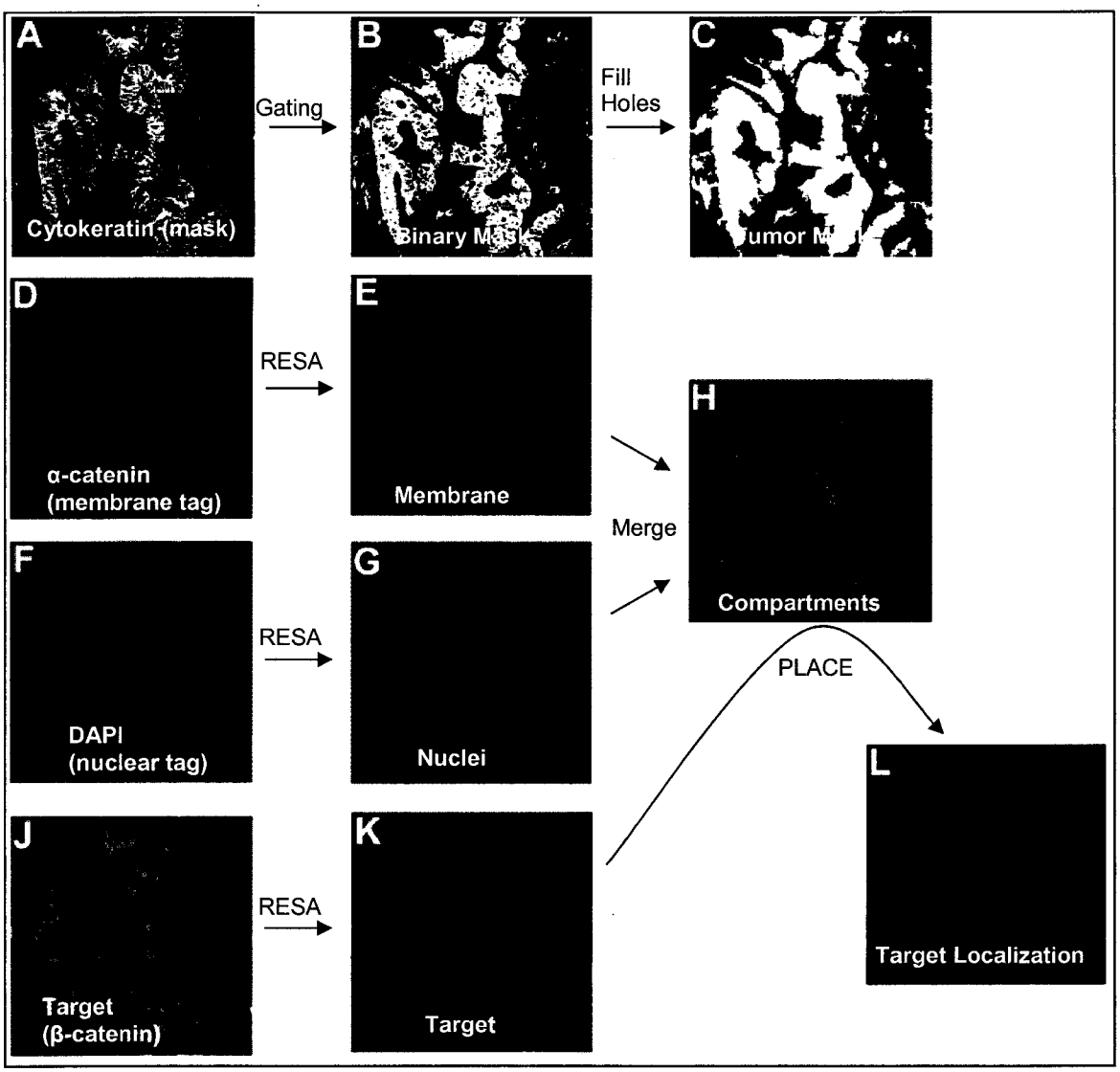

Figure 11. The schematic above demonstrates a step-by-step methodology for RESA and PLACE algorithms used by AQUA in the assessment of β-catenin expression in colon cancer.[226] A) Anti-cytokeratin is used to distinguish colon carcinoma cells from the surrounding stroma. B) Gating of that image creates a binary mask. C) The mask is enhanced by filling holes and removing small objects. D) Anti-α-catenin serves as a membrane tag. E) The membrane tag image is exponentially subtracted using RESA. F) DAPI identifies the nuclei. G) The nuclear tag image is exponentially subtracted using RESA. H) The membrane and nuclear tag images are merged, and overlapping pixels are removed. White pixels represent overlap. J) Anti-β-catenin is the target marker of interest. K) The target marker image is exponentially subtracted using RESA. L) The intensity of the marker is divided into the various subcellular compartments. Graphically, this is represented by red (membrane), green (cytoplasm), and blue (nuclei). In this tumor, β-catenin is predominantly localized to the membrane (red).

The results of this assay (or other quantitative microscopy systems) are a "number" that represents an objective continuous variable for subsequent analysis. This allows statistical analysis of histologic data in a manner more similar to other quantitative

areas of medicine (blood glucose, liver enzymes, or drug levels). Although these systems remove the subjectivity in assessment, there are still other issues that must be systematically addressed, including sample selection (the region analyzed) and a multitude of steps related to processing. However, the addition of quantitative analysis removes the most subjective step and allows the typical rigorous QC and QA of laboratory tests. It is easy to envision future application of these technologies in the clinical lab. Specifically a likely application is the assessment of biopsy tissue for the qualification of cancer patients for new biospecific therapies, based on quantitatively assessed levels of target protein expression.

Statistical Approaches to Tissue Microarray Data

Survival analysis: Kaplan-Meier

In medical research, we often seek to display a summary of the survival experience of a group of patients. Typically, the most convenient method for demonstrating a survival function is by graphical presentation. In this form, it is typically referred to as a survival curve. The horizontal axis usually represents time since diagnosis and the vertical axis represents the probability or chance of survival (or any other well-defined end-point, such as recurrence), expressed as a percentage.[227]

First proposed by Kaplan and Meier in 1958[228], the Kaplan-Meier (K-M) estimate can also be called an actuarial estimate. The Kaplan-Meier method is a nonparametric (actuarial) technique for estimating time-related events. It is a univariate analysis and is an appropriate technique for determining the association of a single variable with survival. It estimates the proportion of individuals alive at a particular time, starting from

the time of diagnosis (time zero). It is especially applicable when length of follow-up time varies from patient to patient, and takes into account those patients lost to follow-up or not yet event-free at the end of study (censored patients, assuming the censoring is non-informative). Since the estimated survival distribution for the cohort study has some degree of uncertainty, 95% confidence intervals may be calculated for each survival probability on the "estimated" curve.

A variety of tests (log-rank, Wilcoxan and Gehen) may be used to compare two or more Kaplan-Meier "curves" under certain well-defined circumstances. Median remission time (the time when 50% of the cohort has reached remission), as well as quantities such as three, five, and ten year probability of remission, can also be generated from the Kaplan-Meier analysis, provided there has been sufficient follow-up of patients. In summary, the Kaplan-Meier technique is a useful method of evaluation for individual nominal (or categorical) markers.

Survival analysis: Cox Proportional Hazard Analysis

In some cases it is necessary to determine whether survival is influenced by one or more factors, called "predictors" or "covariates", which may be categorical (such as the kind of treatment a patient received) or continuous (such as the patient's age, weight, or the dosage of a drug). For simple situations involving a single factor with just two values (such as drug vs. placebo), the method of Kaplan-Meier analysis followed by log-rank testing will suffice for comparing the survival curves of two groups of subjects. For more complicated situations, a special type of regression is required; one that provides assessment of the effect of each predictor on the shape of the survival curve.

To understand the method of proportional hazards, first consider a "baseline" survival curve. This can be thought of as the survival curve of a hypothetical "completely average" subject—someone for whom each predictor variable is equal to the average value of that variable for the entire set of subjects in the study. This baseline survival curve doesn't necessarily have any particular formula representation; it can have any shape whatever, as long as it starts at 1.0 at time 0 and descends steadily with increasing survival time. The baseline survival curve is then systematically "flexed" up or down by each of the predictor variables, while still keeping its general shape.

The proportional hazards method computes a coefficient for each predictor variable that indicates the direction and degree of flexing that the predictor has on the survival curve. Zero means that a variable has no effect on the curve (i.e., it is not a predictor at all); a positive variable indicates that larger values of the variable are associated with greater mortality while a negative variable indicates that larger values are associated with improved survival. Knowing these coefficients, it is possible to construct a "customized" survival curve for any particular combination of predictor values. More importantly, the method provides a measure of the sampling error associated with each predictor's coefficient. This allows for assessment of which variables' coefficients are significantly different from zero, in turn, providing a determination of which variables are significantly related to survival.

Cox analysis incorporates proportional hazards regression to predict relative risk. When incorporating several variables into a Cox model, the relationship between the variables is assessed by multiple regression, taking into account multiple variables and the proportional changes in the dependent variable (survival time and censor status) that

can be expected related to changes in explanatory variables (clinical parameters, protein expression levels). Relative risk is a measure of how much a particular risk factor (say cigarette smoking) influences the risk of a specified outcome (say, death by age 70). For example, a relative risk of 2 associated with a risk factor means that patients with that risk factor have a 2-fold increased risk of having a specified outcome compared to persons without that risk factor. One overall p-value tests the overall null hypothesis that the relative risk of the population is 1.0 and that none of the variables influence patient prognosis. Individual p-values for different markers or clinical variables each have their own p-value that tests the null hypothesis that a variables' particular relative risk is 1.0 in light of other variables.

Hierarchical Cluster Analysis

A major method for analyzing and demonstrating data from gene expression profiling experiments, the use of cluster analysis has increased dramatically over the past few years. Cluster analysis includes a diverse collection of techniques that can be used to classify objects, with the goal of finding subgroups of data within a larger dataset. All cluster analysis algorithms seek to maximize the similarity of "within-cluster" observations while maximizing differences between clusters. The underlying mathematics of most clustering methods are relatively simple but large numbers of calculations are needed. Classification depends on the particular method used, and there are many ways to measure similarity and dissimilarity.

Hierarchical clustering methods attempt to create groups of observations through merging or dividing, with the resultant classification consisting of an increasing number of nested classes. The result resembles a phylogenetic classification, in which

hierarchical tree dendrograms denote the relatedness between genes/samples; branch length denotes the level of similarity. There are two main categories of hierarchical clustering: agglomerative and divisive. Agglomerative clustering methods begin with each observation representing a single cluster. At each step, two clusters are merged until only one cluster remains. The researcher determines the step to stop clustering and, thus, how many clusters to retain. Divisive clustering methods begin in an opposite manner. Initially, all the observations begin in one large cluster, and at each step a cluster is divided until all members represent their own cluster. Again, the researcher determines the number of clusters to retain.

The results of clustering analysis are typically displayed as a two-color heat map, demonstrating both the direction of fold change (indicated by color) and the magnitude of the change (indicated by the intensity/brightness of the color). The phylogenies (one for genes and one for patients/specimens) are displayed adjacent to the heat map. The most popular pieces of software for these analyses—CLUSTER and TREEVIEW—were developed in Michael Eisen's laboratory[118] in order to demonstrate genome-wide expression data from DNA microarray hybridization experiments; standard statistical algorithms are used to arrange genes according to similarity in pattern of gene expression.

Unfortunately, this use of gene expression data does not always identify cancer subtypes that are related to patient survival. There are two main approaches in the literature to identify cancer subtypes. The first approach, described above (e.g., hierarchical clustering), is called "unsupervised" as it does not use any of the clinical information about the patient. There have been a few studies that have demonstrated success in identifying clinically relevant cancer subtypes through unsupervised

hierarchical clustering analysis.[229-233] However, unsupervised learning procedures, by definition, do not use clinical data to identify subtypes, and thus, there is no guarantee that the subtypes they identify will be correlated with clinical outcome. The second approach to identifying subtypes of cancer is based exclusively on clinical data. For example, patients can be assigned to a "low-risk" or "high-risk" subgroup, depending on whether they are alive or their tumor has metastasized after a certain time period. This approach has been used successfully to develop procedures to diagnose patients based on their gene expression profile.[234-237] Unfortunately, this process of grouping patients may not be biologically meaningful, leading to the misclassification of patients in future applications of the model. A third, less commonly used procedure—semi-supervised clustering—was recently proposed by Bair and Tibshirani[238], in which both gene expression data and clinical data is used to identify cancer subtypes. The crux of the idea is to use the clinical data to identify a list of genes that correlate with the clinical variable of interest and then apply unsupervised clustering techniques to this subset of genes.

In summary, hierarchical clustering is a useful tool for visualizing large datasets and generating hypotheses about the relationship of markers and tumors. While it has been the cornerstone of DNA microarray analyses, in which the expression of thousands of genes is simultaneously evaluated in a small cohort of specimens, the procedure is gaining ground in tissue microarray studies, where the expression of a few genes are evaluated in hundreds to thousands of patients. A few groups have demonstrated the ability to immunoprofile cancer through hierarchical clustering of TMA data, including classification by binarized ER, HER2, COX-2, p53 and VEGF expression[239], analysis of breast cancer expression of neuroendocrine markers[240], the relationship between

differential protein expression and cytogenetic alteration patterns[241], and prognosis prediction[242, 243]. Unfortunately, most of these attempts have been made in breast carcinoma and none have been reported for melanoma.

Genetic Algorithms

First introduced by John Holland in 1975[244], Genetic algorithms (GA) are a novel tool for the investigation of combinatorial optimization problems. A number of books have been published in recent years that review the application of genetic algorithms to optimization problems.[245-247] Briefly, genetic algorithms represent a type of cooperative search method, in which a number of searches are run in parallel and information is exchanged between them. They are a class of algorithms that mimic some of the major characteristics of Darwinian evolution. That is, mutations, cross-overs and replication operating on strings, are ultimately subjected to some form of selection. Mutations can be thought of as operations within a single search trajectory, and cross-overs provide a means of information exchange between trajectories.

A general description of GAs follows. An initial population of trial solutions is established, represented by strings. Mutations are introduced independently into each string. After some number of mutations has been performed, new strings are created by cross-over operations. That is, two new population members are created by joining parts of two separate strings. The operation of creating new strings is repeated until a new population of accepted strings is established and then another phase of mutations is entered. Along the way, the new populations are subjected to a fitness function. Usually, only changes that increase fitness are accepted, though, in some cases, less-fit changes may be allowed.

Basic terminology of genetic algorithms, as applied to data in this dissertation, includes genes (algorithms) and chromosomes (solutions). In order to avoid confusion with the original meaning of these biologic terms, both terminologies will be used together.

X-tile Analysis

The ability to parse tumors into subsets based on biomarker expression has many clinical applications; however, there is no global way to visualize the best cut-points for creating such divisions. Robert Camp, in our laboratory, has developed a graphical method, the X-tile plot that illustrates the presence of substantial tumor subpopulations and shows the robustness of the relationship between a biomarker and outcome by construction of a two-dimensional projection of every possible subpopulation.[248]

In theory, associations between tumor biomarker expression and patient outcome should reveal the existence of biologically meaningful tumor classifications; however in practice, there is no universal method for discovering, assessing or displaying such associations. Consequently, studies generally group tumors into set divisions (e.g., quartiles, deciles), which fails to reflect the underlying biology of most markers. Microarray technology has magnified this problem by accelerating the discovery of tumor markers for which there is no known biological basis. In such cases, there is no foreknowledge about how (or whether) a marker parses a population into subsets.

X-tile plots provide a single, global assessment of every possible way of dividing a population into low-, medium-, and high-level marker expression. X-tile data are presented in a right triangular grid where each point represents a different cut-point. The intensity of the color of each cutoff point represents the strength of the association. The

X-tile software allows the user to move a cursor across the grid and provides an "on-the-fly" histogram of the resulting population subsets along with an associated Kaplan-Meier curve. This type of graphical representation can provide insight into the biological nature of a marker (e.g., does it show a linear distribution relative to survival, does it reveal distinct sub-populations, or does it manifest a U-shaped relationship to outcome). Because it is statistically invalid to test multiple divisions and accept the best P value, rigorous statistical evaluation is achieved by defining divisions in a "training set" and then validating them in a separate patient cohort ("validation set"). The X-tile software provides a method of dividing a single cohort into training and validation subsets for P value estimation when separate training and validation cohorts are not available. In addition, the software can perform standard Monte Carlo simulations (e.g., cross-validation) to produce corrected P values to assess statistical significance of data assessed by multiple cut-points.

In summary, X-tile plots present a new tool for (a) the assessment of biological relationships between a biomarker and outcome; and (b) the discovery of population cut-points based on marker expression. Clinically, the ability to effectively define such subpopulations is important for the development of novel therapeutics that may be effective for only a limited subset of tumors. Furthermore, this method may have value in other fields (materials testing, actuarial questions, etc.) where cut-point selection is complicated by time-dependent assessment of outcome.

Model Selection and Model Assessment

Statistical learning—the process of learning from data (i.e., creating a model for outcome prediction)—plays a key role in many areas of science, finance, and industry. In

its simplest form, a prediction model is used to predict an outcome measurement, which can be quantitative (e.g., a stock price) or categorical (e.g., alive or dead), based on a set of features (e.g., diet and clinical measurements). The first step involves a training set of data, in which feature measurements and outcome are observed for a set of objects (e.g., patients). Using this data, a prediction model, or learner, is developed, with the gaol of predicting the outcome for new unseen objects.

The generalization performance of a learning method relates to its prediction capability on independent test data. Assessment of this performance is critical, as it guides the choice of learning method or model, and provides a measure of the quality of the ultimately chosen model. There are, in fact, two separate goals at hand:

Model selection: estimating the performance of different models in order to choose the (approximate) best one.

Model assessment: having chosen a final model, estimating its prediction error (generalization error) on new data.

In a data-rich situation, the best approach for both goals is to randomly divide the dataset into three parts: a training set (typically 50%), a validation set (usually 25%), and a test set (also 25%). The *training set* is used to fit the models; the *validation set* is used to estimate prediction error for model selection; the *test set* is used for assessment of the generalization error of the final chosen model. In many cases, there is insufficient data to split into three parts. There is no 'standard' regarding how much training data is enough, but a major factor in this consideration is the signal-to-noise ratio of the underlying function, as well as the complexity of the models being fit to the data. There are a couple statistical methods available for approximation of the validation step either analytically

(e.g., Akaike or Bayesian information criterion, minimum description length, structural risk minimization) or by efficient sample re-use (e.g., cross-validation and bootstrapping). In addition to assisting in model selection, these methods are also helpful in estimating test error.[249]

Chapter 2: Subcellular Localization of Activating Transcription Factor 2 in Melanoma Specimens Predicts Patient Survival

Abstract

The transcription factor activating transcription factor 2 (ATF2) has been shown to be associated with melanocytic oncogenesis and melanoma tumor proliferation in preclinical models. The clinical significance of ATF2 expression is unknown. To determine the prognostic value of ATF2 in melanoma, we evaluated the pattern and level of ATF2 expression in a large cohort of melanoma specimens. Immunohistochemical staining was performed on a tissue microarray representing 544 patients with a mean follow-up time of 60 months. Expression was evaluated semiquantitatively and correlated with overall survival and other clinicopathological data. Strong cytoplasmic ATF2 expression was associated with primary specimens rather than metastases ($P < 0.0001$) and with better survival ($P = 0.0003$). Strong nuclear ATF2 expression was associated with metastatic specimens ($P < 0.0001$) and with poor survival ($P = 0.0008$). Patients who had both weak cytoplasmic and strong nuclear ATF2 staining had the worst outcome, both among the full cohort of patients ($P < 0.0001$) and among the patients with localized disease ($n = 269$; $P < 0.0001$). On multivariate analysis of the primary cutaneous specimens, weak cytoplasmic staining and strong nuclear staining was an independent predictor of poor outcome, as was Clark level. Nuclear ATF2 is likely to be transcriptionally active, whereas cytoplasmic ATF2 probably represents an inactive form. These findings support other preclinical findings in which transcriptionally active ATF2 is involved in tumor progression-proliferation in melanoma. Moreover, our findings suggest that ATF2 might be a useful prognostic marker in early-stage melanoma.

Introduction

The only clinically reliable markers used to predict outcome in malignant melanoma are Breslow depth, Clark level of invasion, presence of ulceration and lymph node involvement.[19] These parameters form the basis of the new American Joint Committee on Cancer Staging System. However, within each stage there is significant variability in outcome, and while the staging is helpful in determining prognosis and therapy at the time of diagnosis, more accurate measures based on tumor biology are needed.[19] Better predictors of poor outcome in resected melanoma could enhance our ability to appropriately select patients in need of adjuvant therapy.

Numerous tissue and serological markers have been studied, as reviewed by Li *et al.*[250] Among them, a number of transcription factors, including Activating Transcription Factor 2 (ATF2), have been shown to be associated with tumor growth and metastasis[251, 252] in cell culture and animal models, but their prognostic role in melanoma has not been determined. ATF2 is among the primary transcription factors regulated by p38, MAP Kinase and JNK signaling pathways.[253, 254] Phosphorylation of ATF2 by these kinases is central in determining its stability[255] and transcriptional activity, which is dependent upon its heterodimerization with other members of the bZIP family, c-Jun, CREB, NFkB and retinoblastoma (Rb).[253, 256-258] ATF2 plays an important role in acquisition of resistance of melanoma cells to chemotherapeutic drugs and radiation.[259-261] Inhibition of ATF2 activity efficiently inhibits melanoma growth, ability to metastasize, and sensitizes melanoma to a range of chemotherapeutic agents and radiation.[262, 263]

In this study, we sought to evaluate the prognostic role of ATF2 by studying the pattern and levels of ATF2 expression using a large cohort melanoma tissue microarray, and associating expression with clinical and pathologic data.

Materials and Methods

Tissue Microarray Construction:

The tissue microarray was constructed as previously described.[150] A total of 570 tissue cores (553 melanomas with duplicate spots for 9 patients, 17 normal skin) measuring 0.6 mm were spaced 0.8 mm apart on a single glass slide. The cohort was constructed from paraffin-embedded formalin-fixed tissue blocks obtained from the Yale University Department of Pathology archives. The specimens were resected between 1959 and 1994, with a follow-up range between 2 months and 38 years with a median follow-up time of 60 months. Treatment information was not available for the entire cohort. Some of the stage III patients were treated with interferon based therapy, and the stage IV patients were treated with a range of therapies including chemotherapy, biological therapy, vaccine therapy and supportive care. Slides from all blocks were reviewed by a pathologist to select representative areas of invasive tumor to be cored. The cores were placed on the tissue microarray using a Tissue Micorarrayer (Beecher Instruments, Silver Spring, MD). The tissue microarrays were then cut to 5 μm sections and placed on glass slides using an adhesive tape-transfer system (Instumedics, Inc., Hackensack, NJ) with UV cross-linking.

Immunohistochemistry:

The tissue microarray slide was deparaffinized by rinsing with xylene, followed by two changes of 100% ethanol and two changes of 95% ethanol. The slides were then

boiled in a pressure cooker containing 1 mM EDTA (pH 7.5) for antigen retrieval. Endogenous peroxidase activity was blocked with 2.5% methanol in hydrogen peroxide for 30 minutes at room temperature. After washing with Tris Buffered Saline, the slides were incubated at room temperature for 30 minutes in 0.3% BSA[1]/1X TBS[2] to reduce non-specific background staining. The primary antibody, rabbit polyclonal anti-ATF2 IgG (Santa Cruz Biotechnology, Inc., Santa Cruz, CA) was then added at a dilution of 1:50, and the slides were incubated overnight at 4°C in a wet chamber, and then rinsed three times in 1X TBS/0.05% Tween-20. Biotinylated goat anti-rabbit IgG (Vector Laboratories, Burlingame, CA) was added for 1 hour, and the slides were washed in TBS-Tween as above, incubated for with VECTASTAIN® ABC-AP Reagent (Vector Laboratories, Burlingame, CA) for 1 hour, washed again in TBS-Tween as above and incubated for 30 minutes with an alkaline phosphatase substrate solution (Vector Laboratories). The slides were then rinsed in water, counterstained with hematoxylin and mounted with Immunomount (Shandon, Pittsburgh, PA).

Evaluation of the Immunohistochemical Staining:

The regions of most intense staining were scored by eye for each spot. Cytoplasmic and nuclear staining of the melanoma cells were scored separately. Because of the small size of the histospot (0.6 mm in diameter), no area variable was included in the scoring. The staining was graded using the following scale: 0 - no staining; 1 - weak staining; 2 - moderate staining; 3 - intense staining. Specimens with no invasive melanoma, or specimens that were not interpretable were excluded from the analysis. The tissue microarray was scored separately by two independent observers (A.B. and

[1] Bovine Serum Albumin
[2] Tris Buffered Saline

H.K.), with a very high correlation between scorers ($P<0.0001$). A consensus score was determined for spots with discrepant scoring between the observers.

Statistical Analysis:

JMP 5.0.1 and Statview 5.0.1 (SAS Institute Inc., Cary, NC) software were used for data analyses. The correlation between the consensus score and the relationship of ATF2 expression and clinicopathological parameters were done using the Chi Square test. The prognostic significance of the parameters was assessed for predictive value using the Cox proportional hazards model with overall survival as an end point. Survival curves were calculated using the Kaplan-Meier method, with significance evaluated using the Mantel-Cox long-rank test.

Results

Immunohistochemical Staining of Melanoma Tissue Microarrays

Of the 553 melanoma tumors on the tissue microarrays, 479 (87%) were interpretable for cytoplasmic and nuclear ATF2 staining. Spots that were deemed uninterpretable had insufficient tumor cells in the spot, loss of tissue in the spot or an abundance of necrotic tissue. Of the 479 interpretable specimens, 400 (84%) also had associated survival information. Figure 12 demonstrates histospots representative of scores 3+ for cytoplasmic and for nuclear staining. The cases included 269 primary cutaneous melanoma specimens, 20 local recurrences, 18 melanomas originating in mucous membranes (vulva, anus, nasal mucosa and rectal), 118 lymph node metastases, 68 cutaneous metastases and 51 distant metastases. The site was not known for 4 of the patients. There was a strong correlation between nuclear ATF2 expression and lymph node or metatstatic sites (chi squared test $P<0.0001$), while cytoplasmic ATF2 expression correlated with primary lesions ($P<0.0001$).

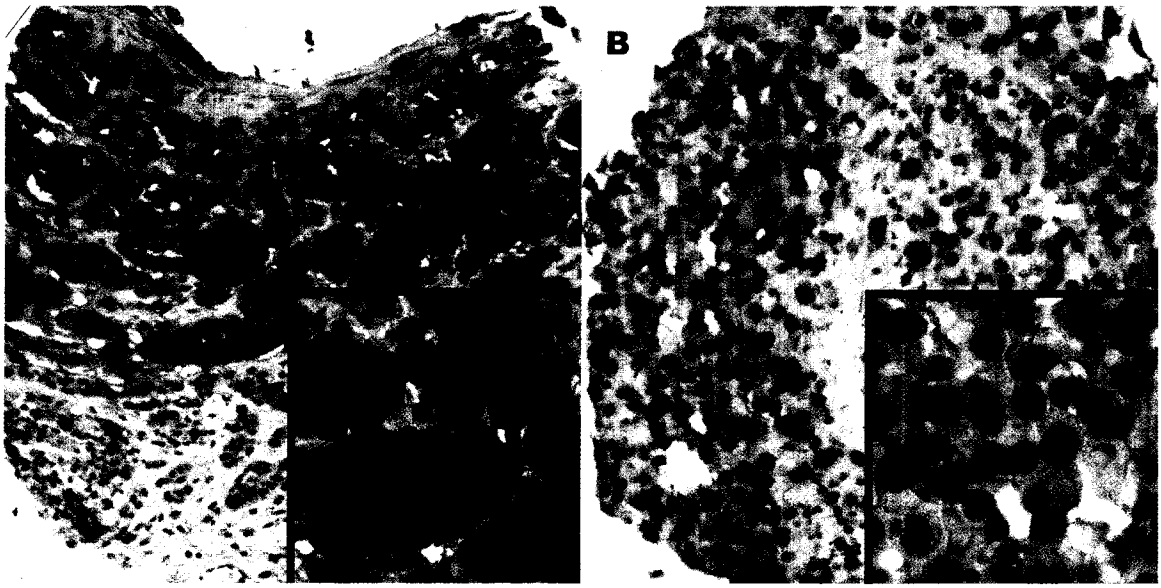

Figure 12. Immunohistochemical staining on representative histospots showing strong cytoplasmic ATF2 staining (A) and strong nuclear ATF2 staining (B). The Figures are at 10X magnification, and the insets at 60X magnification.

Survival Analysis

The cytoplasmic and nuclear ATF2 expression levels were each evaluated for association with overall survival. Kaplan Meier survival curves generated for cytoplasmic and nuclear ATF2 were split by ordinal score, as shown in Figure 13. These curves show that increased cytoplasmic expression was correlated with better outcome (P=0.0005). Conversely, increased nuclear ATF2 staining was associated with worse outcome (P=0.0013). Although these data are only semi-quantitative, the curves suggest a splitting of the data to define scores of 0 and 1 as "low" or "negative" expression and 2 and 3 as "high" or "positive" for both nuclear and cytoplasmic staining. The curves for scores of 0 and 1 overlap each other, likely secondary to the difficulty in determining the difference between absent or very weak staining by eye, particularly for weak or absent nuclear staining in the presence of strong cytoplasmic staining and vice versa. Therefore

the designations of "high" or "low" expression are used for the remainder of the analyses. This result is shown in a Kaplan Meier plot in Figure 13.

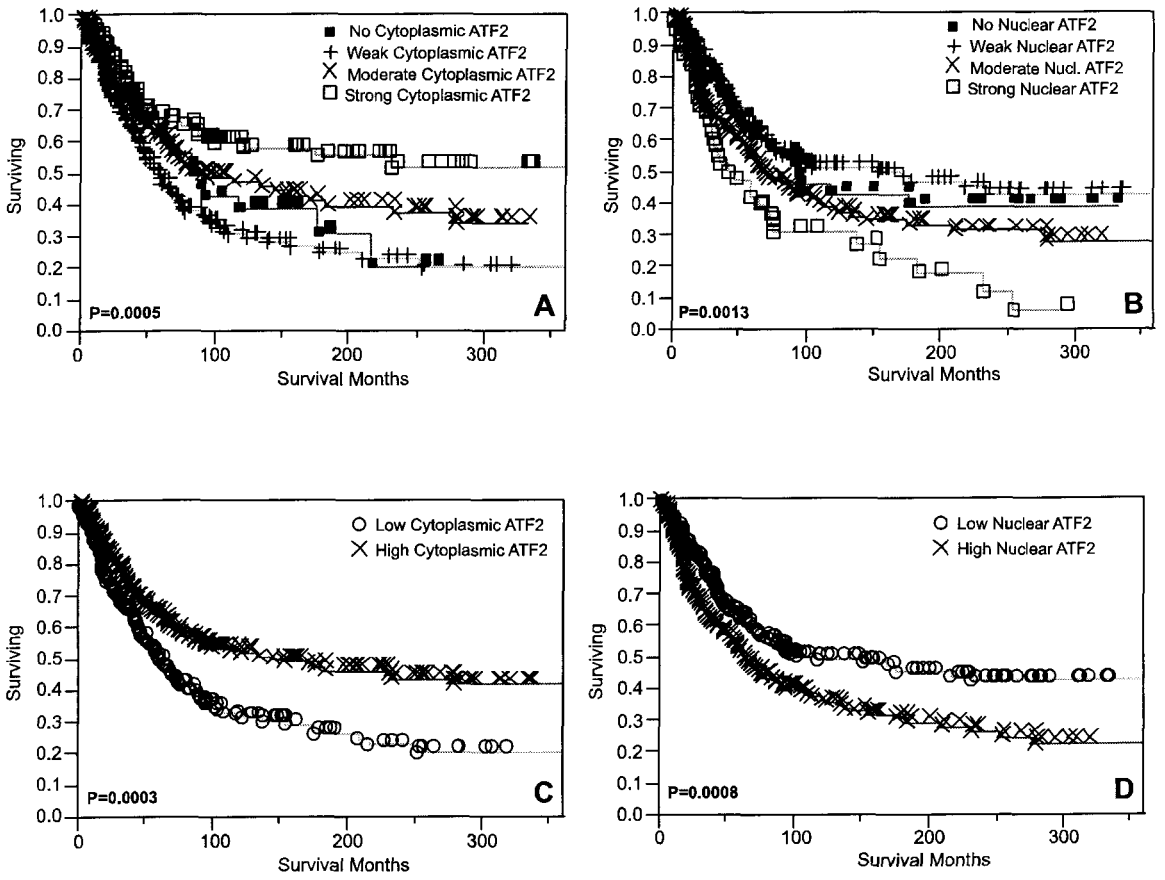

Figure 13. Kaplan-Meier survival curves for ATF2 staining for the entire cohort of patients over a 30 year period, with time given in months: (A) The four intensities of ATF2 cytoplasmic staining (0,1,2,3) (B) The four intensities of ATF2 nuclear staining (0,1,2,3) (C) High and low cytoplasmic staining for ATF2 (D) High and low nuclear staining for ATF2.

There were a relatively large number of patients that had high cytoplasmic ATF2 expression with low nuclear expression and vice versa. Therefore to further stratify the patients, they were divided into three risk groups: 1) high cytoplasmic expression, low nuclear expression, 2) low cytoplasmic expression and high nuclear expression and 3) high cytoplasmic and nuclear expression or low cytoplasmic and nuclear expression. The

Kaplan Meier survival curves for these three groups of patients are shown in Figure 14(A).

For clinicians treating melanoma patients, perhaps the greatest need for determining prognosis occurs at initial presentation, when patients have a biopsy performed on a changing skin lesion. Therefore, further survival analysis was performed using the primary skin lesions only. When dividing the primary skin lesions into the three ATF2 prognostic groups mentioned above, patients with high cytoplasmic, low nuclear ATF2 expression did better than those with low cytoplasmic, high nuclear expression, and the group with low cytoplasmic, low nuclear or high cytoplasmic, high nuclear expression demonstrated intermediate overall survival ($P<0.0001$), as can be seen in Figure 14(B).

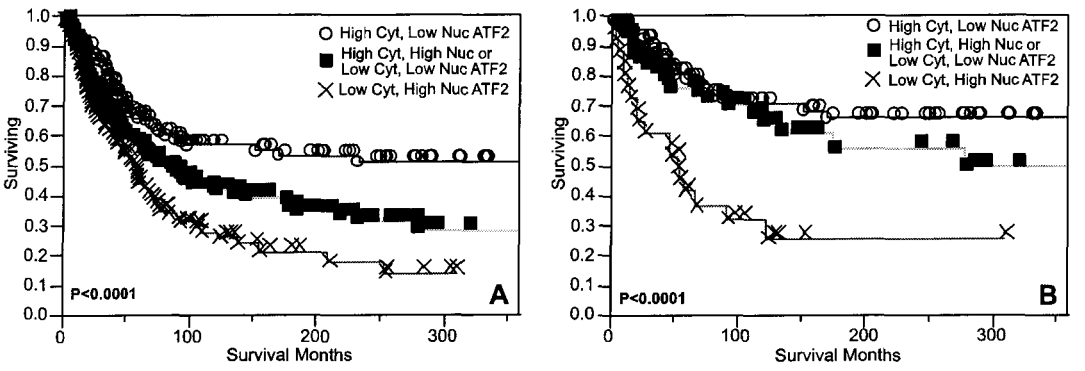

Figure 14. Kaplan Meier survival curves for 3 risk groups of patients: low risk patients (high cytoplasmic and low nuclear ATF2 expression), intermediate risk patients (high cytoplasmic and high nuclear or low cytoplasmic and low nuclear ATF2 expression) and high risk patients (low cytoplasmic and high nuclear ATF2 expression) as shown in the figure legend. Curves include (A) all patients and (B) primary cutaneous lesions only.

Univariate analysis was performed using the Mantel Cox test. High cytoplasmic ATF2 expression was associated with good overall survival; hazard ratio=0.618 (95%

C.I.[3] 0.474-0.806, P=0.0003). High nuclear ATF2 expression was associated with poor overall survival; hazard ratio=1.25 (95% C.I. 1.1-1.4, P=0.0009), and the combination of low cytoplasmic ATF2 and high nuclear ATF2 was associated with worse survival, hazard ratio 1.33 (95% C.I. 1.15-1.53, P<0.0001). The pattern of ATF2 expression for primary and regional/metastatic disease and its association with survival is shown in Table 8. The ATF2 expression pattern was only predictive of survival among the primary specimens, and not the regional/metastatic specimens.

[3] Confidence Interval

Table 8. Univariate analysis of ATF2 expression by tumor site and subcellular localization.

Location of Lesion	Cytoplasmic ATF2	Count	Median Survival Months (Range)	Hazard ratio (95% confidence interval)	P value
Primary Lesions	Low	70	47 (1-463)	0.66 (0.52-0.85)	0.001
	High	157	97 (0-444)		
Metastatic lesions	Low	138	47 (1-305)	1.02 (0.86-1.2)	0.80
	High	93	39 (1-415)		

Location of Lesion	Nuclear ATF2	Count	Median Survival Months (Range)	Hazard ratio (95% confidence interval)	P value
Primary Lesions	Low	153	83 (0-463)	1.37 (1.08-1.74)	0.011
	High	74	77 (1-377)		
Metastatic lesions	Low	98	44 (4-415)	1.03 (0.88-1.23)	0.70
	High	133	42 (1-387)		

Location of Lesion	ATF2 Risk	Count	Median Survival Months (Range)	Hazard ratio (95% confidence interval)	P value
Primary Lesions	Low	111	93 (0-444)		0.0004
	Intermediate	88	77 (1-463)	0.81 (0.57-1.13)	
	High	28	52 (1-309)	2.14 (1.46-3.04)	
Metastatic lesions	Low	38	41 (6-415)		0.64
	Intermediate	115	46 (1-387)	0.90 (0.71-1.13)	
	High	78	43 (1-305)	1.04 (0.81-1.33)	

Clinicopathological Correlations and Multivariate Analyses

Using the Cox Proportional Hazards Model, we performed multivariate analyses to assess the independent predictive value of ATF2 expression among the primary cutaneous lesions. We included the following prognostic variables for melanoma,; Breslow depth, Clark level, ulceration, microscopic satellites and tumor infiltrating lymphocytes at diagnosis. We used a combined cytoplasmic and nuclear ATF2 risk grouping with low cytoplasmic and high nuclear ATF2 staining presenting the highest risk group. Our high risk ATF2 pattern remained an independent prognostic indicator in primary lesions, as did Clark level. Results of the multivariate analysis are shown in Table 9.

Table 9. Multivariate Analysis of ATF2 Expression Pattern and Other Histopathological Variables among Primary Lesions

Variable	Hazard Ratio (95% confidence interval)	Likelihood-Ratio χ^2	P value
Clark Level (I-III vs. IV-V)	1.67 (1.17-2.47)	8.25	0.0041
Breslow (≤1mm vs. >1mm)	1.28 (0.80-2.07)	1.08	0.30
TILs (present vs. absent)	1.13 (0.83-1.51)	0.63	0.43
Ulceration (present vs. absent)	0.83 (0.63-1.10)	1.73	0.19
Microscopic Satellites (present vs. absent)	0.75 (0.57-1.01)	5.00	0.025
ATF2 Risk (high vs. intermediate+low)	1.81 (1.34-2.40)	13.6	0.0002

Correlation between clinicopathological variables and the ATF2 risk pattern was further examined. The high risk ATF2 pattern was most strongly associated with thick lesions ($P < 0.0001$), and had a weaker association with Clark level ($P = 0.01$). There was

no significant association between the pattern of ATF2 expression and the site of primary lesion, age or gender.

Discussion

Numerous preclinical studies have shown that ATF2 contributes to melanoma growth and metastasis, tumor cell survival and resistance to chemotherapy and radiation. Here we demonstrate, for the first time, that the ATF2 expression pattern is associated with patient survival.

Our data show that strong nuclear ATF2 expression was more frequent in metastatic sites (lymph nodes, bone metastases or visceral metastases) than in primary cutaneous specimens ($P<0.0001$). Furthermore, our data show that nuclear ATF2 expression is a strong predictor of poor survival and that cytoplasmic ATF2 expression is a strong predictor of good outcome in melanoma patients. Among the primary cutaneous specimens, patients that had weak cytoplasmic and strong nuclear staining had poor survival ($P<0.0001$), and vice versa for strong cytoplasmic and weak nuclear staining. The expression pattern of ATF2 retained independent prognostic value on multivariate analysis, as did Clark level. Breslow depth was predictive of outcome on univariate analysis. However, when evaluated in multivariate analyses with ATF2, it was not an independent predictor of survival. This is likely due to the correlation between Breslow depth and ATF2 expression.

Our data suggest that subcellular ATF2 localization might be a very useful prognostic marker in primary cutaneous melanoma, and might affect decisions regarding patient management, such as the appropriateness of staging evaluation and adjuvant therapy for patients with early stage melanoma.

ATF2 has been primarily implicated as a transcription factor which heterodimerizes with c-Jun and mediates transcriptional activities by Jun responsive elements.[253, 264] ATF2 is among early response genes that are activated following stress and DNA damage, depending on its phosphorylation by upstream kinases, including JNK and p38. ATF2 has been identified as one of the primary transcription factors that bind to Jun2-like elements in human melanoma cells.[259] Earlier studies that elucidated the possible role of ATF2 in human melanoma have established it plays an important role in the acquisition of resistance to chemotherapy and radiation therapy.[259-261] ATF2 alters melanoma susceptibility to undergo apoptosis, in part, due to its ability to alter the balance between TNF and Fas signaling.[261] Inhibition of ATF2 activities, either by co-expression with its dominant negative forms or via short peptides that out-compete the endogenous protein, was found to be an efficient mechanism for sensitizing human and mouse melanoma cells to radiation-induced apoptosis. Furthermore, expression of a small peptide that abolishes ATF2 transcriptional activities inhibited melanoma growth in several mouse tumor models.[262, 263] Collectively, these studies suggest a critical role for ATF2 in melanoma progression and resistance to therapy.

The current findings are compatible with the preclinical data and provide insight into the importance of this transcription factor in the development of melanoma. Of particular interest is the finding that nuclear localization of ATF2 correlates with poor prognosis. As a transcription factor, ATF2 is active within the nuclear compartment, where it elicits its transcriptional activities. Strong nuclear staining of ATF2 therefore suggests that ATF2 is constitutively active in these tumors. These findings are consistent

with the notion that it is necessary to inhibit ATF2 activities in order to sensitize these tumors to treatment.

ATF2 phosphorylation is a prerequisite for its stability and transcriptional activities.[255, 258] ATF2 kinases are often active in melanoma cells[265], thereby enabling its constitutive phosphorylation and activity. Interestingly, ERK has been shown to be capable of phosphorylating ATF2 on the same residues as Jnk[263], thereby establishing a possible link between B-RAF, which is constitutively active in a large percentage of human melanoma tumors[266], and the activation of ATF2. Nevertheless, the possible existence of another kinase which may be activated in the course of melanoma progression, and which would trigger the nuclear localization of ATF2, cannot be excluded.

In summary, our data suggest that the level and localization of ATF2 expression may be clinically useful for assessing prognosis, particularly in primary cutaneous melanoma specimens, warranting prospective confirmation. Furthermore, our findings suggest that ATF2 might be a useful target for new drug development.

Chapter 3: Automated Quantitative Analysis (AQUA) of HDM2 Expression in Malignant Melanoma Shows Association with Early Stage Disease and Improved Outcome

Abstract

The incidence of cutaneous malignant melanoma continues to increase every year, and this disease remains the leading cause of skin cancer death in industrialized countries. In spite of the aggressive nature of advanced melanoma, there are no standard biological assays in clinical usage that can predict metastasis. This may be due, in part, to the inadequacy of reproducible assessment of protein expression using traditional immunohistochemistry. We have previously described a novel method of quantitative assessment of protein expression (AQUA) with the continuity and accuracy of an ELISA assay but with maintenance of critical spatial information. Here, we modify this technology for the evaluation of protein expression in melanoma. Using a tissue microarray cohort of 405 melanoma lesions and 17 normal skin samples, we analyzed expression of HDM2, the human homolog of MDM2 (murine double minute 2) with AQUA. We show that expression levels in the nucleus are significantly higher in primary melanomas than in metastatic lesions. Furthermore, high levels of expression are predictive of better outcome. This study demonstrates that quantitative assessment of protein expression is useful in melanoma to validate potential tissue biomarkers, and suggests that HDM2 may be a valuable prognostic tool for management of malignant melanoma.

Introduction

Malignant melanoma is currently the malignancy with the most rapid increase in incidence in the United States.[1, 267] The fifth most common cancer[2], melanoma is the most common fatal malignancy among young adults[3] with 53,600 new cases diagnosed in 2002[268]. Current estimates predict that 1 in 71 individuals will develop melanoma during their lifetime, up from an initial estimate of 1 in 600 in 1960 and 1 in 150 in 1985.[1]

A number of clinical and pathologic factors have been described as markers of prognosis in cutaneous malignant melanoma, however, there are currently no routinely used, broadly accepted molecular, or immunohistochemical markers to define subsets of this neoplasm[15] or predict outcome. The current methods of prognosis in cutaneous melanoma have not changed much since the 1970s when Breslow[28] and Clark[29] first published reports indicating the importance of dermal invasion in prognosis. The models of Breslow and Clark remain the most powerful and reliable predictors of survival in primary melanoma[42], in spite of the molecular "revolution" of the past 30 years.

To develop a better understanding of melanoma biology and development, as well as discover molecular markers of potential benefit in melanoma prognosis, a number of studies have evaluated immunohistochemical (IHC) markers on an individual basis and in numerous relatively small cohorts. Very few, however, have been performed on melanoma tissue microarrays[269, 270] and none have made use of quantitative analysis. Differences in expression levels in the tissues have been limited to those that are easily detectable by the human eye. The current IHC technology is susceptible to high levels of inter- and intra-observer variability and fraught with variability as a function of the lack of standardization of antibody-based techniques.[218]

Tissue microarrays provide a highly efficient and economical way to evaluate hundreds of tumors on a single slide.[149] The use of tissue microarray (TMA) technology eliminates the slide-to-slide variability inherent to IHC as all tissues are present on the same slide and are exposed to the same experimental conditions. The use of archival tissues allows for a retrospective study with the benefit of long-term patient follow-up. In addition to improving our understanding of key molecular events in cancer progression, TMAs provide an excellent mechanism for the discovery of outcome predictor models, particularly when coupled with quantitative analysis.

We have developed a system for compartmentalized, automated quantitative analysis of histological sections (AQUA).[271] AQUA provides highly reproducible analysis of target signal expression in tissues on a continuous scale, while preserving spatial information, particularly subcellular localization. Quantitative analysis enables precise discrimination of expression levels in tissues, providing measurements on a continuous scale not previously attainable by traditional, or manual, scoring methods. The use of this technology was originally described in colon cancer[271], and has since been applied to breast[272] and prostate[273] carcinoma. Briefly, the system identifies and tags tumor tissue within each histospot, based on the expression of tissue specific proteins, such as cytokeratin in carcinomas, and then evaluates the expression level of a target antigen within the 'tumor mask' and inside user-defined subcellular compartments. For this study, the AQUA system was modified to accommodate melanoma by substituting S100 protein for cytokeratin (Figure 15). A review of the pertinent literature demonstrated that S100 is expressed in 97.4% of all melanomas[274], and some investigators suggest this number may exceed 98%[275]. Here, we validate the technology

by assessing the expression of HDM2 (human homologue of 'murine double minute 2') and demonstrate its utility in evaluating a prognostic marker in a large retrospective cohort.

HDM2 is a transcriptional target of the tumor suppressor protein p53, that, in turn, marks p53 for degradation.[276-278] It is predicted that disruption of this negative feedback loop, through either p53 mutation or overexpression of HDM2, would be a negative prognostic marker for cancer progression. The association between HDM2 and clinical outcome has been investigated intensively in a number of cancers[279] with the anticipation of using HDM2 as a clinical prognostic marker. However, only a handful of studies have evaluated HDM2 expression in melanoma.[269, 280, 281] In the largest study, Polsky *et al.* demonstrated that over-expression of HDM2 in a cohort of 134 melanoma patients unexpectedly correlated with improved clinical outcome, having a statistically significant association with longer disease free- and overall survival.[109] The quantitative assay we describe in the work confirms and extends these observations.

Materials and Methods

Tissue Microarray Construction:

The tissue microarray was constructed as previously described.[150, 282] A total of 570 tissue cores representing 542 total melanoma cases and a small series of controls measuring 0.6 mm were spaced 0.8 mm apart on a single glass slide. The cohort was constructed from formalin-fixed paraffin-embedded tissue blocks obtained from the archives of the Department of Pathology at Yale University School of Medicine. A pathologist examined each case to select the region for inclusion in the TMA. Core-biopsies from the specimens were placed on the tissue microarray using a Tissue Micorarrayer (Beecher Instruments, Sun Prairie, WI). The tissue microarrays were then cut to 5-μm sections and placed on glass slides using the adhesive tape transfer system (Instumedics, Inc., Hackensack, NJ) with UV cross-linking. The specimens were all drawn from archives of tumors resected between 1959 and 1994, with a follow-up range of 2 months and 38 years (median follow-up time, 60 months). The cohort characteristics are demonstrated in Table 1. For the primary cutaneous lesions (269), a single reviewer measured Breslow depth, Clark level, microscopic satellites, tumor infiltrating lymphocytes, and the presence of ulceration. Treatment information was not available for the entire cohort. Some of the stage III patients were treated with Interferon-based therapy, and the stage IV patients were treated with a range of therapies including chemotherapy, biological therapy, vaccine therapy, and supportive care.

Immunohistochemistry:

The tissue microarray slide was stained as described previously.[271] In brief, the slides were deparaffinized by rinsing with xylene, followed by two changes of 100%

ethanol and two changes of 95% ethanol. Antigen retrieval was performed in a pressure cooker containing 1 mM EDTA (pH 7.5), and endogenous peroxidase activity was blocked with 2.5% hydrogen peroxide in methanol for 30 min at room temperature. The slide was washed with TBS, incubated in 0.3% BSA/1X TBS for 30 min at room temperature to reduce nonspecific background, and then stained with the a combination of anti-MDM2 mouse mAb 1B10 (1:100, Novocastra, Ltd., Newcastle upon Tyne, UK) plus anti-S100 rabbit polyclonal (1:6,000, DAKO Corporation, Carpinteria, CA) diluted in BSA/TBS, at 4°C overnight. The 1B10 mAb was chosen because it was validated by numerous studies in which HDM2 expression was assessed in tumors relative to normal tissues.[283-285] The secondary antibodies Alexa 488-conjugated goat anti-rabbit (1:100, Molecular Probes, Eugene, OR) plus Envision anti-mouse (neat, DAKO) diluted in BSA/TBS were applied for 1 hour at room temperature. DAPI (4, 6-Diamidino-2-phenylindole) was included with the secondary antibodies to visualize nuclei. The slide was washed with BSA/TBS (3X for 5 min), and then incubated with Cy5-tyramide (Perkin Elmer Life Science Products, Boston, MA), activated by HRP resulting in the deposition of numerous covalently associated Cy5 dyes immediately adjacent to the HRP-conjugated secondary antibody. Cy5 was used because its emission peak (red) is well outside of the green-orange spectrum of tissue autofluorescence. The slides were sealed with cover-slips with an antifade-containing mounting medium (with 0.6% n-propyl gallate)

Automated Image Acquisition and Analysis:

The AQUA automated image acquisition and analysis was performed as described.[271] Briefly, images of the TMA were captured through an Olympus BX51

microscope with automated *x*, *y*, *z* stage movement using an Olympus Motorized Reflected Fluorescence System and software (IP lab v3.54, Scanalytics, Inc.), equipped with Cooke Sensicam QE High Performance camera. Low power images of the microarray were stitched together using multiple low-resolution images of the microarray (64 x 64 pixel) at approximately 7-micron resolution. Histospots were identified employing the signal from DAPI and/or S100 tags. Rows and columns of the histospots were then identified, missing histospots filled in, allowing each histospot to be identified by its coordinates, and recorded based on its position in the grid. Subsequently, monochromatic, high-resolution (1024 x 1024 pixel, 0.5-micron resolution) images were obtained of each histospot, both in the plane of focus, and 8 microns below it, recorded in an image stack as bitmaps. A resolution of 0.5 microns is suitable for distinguishing between large subcellular compartments such as the cell membrane/cytoplasm and nuclei. Images were obtained using a pixel intensity dynamic range of 0–1024.

A visual demonstration of the AQUA analysis process is depicted in Figure 15. For each histospot, areas of tumor are distinguished from stromal elements by creating a *tumor mask* from the S100 protein signal, visualized under the Alexa 488 fluorophore. The tumor mask is determined by 'gating' the pixels in this image, in which an intensity threshold is set by visual inspection of histospots (ranging from lowest to highest intensity), and each pixel is recorded as "on" (tumor) or "off" (non-tumor) based on the threshold. In addition, small objects (< 50 pixels) are removed and small holes filled. The DAPI image, used to identify the nuclei, is subjected to RESA (rapid exponential subtraction algorithm), which improves signal-to-noise ratio by subtracting the out-of-focus image from the in-focus image, in order to clearly define the *nuclear*

compartment.[271] Removal of the pixels assigned to the nuclear compartment from the tumor mask provides a designation of the *cytoplasmic compartment.* After application of RESA, the signal intensity of the target antigen, acquired under the Cy5 signal (HDM2), is scored on a scale of 0-1024, and the AQUA score within the sub-cellular compartments (i.e., nucleus, cytoplasm) is calculated by dividing signal intensity by the area of the specified compartment. This score has three significant figures and is directly proportional to the number of molecules per unit area.

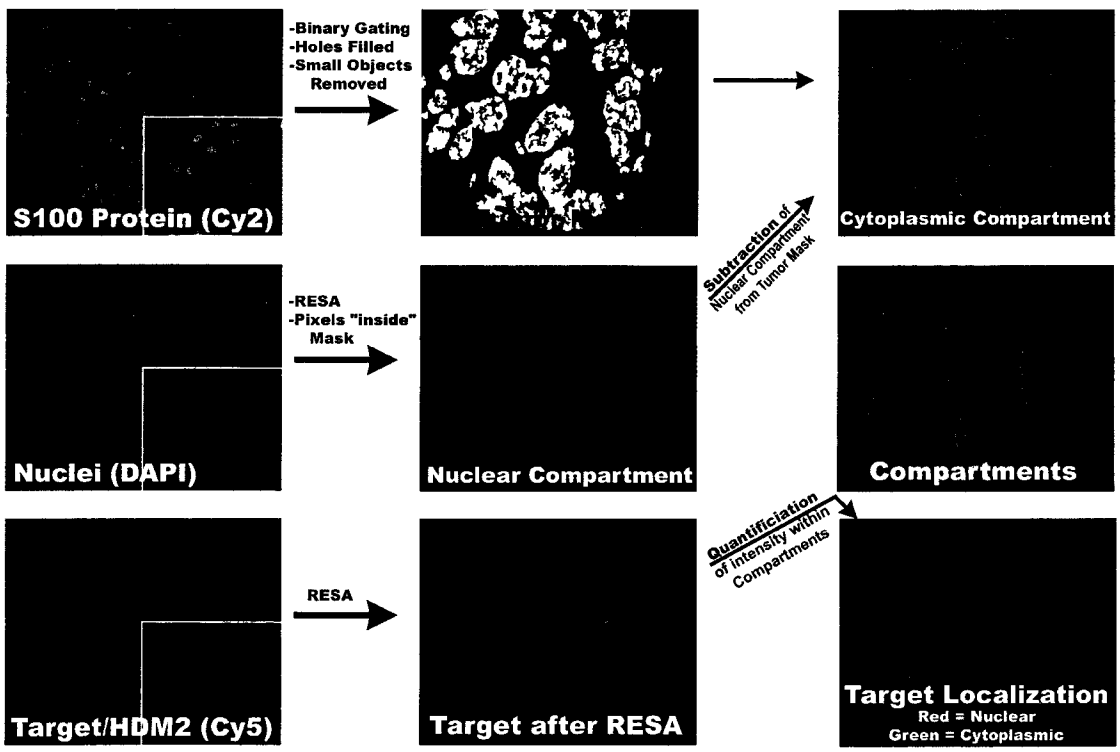

Figure 15. Schematic demonstration of AQUA protocol applied to melanoma. Images on the left are raw. Images on the right have been generated by AQUA. The top horizontal set of panels demonstrates tumor mask in a melanoma histospot, based on S100 protein expression (Alexa 488), distinguishing tumor cells from stroma. The S100 image is gated to form a binary mask. This binary image is enhanced by filling holes and removing small objects. DAPI is used to tag the nuclei, and after application of RESA (Rapid Exponential Subtraction Algorithm) and identification of only those pixels within the tumor mask, this image designates the nuclear compartment. After application of RESA to the Alexa 488 image, the nuclear compartment is subtracted from the tumor mask to provide a designation of the cytoplasmic compartment. An image of the target-specific marker, HDM2, is taken (Cy5), and after exponential subtraction using RESA, the intensity of the marker is divided into the subcellular compartments by pixel-based locale assignment for compartmentalization of expression (PLACE algorithm). An AQUA score (intensity/area) is generated for the target within the subcellular compartments. This information is graphically represented by the target localization image.

Data Analysis:

Histospots containing <10% tumor as assessed by *mask area* were excluded from further analysis. Previous studies have demonstrated that the staining from a single histospot provides sufficient representative sample to judge outcomes.[286, 287] In the case of HDM2, staining was always nuclear; analyses using the nuclear-specific AQUA score of HDM2 yielded parallel results to analyses using the total AQUA score. Univariate survival analyses were assessed using the Kaplan-Meier method for nominal variables and the Cox regression method for continuous variables. Multivariate analyses were performed with the Cox proportional hazards model. Mantel-Cox log-rank score was used to assess statistical significance. Analyses were performed with JMP 5.0.1 (SAS Institute Inc., Cary, NC). Patients were deemed uncensored if they died of melanoma within 30 years of their initial date of diagnosis.

Results and Discussion

Validation of Microarray Cohort:

We sought to validate our tissue microarray cohort of 542 melanomas using several traditional histopathological markers of malignancy. As described previously[282] and demonstrated in Table 10, unique patient-specific cases on the TMA include 287 primary specimens, 233 metastatic specimens, and 20 local recurrences. Using univariate analysis of long-term disease-related survival, primary versus metastatic status predicted improved survival ($p<0.0001$). (Figure 16A) For the primary cutaneous specimens, we found that tumor depth (Breslow and Clark) ($p<0.0001$), ulceration status ($p=0.0028$),

microscopic satellitosis ($p<0.0001$), tumor infiltrating lymphocytes (TILs) ($p=0.0007$), and histologic subtype were all significant predictors of survival (Figure 16B-F).

Table 10. Tissue Microarray Characteristics

Primary Lesions (287)	269 Cutaneous 18 Mucosal
Metastatic Lesions (233)	118 Lymph Node 65 Cutaneous & Subcutaneous 11 Lung 8 Bone 2 Brain 26 Other Distant 3 Unknown
Local Recurrences (20)	
Unknown (2)	

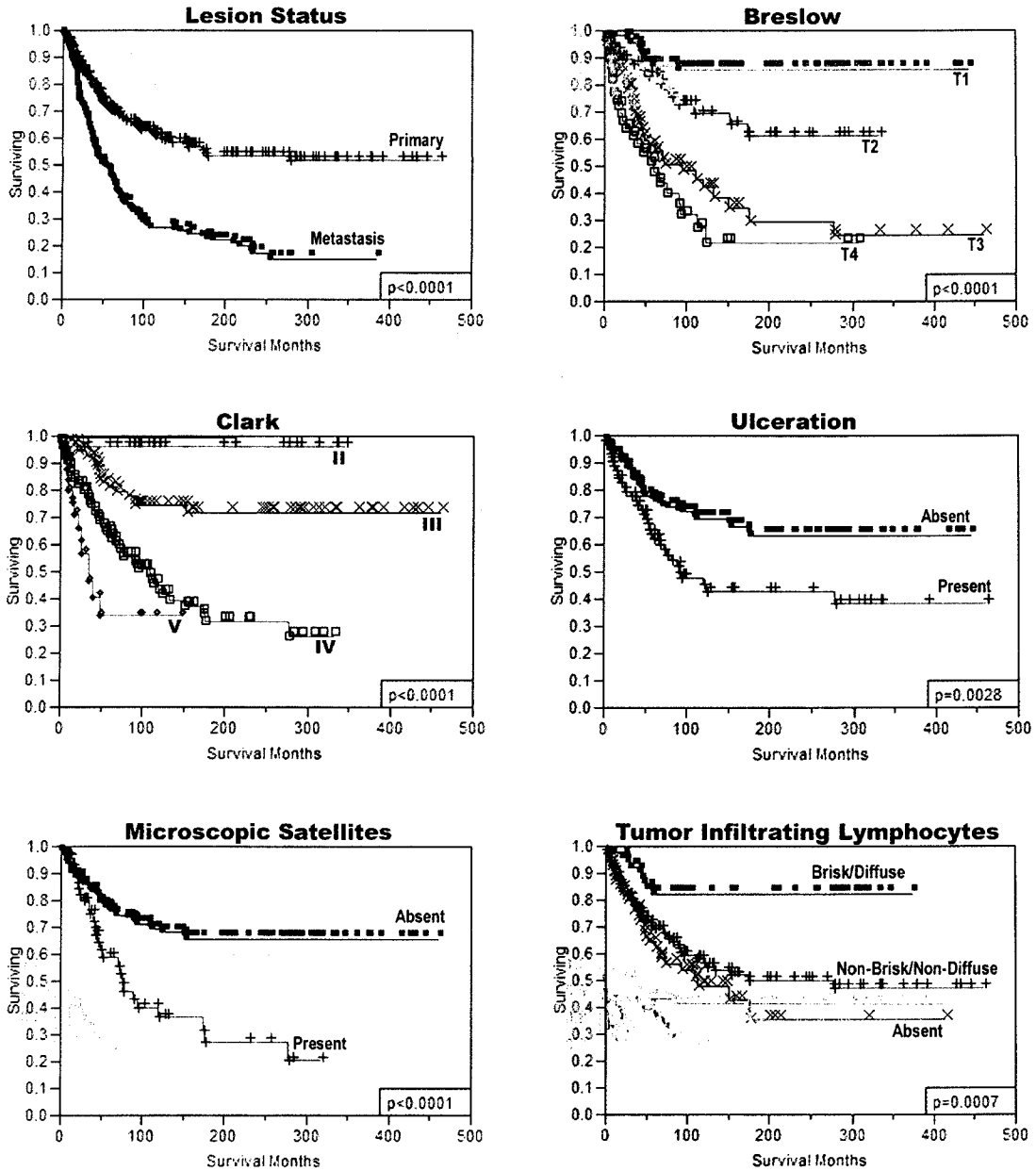

Figure 16. Melanoma TMA characteristics. Kaplan-Meier survival curves demonstrating disease-specific survival based on lesion location (i.e., primary versus metastatic), as well as the role of standard histopathological criteria on survival in this cohort, which includes Breslow depth (T1-T4), Clark levels (II-V), the presence or absence of ulceration, the presence or absence of microscopic satellites and presence of infiltrating lymphocytes.

Automated Analysis of HDM2 Expression in Melanoma:

After image acquisition for each histospot, AQUA was performed to establish the intensity of HDM2 expression per unit area within each histospot (Figure 15). HDM2 expression was confined to the cell nuclei, and analysis of AQUA scores of HDM2 within the nuclear compartment yielded similar results to analysis of HDM2 expression within the overall tumor mask, suggesting nearly all of the expression is in the nucleus.

AQUA score calculation results in a continuous scale in contrast to manual scoring, which is based on an ordinal scale with arbitrary values. Regression analysis has previously demonstrated a good correlation between the two methods.[271, 272] Of the 542 total histospots, 405 contained sufficient tumor tissue to provide an AQUA score for HDM2. The loss of histospots is random, but reduces the number of cases available for analysis in remainder of this study. Of the 405 cases analyzed, 200 were primary lesions and 190 were metastases, 13 were local recurrences, and 2 were of unknown origin. AQUA scores in the melanoma-specific nuclear compartment of all specimens ranged from 19.62-150.72 and from 21.84-145.98 within nuclear compartment of primary lesions. The histogram in Figure 17A demonstrates the continuous nature and bell-shaped distribution of the AQUA scores for all of the specimens. Note that in other systems, we have evidence that the scores are directly proportional to the number of molecules per unit area. This is probably also true for HDM2, but purified protein standard controls were not available to validate this prediction.

HDM2 expression in the primary lesions was compared to expression in cutaneous metastases, lymph node metastases, and distant metastases. Figure 17B shows that loss of HDM2 is more common in later stage disease. This may be related to specific

classes of tumor with low expression having a great propensity for progression. The significance of the difference between the means of the AQUA scores for each tissue type (i.e., skin metastases, lymph node metastases, distant metastases) from the AQUA scores of primary lesions was determined by t-tests, demonstrated in the Table 11.

Table 11. HDM2 Protein Expression within Tumor Nuclei by AQUA Analysis

	n	Mean	SE	95% CI	Comparison with Mean of Primaries				
					Difference	Std Error	t test	DF	p value
Primaries	200	65.73	1.57	62.63-68.83					
Skin Mets	52	58.37	3.24	51.98-64.76	7.36	3.64	2.02	250	0.0445
LN Mets	98	53.72	2.28	49.23-58.21	12.01	2.78	4.31	296	<0.0001
Distant Mets	40	49.22	3.52	42.28-56.15	16.51	3.86	4.28	238	<0.0001
All Mets	190	54.05	1.63	50.85-57.24	11.68	2.27	5.15	388	<0.0001

Mets, metastatic tumor; LN, lymph node; CI, confidence interval

Survival Analysis:

Since the AQUA scores are of a continuous nature, the HDM2 expression scores were analyzed by univariate Cox regression. This univariate parametric survival analysis demonstrated that high HDM2 expression was associated with improved survival in all specimens (p=0.0154), and in the primary lesions alone (p=0.0318). However, when HDM2 expression was evaluated in only the metastatic specimens, it did not show a significant association with survival (p=0.9330). To graphically depict the influence of HDM2 on survival in melanoma, the scores were divided into quartiles and Kaplan-Meier survival curves were constructed for HDM2 expression. The p values for these curves were determined by the Mantel-Cox log-rank method. Assessment of survival in all

specimens demonstrated that high expression of HDM2 is associated with better disease-specific survival (p=0.0382) (Figure 17C). Examination of HDM2 expression in relation to survival in only the primary specimens followed the same trend, revealing improved outcome for high expressers (p=0.0211) (Figure 17D). The quartile cut-points established for AQUA scores in all specimens were maintained in evaluation of the primary lesions.

Clinicopathologic Correlations:

Table 11 and Figure 17B demonstrate that decreased expression of HDM2 is associated with metastasis. Within primary lesions, there is a relationship between HDM2 expression and lesion progression. Table 12 demonstrates that HDM2 exhibits an association with Breslow thickness, Clark level, and tumor infiltrating lymphocytes, but not with microscopic satellites, ulceration, primary tumor location, age, or sex. These data indicate that HDM2 expression decreases as lesions progress deeper into the dermis (Breslow thickness and Clark level). Multivariate analysis revealed that HDM2 is not independently predictive presumably due to its tight association with variables defining depth of invasion (data not shown).

Table 12. HDM2 Expression and Clinicopathologic Features of Primary Lesions

Factor	HDM2 Expression within Tumor Nuclei (Quartiles)				P value
	Bottom 25% (n=31), No. (%)	25-50% (n=48), No (%)	50-75% (n=55), No (%)	Top 25% (n=66), No (%)	
Breslow Thickness					
≤1mm (T1)	0 (0)	10 (17.9)	16 (28.6)	30 (53.6)	<0.0001
1.01-2.0mm (T2)	7 (15.6)	10 (22.2)	15 (33.3)	13 (28.9)	
2.01-4mm (T3)	9 (18.8)	16 (33.3)	13 (27.1)	10 (20.8)	
≥4mm (T4)	12 (30.8)	9 (23.1)	8 (20.5)	10 (25.6)	
Unknown	*3*	*3*	*3*	*3*	
Clark Level					
I	0 (0)	0 (0)	0 (0)	0 (0)	0.0029
II	0 (0)	0 (0)	8 (38.1)	13 (61.9)	
III	10 (14.7)	19 (27.9)	18 (26.5)	21 (30.9)	
IV	14 (17.5)	19 (23.8)	23 (28.8)	24 (30)	
V	3 (15)	8 (40)	4 (20)	5 (25)	
Unknown	*4*	*2*	*2*	*3*	
TILs					
Brisk/Diffuse	1 (2.1)	11 (23.4)	14 (29.8)	21 (44.7)	0.0392
Nonbrisk/Nondiffuse	20 (20.2)	26 (26.3)	26 (26.3)	27 (27.3)	
Absent	7 (16.3)	9 (21.0)	13 (30.2)	14 (32.6)	
Unknown	*3*	*2*	*2*	*4*	
Age					
<60	9 (8.9)	27 (26.7)	30 (29.7)	35 (34.7)	0.1797
≥60	17 (20.2)	20 (23.8)	22 (26.2)	25 (29.8)	
Unknown	*5*	*1*	*3*	*6*	
Ulceration					
Present	12 (20.3)	15 (25.4)	17 (28.8)	15 (25.4)	0.2585
Absent	14 (11.4)	28 (22.8)	35 (28.5)	46 (37.4)	

Factor	HDM2 Expression within Tumor Nuclei (Quartiles)				P value
	Bottom 25% (n=31), No. (%)	25-50% (n=48), No (%)	50-75% (n=55), No (%)	Top 25% (n=66), No (%)	
Unknown	*5*	*5*	*3*	*5*	
Sex					
Male	12 (14.3)	19 (22.6)	27 (32.1)	26 (31.0)	0.5304
Female	15 (15.3)	25 (25.5)	22 (22.5)	36 (36.7)	
Unknown	*4*	*4*	*6*	*4*	
Microscopic Satellites					
Present	7 (18.0)	9 (23.1)	8 (20.5)	15 (38.5)	0.5535
Absent	19 (13.5)	33 (23.4)	44 (31.2)	45 (31.9)	
Unknown	*5*	*6*	*3*	*6*	
Primary Tumor Location					
Axial	12 (15)	20 (25)	24 (30)	24 (30)	0.5701
Extremity	9 (9.5)	26 (27.4)	25 (26.3)	35 (36.8)	
Unknown	*10*	*2*	*6*	*7*	

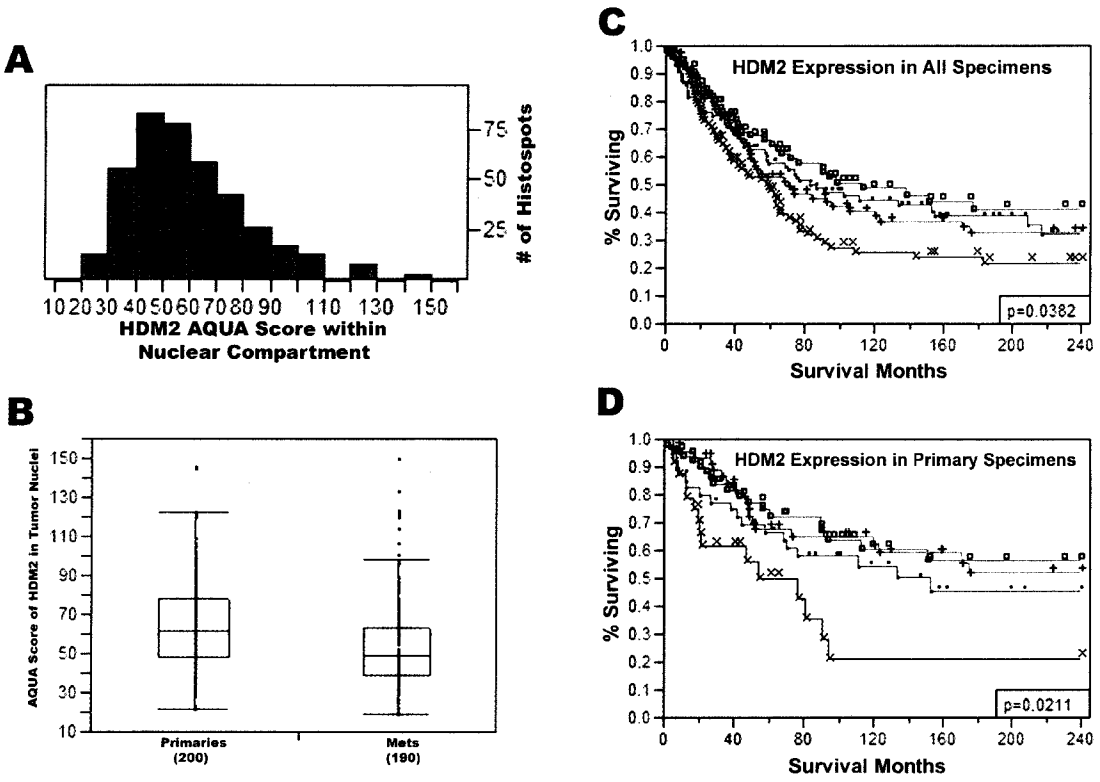

Figure 17. (A) HDM2 protein expression histogram for AQUA analysis within the nuclear compartment of the tumor mask. The histogram demonstrates the ability of AQUA to give a continuous readout of HDM2 protein expression. (B) One-way analysis of AQUA scores demonstrating significantly higher levels of HDM2 in primary melanoma compared to metastatic lesions (mets). Further stratification (primary, cutaneous metastases, lymph node metastases, distant metastases) demonstrates that there is a significant decrease in HDM2 expression as lesions progress to more advanced stages (refer to Table 2). (C) Kaplan-Meier survival plot of HDM2 expression in all specimens based on AQUA score demonstrating stratification by quartiles. (D) Kaplan-Meier survival plot of HDM2 expression in only the primary lesions. For C & D: x, Bottom 25%; ·, 25-50%; +, 50-75%; □, Top 25%.

Discussion

HDM2 overexpression correlated positively with poor prognosis in sarcoma, glioma, and pediatric acute lymphocytic leukemia, but negatively for non-small cell lung cancer, ERα-positive breast carcinoma, and melanoma.[279] Pathologist-based, traditional analysis of HDM2 expression in a melanoma cohort of 134 patients demonstrated that HDM2 over-expression was unexpectedly associated with improved survival.[109] The method of scoring used by Polsky *et al.* was based on a scale of nuclear immunoreactivity, ranging from undetectable (0%) to homogeneous staining (100%). Their choice of cut point was based on prior experience with this antibody in other cancers (i.e., bladder, prostate, squamous cell carcinomas, and sarcomas), in which the 20% cut point stratified patients in a clinically relevant fashion, but they acknowledged that the appropriate cut points for cutaneous melanoma remain to be established.[109] The continuous nature of AQUA scores makes it difficult to determine a cut-point for survival analyses; however, expression of HDM2 diminished as lesions became more invasive (Table 11 & Table 12, Figure 17B). Therefore, the AQUA scores of HDM2 expression were stratified into quartiles and survival curves were plotted to predict outcome. In concordance with Polsky *et al.*, we also found that high expression of HDM2 predicted a favorable prognosis (Figure 17C). The ability to predict survival was more apparent when the analysis was limited to primary lesions (Figure 17D).

The apparent paradox of HDM2 over-expression having a protective effect, was suggested to indicate the presence of a functional p53 exerting an inhibitory effect on tumor proliferation and activating the HDM2 promoter as part of its normal autoregulatory feedback loop.[109] The p53 tumor suppressor plays a critical role in the

cellular response to DNA damage, preventing altered, pre-malignant cells from progressing to cancer. In response to DNA damage, the p53 protein initiates a variety of stress-specific transcriptional response programs that lead to growth arrest, apoptosis, or senescence.[276] In addition to inducing these response programs, p53 also tightly regulates its own intracellular level via an autoregulatory feedback loop with HDM2. Transcription of HDM2 is stimulated by p53, and HDM2, in turn, directly ubiquintinates p53 and targets it to proteasomal degradation.[278] Recent experiments by Lahav *et al.* on the dynamics of the p53-MDM2 feedback loop demonstrate that this negative-feedback system functions in a 'digital' fashion, in which expression of repair enzymes occurs in defined linear quanta rather than a binary switch-like (all-or-nothing) response.[288] Cells probably express frequent pulses of HDM2 induction when exposed to damage, and histologic sections may represent a snapshot of this dynamic result. That is, a set of cells undergoing pulses that are more frequent would be more likely to be expressing HDM2 at the time of excision and fixation.

However, in light of all the examples demonstrating the regulatory functions of MDM2/HDM2 on p53, there is mounting evidence demonstrating p53-independent functions of HDM2.[289] This protein has been shown to interact with multiple factors (e.g., ARF, MDMX, ATM, c-abl, HIF-1α, RB, PML, E2F) that can play a role in transformation, affecting cell cycle control, differentiation, DNA synthesis, RNA biosynthesis, transcription, and cell surface receptor turnover.[290] Like p53, which plays roles in both transcriptional regulation and mediation of apoptosis in mitochondria[291], HDM2 may also have a second role, unrelated to its interaction with p53. It should also be noted that a number of other oncoproteins, such as Ras[292, 293], Raf-1[294], and Bcl-2[295],

have recently been shown to possess secondary, growth inhibitory functions. These dual-function oncoproteins, including HDM2, may be essential to the proliferation of normal cells equipped with growth suppressor activities that have not been fully characterized.[296]

The AQUA system provides a unique method for the analysis of tissue microarrays not previously possible using standard pathologist-based techniques. The system is precise, highly reproducible and quantitative resulting in continuous measurements similar to that obtained from ELISA assays. In addition, AQUA allows for accurate subcellular localization, with the ability to discriminate between the cytoplasmic and nuclear compartments in melanoma cells. With increased resolution, the analyses will expand to include additional 'virtual' compartments (e.g., mitochondria, lysosomes, endoplasmic reticulum, Golgi, etc.). The system has been effectively demonstrated on colon[271], breast[272], and prostate[273] carcinomas. The automated nature of this technology can allow high-throughput screening of tissue microarrays, facilitating their use in discovery of chemotherapeutic targets and biomarker validation.

In summary, AQUA-based analysis was used to demonstrate that HDM2 is a marker of melanoma progression. As might be expected of a marker of progression, it is also useful for prognostication independent of all conventional histologic markers except those related to tumor depth of invasion. In primary lesions, this biomarker may represent a mechanism to predict survival in a tumor type without standard molecular tools for prediction of outcome.

Chapter 4: Automated Quantitative Analysis of AP-2 subcellular expression in Melanoma Tissue Microarrays Correlates with Survival Prediction

Abstract

The activator protein-2α (AP–2) transcription factor plays a key role in regulating the expression of many genes involved in tumor growth and metastasis of human melanoma. Loss of AP-2 expression has been shown to result in the deregulation of several genes with AP-2 binding motifs such as c-Kit, MCAM/MUC18, MMP-2, and PAR-1 expression, all of which contribute to the increased metastatic potential of human melanoma. In this study, we sought to assess the prognostic significance of AP-2 expression and its role in the transition of nevi to radial growth phase (RGP) and to vertical growth phase (VGP, metastatic phenotype) in human melanoma. Two cohorts were analyzed using the tissue microarray format. The first was a "progression" array containing melanoma specimens from M.D. Anderson Cancer Center representing 168 melanocytic cores (84 individual cases) from benign nevi (BN, 19), dysplastic nevi (DN, 21), radial and vertical growth phase melanoma (MM, 22) and metastatic melanoma (MMM, 27). The second array was a retrospective cohort collected at Yale University representing 214 primary melanomas and 293 metastases with long term clinical follow up. The MDCC array was analyzed using Laser Scanning Cytometry (LSC) and Yale array was analyzed using Automated Quantitative Analysis (AQUA) systems for analysis of AP-2 expression, respectively. Both systems permit the continuous and quantitative analysis of protein expression at the single cell level, including sub-cellular localization, in tissue sections. Analysis of total AP-2 expression using two, independent quantitative systems revealed no correlation with diagnosis group (i.e., BN, DN, MM, or MMM).

Laser Scanning Cytometry (LSC)-mediated sub-cellular analysis demonstrated that the nuclear expression of AP-2 was highest in the BN group (11.85%) and significantly decreased in each phase of melanoma progression to 0.39% in the MMM group. Using Automated Quantitative Analysis (AQUA™)-based analysis, neither nuclear nor cytoplasmic expression levels correlated with outcome. However, the ratio of cytoplasmic over nuclear AP-2 was highly predictive of outcome in the entire population, as well as in the primary tumors alone. Furthermore, the AP-2 ratio directly correlated with other clinicopathological factors such as Breslow depth ($R=0.334$, $p < 0.001$). Employing two different automated quantitative systems, we demonstrate that a high level of AP-2 expression in the cytoplasm relative to the nucleus correlates with poor prognosis. Together, these results confirm the biological hypothesis and provide quantitative evidence that the loss of AP-2 expression in the nucleus is associated with malignant transformation and progression of melanoma.

Introduction

The incidence and mortality rate of melanoma has increased significantly over the last fifty years, with more than 59,000 new cases expected this year.[297] This increase in incidence combined with the lack of effective therapy for advanced melanoma emphasizes the need to develop better markers that correlate with clinical outcome. Since the 1970s, the Breslow depth and Clark level of invasion remain the most widely used and reliable predictors of survival in primary melanoma.[298, 299] However, within each stage of melanoma there is a significant variability in outcome. Thus, more accurate molecular markers for melanoma progression are needed to stratify and treat patients with malignant melanoma.

Previously, our collaborators have shown that the 52-KDa transcription factor Activator Protein 2-α (AP-2) is involved in the progression and metastasis of human melanoma through the regulation of several target genes such as c-KIT, MCAM/MUC18, E-cadherin, p 21, PAR-1 and MMP-2 genes.[300-305] The loss of AP-2 results in the suppression of endogenous AP-2 transactivator function that may inhibit melanoma cells to respond to growth and differentiation-regulatory signals.[306, 307] Furthermore, inactivation of AP-2 by means of dominant-negative AP-2 gene resulted in an increase of tumorigenicity and metastasis potential in primary cutaneous melanoma cells.[302] Indeed, screening human melanoma cells *in vitro* for AP-2 protein expression has shown that the majority of highly metastatic cells express low levels of nuclear AP-2.[308]

Few studies have evaluated AP-2 immunohistochemical staining in melanoma prognosis.[306, 309] These studies, however, were based on individual cases or on small patient cohorts using semiquantitative methods. Manual quantification is limited by the

pathologist's ability to detect low level staining patterns with the eye, rapidly and reproducibly score on a continuous scale, and accurately quantify subcellular expression levels. In addition, the analysis of histological sections is complicated by the fact that tumor tissue contains a heterogeneous mixture of cell types, necrotic regions and extracellular material. Better research tools are needed to facilitate discovery of molecular markers of prognosis that reduce variability often observed using antibody-based techniques.

Tissue microarrays provide a high-throughput approach to simultaneously screen hundreds of patient samples in a uniform fashion.[310, 311] Analysis of tissue arrays permit the molecular profiling of a large number of different molecules at the DNA, RNA, and protein levels that are potentially involved in tumor development and/or progression.[312, 313] Microarray technology reduces the variability between specimens because all tissue cores on the slide are simultaneously exposed to the same technical conditions. Another benefit of tissue microarrays is that automated quantitative analysis systems such as LSC or AQUA can be used to generate accurate, reproducible measurement of antigen levels.[314-316] Consistent measurements made across thousands of cells can help identify subtle differences in expression that are not easily detectable by the human eye.[317] Furthermore, quantitative analysis provides continuous scoring as opposed to pathologist-based categorical scoring. This is particularly important when validating putative prognostic markers that display large variation in expression, especially when analyzing a large cohort as in a tissue microarray.

Here we report two innovative, automated quantitative analysis systems, LSC and AQUA, to measure the subcellular expression of AP-2 in two independent melanoma

tissue microarrays. The LSC platform combines features of both flow and static image cytometry analysis. LSC data acquisition captures quantitative information by detecting single cell nuclei in tissue sections, eliminating the need to acquire multiple images for performing complex algorithms. For this study, LSC-mediated analysis of AP-2 was performed by using Melanoma Antigen Recognized by T Cells 1(MART-1) to detect melanocytic cells. MART-1 or Melan-A is a recently discovered melanocyte differentiation antigen recognized by autologous cytotoxic T lymphocytes.[318] The gene that encodes MART-1 is expressed in retina, skin, and melanocytic cell lines thereby making it an ideal marker for automated detection of melanocytes.[319]

AQUA uses a pair of novel algorithms that allow highly reproducible analysis of target expression in subcellular compartments in tissue sections. Validation using the AQUA system has been previously reported.[314] This system identifies tumor tissue within each histospot based on the expression of tissue-specific proteins (such as S100) and then evaluates the expression of target antigen, e.g., AP-2, within the tumor mask and inside user defined subcellular compartments. Because S100 is expressed in 98% of all melanomas[320], this protein has been used to create the tumor mask in melanoma.[315, 321] Recently, AQUA was used to demonstrate that HDM2 is a marker of melanoma progression and may be used to predict survival in primary lesions.[315] Thus, AQUA is designed to read tissue microarrays and optimized for high throughput quantitative analysis.

We hypothesized that AP-2 should be active in the nucleus while cytoplasmic expression should be associated with loss of function. Employing two independent automated quantitative analysis systems, we further demonstrate herewith that the loss of

AP-2 in the nucleus is a crucial event in the progression of human melanoma and that subcellular localization of AP-2 is the critical factor in predicting survival.

Materials and Methods

Patients and Case Selection

Specimens obtained from the Department of Pathology, M.D. Anderson Cancer Center consisted of 84 cases comprised of melanocytic lesions including benign nevus (19), dysplastic nevus (21), primary melanoma (22, including superficial spreading, nodular, acral, and lentigo malignant melanoma, and metastatic melanoma (27) to subcutaneous tissue, lymph node and visceral organs, and normal melanocyte controls (8). Specimens obtained from the Department of Pathology, Yale University consisted of 214 primary melanomas, 293 metastases, 14 local recurrences, 22 nevi and 15 cell block controls. The specimens were resected between 1959 and 1994, with a median follow-up time of 60 months. Both studies involving human tissues were approved by the Institutional Review Board at each institution.

Tissue Microarray Construction

Tissue sections from each block were stained with hematoxylin and eosin (H&E) and reviewed by a pathologist to define the selective areas to be punched. To preserve the original tissue block, either 0.6 mm (biopsies) or 1.0 mm (excision specimens) cylindrical cores of tissue were punched out from donor blocks. Selected tissue cores were inserted in a standard 4.5 x 2 x 1 cm recipient block using a Tissue Microarrayer (Beecher Instruments, Silver Spring, MD, USA) with an edge-to-edge distance of 0.1 or 0.15 mm.

The tissue microarrays were then cut to 5 μm sections and placed on glass slides using an adhesive tape transfer system (Instumedics, Inc., Hackensack, NJ) with UV cross-linking. One section from each array was stained with H&E to verify the presence of diagnostic lesional cells and to facilitate case selection for LSC and AQUA-mediated quantitative analysis. At least two cylindrical cores from each case were obtained to construct the three tissue microarrays evaluated at M.D. Anderson Cancer Center as previously described[316]. Two tissue microarrays were constructed at Yale University, with cores (0.6mm) taken from different parts of the tumor for each microarray as previously described[315].

Immunofluorescent Detection of MART-1 and AP-2 for Laser Scanning Cytometry Analysis

Sections (5 μm) were prepared from each block, deparaffinized in xylene, rehydrated in alcohol, and transferred to PBS. Antigen retrieval was performed by steaming using antigen retrieval solution (Dako, Carpinteria, CA) by boiling tissues in 10 mM citrate buffer, pH 6.0 for 10-20 minutes followed by cooling at room temperature for 20 minutes. Next, tissues were washed three times for 3 minutes with PBS and incubated with protein block (5% normal horse serum in PBS) for 15 minutes at room temperature. Protein block was drained, and tissues were incubated with a 1:50 dilution of rabbit anti-AP-2 (Serotec, Raleigh, NC) in protein block overnight at 4°C. Tissues were washed with PBS three times for 3 min. Avoiding exposure to light, tissues were incubated with a 1:400 dilution of secondary goat anti-rabbit conjugated to Alexa 488 for 2 h at room temperature. Tissues were washed with PBS containing 0.1% Brij for 3 minutes two times, and once with PBS for 3 minutes. Next, tissues were incubated with a 1:200

dilution of mouse monoclonal anti-MART-1 (Dako) in protein block overnight at 4°C. Tissues were washed with PBS three times for 3 min and then incubated with a 1:400 dilution of secondary anti-mouse conjugated to phycoerythrin (PE). Tissues were washed with PBS three times for 3 minutes and incubated with 1 μg/ml propidium iodide for 10 minutes at room temperature to counterstain total cell nuclei.

Laser Scanning Cytometry Analysis

Laser Scanning Cytometry (CompuCyte Corporation, Cambridge, MA) combines flow cytometry, image analysis, and automated fluorescence microscopy to enable fluorescence-based quantitative measurements at the single cell level. The LSC consists of an Olympus BX50 fluorescent microscope and a computer controlled optics unit coupled to an Argon, HeNe, and Violet laser. Multiple lasers are used to simultaneously excite different fluorochromes in cellular specimens that emit discrete wavelengths detected by a set of photomultiplier tubes. Together these features permit the ability to generate high-content stoichiometric data on heterogeneous populations of large numbers of cells. Thus, the LSC was used very much like a fluorescent activated cell sorter (FACS) to obtain three-color immunofluorescence intensity information from the tissue microarrays.

We selected each fluorochrome based on the experimental endpoint of the study and compatibility with the LSC. Importantly, each probe was independently tested to ensure non-overlapping emission between filters. Propidioium iodide was used as a nuclear counterstain to contour and quantify single cells within each tissue core. To determine subcellular expression of AP-2, the peripheral contouring feature was selected to simultaneously analyze the cytoplasmic versus nuclear expression level. Using the

Wincyte™ software, Argon and HeNe lasers were selected with the appropriate filters to detect red (cell nuclei), long-red (MART-1) and green (AP-2) fluorescence. Once the scan region was selected using the epifluorescent microscope, slides were scanned using a 200x objective and detector gain voltages were set so that a maximum of 50% saturation was achieved for the brightest maximum pixel event scanned for each fluorochrome. The minimum area threshold was set to optimize contouring of single cell nuclei. To determine the percentage of MART-1-positive/AP-2-positive cells, a scattergram was created to define four quadrants that determined which cells were positive. Each gate of the scattergram was set based on the fluorescent properties of the negative control sample stained with each fluorescent probe. Once each slide was scanned, the data file was replayed to determine the percentages of each cell population, e.g., MART-1-positive/AP-2-positive cells for each tissue core. AP-2-positive cells were analyzed separately for nuclear or cytoplasmic expression. The relocation feature was used to confirm positive cellular expression.

Immunofluorescent Detection of S100 and AP-2 for AQUA Analysis

The tissue microarray slide was stained as described previously.[314, 315] In brief, the slides were deparaffinized by rinsing with xylene, followed by two changes of 100% ethanol and two changes of 95% ethanol. Antigen retrieval was performed in a pressure cooker containing 6.5 mmol/L citrate (pH 6.0) and endogenous peroxidase activity was blocked with 2.5% hydrogen peroxide in methanol for 30 minutes at room temperature. The slide was washed with Tris-buffered saline (TBS), incubated in 0.3% BSA/1X and TBS for 30 minutes at room temperature to reduce nonspecific background, and then stained with a combination of rabbit anti-AP-2 (C18) (1:1600, Santa Cruz Biotechnology)

and mouse monoclonal anti-S100, AM058 (Biogenex, San Ramon, CA) diluted in BSA/TBS at 4°C overnight. The secondary antibodies, Alexa 546-conjugated goat antirabbit (1:200, Molecular Probes, Eugene, OR) plus Envision antirabbit (neat; DAKO) diluted in BSA/TBS were applied for 1 hour at room temperature. 4', 6-Diamidino-2-phenylindole (DAPI) was included with the secondary antibodies to visualize nuclei. The slide was washed with BSA/TBS (three times for 5 minutes) and then incubated with Cy5-tyramide (Perkin-Elmer Life Science Products, Boston, MA) and activated by horseradish peroxidase, resulting in the deposition of numerous covalently associated Cy5 dyes immediately adjacent to the horseradish peroxidase-conjugated secondary antibody. Cy5 was used because its emission peak (red) is well outside of the green-orange spectrum of tissue autofluorescence. The slides were sealed with coverslips with an antifade-containing mounting medium (with 0.6% n-propyl gallate).

Automated Image Acquisition and Analysis.

The AQUA automated image acquisition and analysis was performed as described previously.[314] Briefly, images of the tissue microarray were captured through an Olympus BX51 microscope with automated x, y, and z stage movement with an Olympus Motorized Reflected Fluorescence System and software (IP lab v3.60, Scanalytics, Inc., Fairfax, VA) equipped with Cooke Sensicam QE High Performance camera. Low-power images of the microarray were stitched together with multiple low-resolution images of the microarray (64 X 64 pixels) at ~7-μm resolution. Areas of tumor were distinguished from stroma and non-melanoma tissue by creating a mask with the S100 signal tagged with Alexa 546. Expression of S100 protein was used to identify the tumor mask and 4', 6-diamidino-2-phenylindole (DAPI) was used to identify the nuclear compartment.

Areas of the tumor mask without DAPI were considered 'nonnuclear' or 'cytoplasmic'. The target marker, AP-2, was visualized with Cy5 (red). Rows and columns of the histospots were then identified, missing histospots filled in, allowing each histospot to be identified by its coordinates, and recorded based on its position in the grid. Subsequently, monochromatic, high-resolution (1024 X 1024 pixel, 0.5-μm resolution) images were obtained of each histospot, both in the plane of focus, and 8 μm below it, and recorded in an image stack as bitmaps. A resolution of 0.5 μm is suitable for distinguishing between large subcellular compartments such as the cell membrane/cytoplasm and nuclei. The AP-2 signal from the cytoplasmic and nuclear compartment within the S100 tumor mask was measured on a scale of 0 to 4095 and expressed as target signal intensity relative to the respective cytoplasmic or nuclear compartment area.

Statistical Analysis

The number of MART-1 and AP-2 positive cells was compared between the diagnosis groups using a Kruskal-Wallis test or a Wilcoxon rank-sum test, as appropriate. The M.D. Anderson Cancer Center tissue microarray was designed to assess markers along the progression of normal melanocytic lesions to metastatic melanoma and was not designed to be a prognostic array. Therefore, sub-cellular localization of AP-2 expression from the Yale University tissue microarray was used to determine its association with melanoma-specific survival. The association between the consensus score and AP-2 expression and clinicopathological parameters was assessed using the Chi-square test. The prognostic significance of the clinicopathological parameters was assessed for predictive value using the univariate and multivariate Cox proportional hazards model with melanoma-specific survival as an end point. Survival curves were

calculated using the Kaplan-Meier method, with significance evaluated using the Mantel-Cox log-rank test. All analyses were performed using JMP or SAS (SAS Institute Inc., Cary, NC) at a significance level of 5%.

Results

Immunofluorescent staining of Melanoma Tissue Microarrays.

Previously, it has been reported that the progression of human melanoma is associated with the loss of nuclear AP-2 expression in metastatic melanoma.[301-303, 306, 309] Our results have been confirmed by other studies using tumor specimens. These studies, however, were based on standard immunohistochemical analyses of total cellular AP-2 expression in primary tumors or human melanoma cell lines using semiquantitative methods.

To simultaneously measure AP-2 expression in MART-1 or S100-positive cells by LSC or AQUA, respectively, specific labeling conditions were established for optimal data acquisition. For LSC, we selected fluorescent probes that were compatible with the laser and filter configuration to minimize non-specific emission and false-positive signals. Likewise, probes outside the spectrum of tissue autofluorescence were selected for use with the AQUA system Tissue microarrays stained with anti-MART-1 (Figure 18A) or S100 (Figure 18B) and anti-AP-2 were visually inspected to verify the quality of immunofluorescent antigen detection. A serial section from each tissue microarray was stained with hematoxylin and eosin (H&E) to pathologically verify the presence of diagnostic lesional cells and facilitate selection of the scan region, excluding unwanted or necrotic regions from the analysis. Tissue cores deemed uninterpretable had insufficient tumor cells in the spot, loss of tissue, or large areas of necrotic tissue.

A

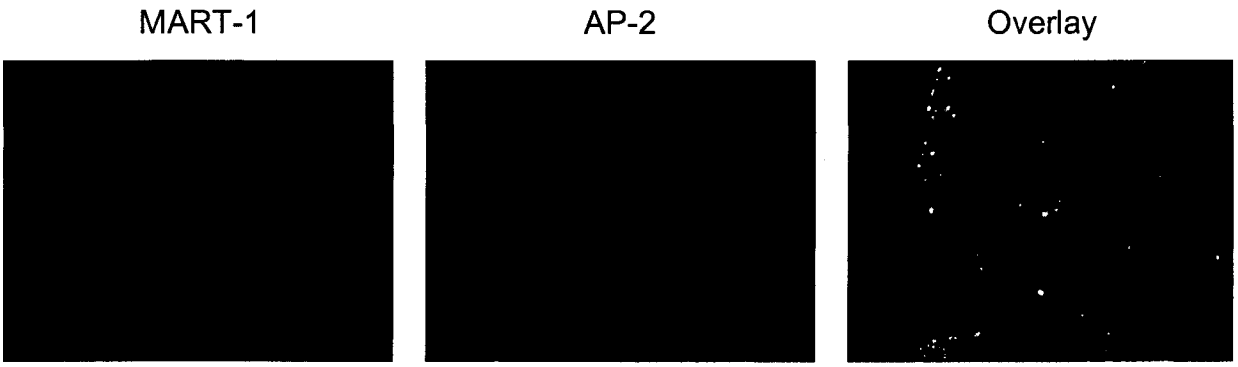

B

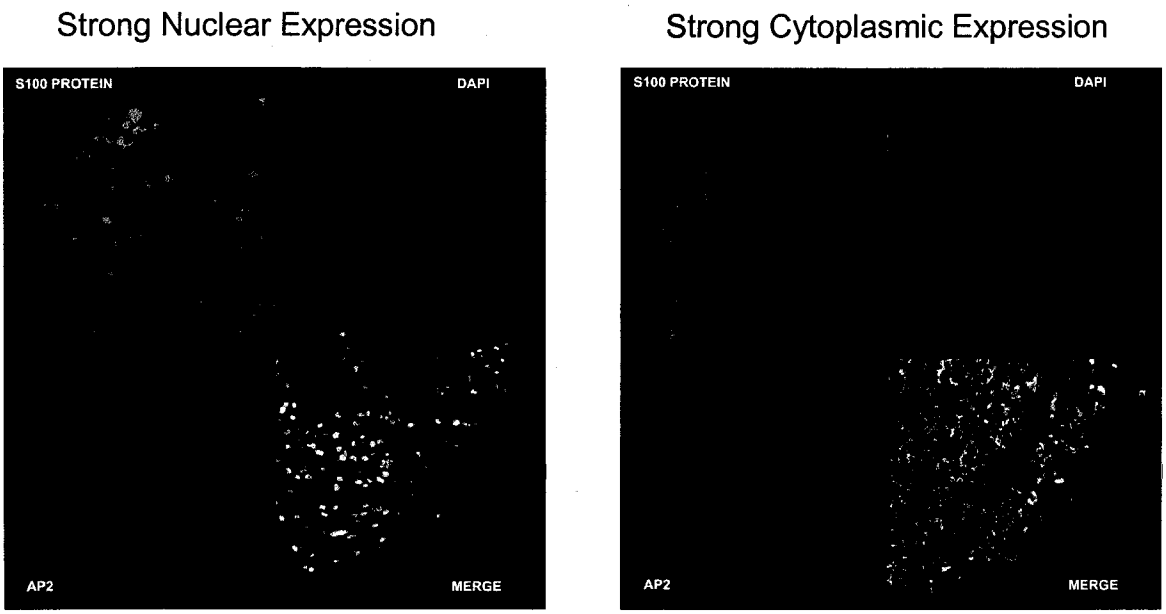

Figure 18. Automated detection of AP-2 in melanocytes. Tissue microarrays were immunofluorescently stained for *A*, MART-1 (red) or *B*, S100 and AP-2 (green) as described in Materials and Methods. *A*, A representative LSC-generated image of a case from a DN reveals optimization of antigen detection for MART-1 and AP-2. Co-localization of MART-1 and AP-2-positive cells appears yellow in the overlay image. Original magnification, x200. *B*, Representative images display tissue cores evaluated by the AQUA system for compartment-specific expression of AP-2. S100 protein (visualized under the 546 wavelength; green) defines the melanoma mask and DAPI (blue) defines the nuclear compartment. The compartment-specific AQUA scores were determined within the melanoma nuclear and melanoma non-nuclear (i.e., cytoplasmic) compartments. Note that the primary melanoma displays strong AP-2 nuclear expression (nuclear compartment, 842; cytoplasmic compartment, 270) and the metastatic melanoma core reveals strong AP-2 cytoplasmic staining (cytoplasmic compartment, 781; nuclear compartment, 490).

Automated Analysis of AP-2 Expression in Melanoma.

The M. D. Anderson tissue microarray was designed to assess markers in the progression of melanoma and not prognosis. Therefore, LSC- and AQUA-based analyses were used to characterize the subcellular expression pattern of AP-2 in each diagnosis group. Peripheral contouring capabilities of the LSC permit the simultaneous measurement of expression in the cytoplasm and nuclear compartment of each cell nuclei (Figure 19A). Because expression of MART-1 has been shown to be a prognostic factor for cutaneous melanoma [322], we first used the LSC to measure the number of MART-1-positive cells in each diagnostic group (Figure 19B, quadrants 2 and 4). Importantly, three-color quantitative analysis demonstrated no significant difference in the number of MART-1-positive cells between the benign nevi, dysplastic nevi, primary or metastatic melanoma groups (Table 13). We therefore used MART-1 as a melanocytic reference for LSC automated analysis of AP-2 in each diagnostic group. After scanning each tissue microarray, the nuclear and cytoplasmic levels of AP-2 in MART-1-positive cells were determined by selecting each case using LSC-generated coordinate position maps and replaying the data file (Figure 19B). LSC-mediated analysis revealed a statistically significant decrease ($p < 0.0001$) in nuclear expression of AP-2 in the benign nevi group (11.85%) to a complete loss of AP-2 (0.39%) in the metastatic melanoma group (Figure 19C). In contrast, cytoplasmic expression of AP-2 significantly increased ($p < 0.001$) with melanoma progression (Figure 19D).

A

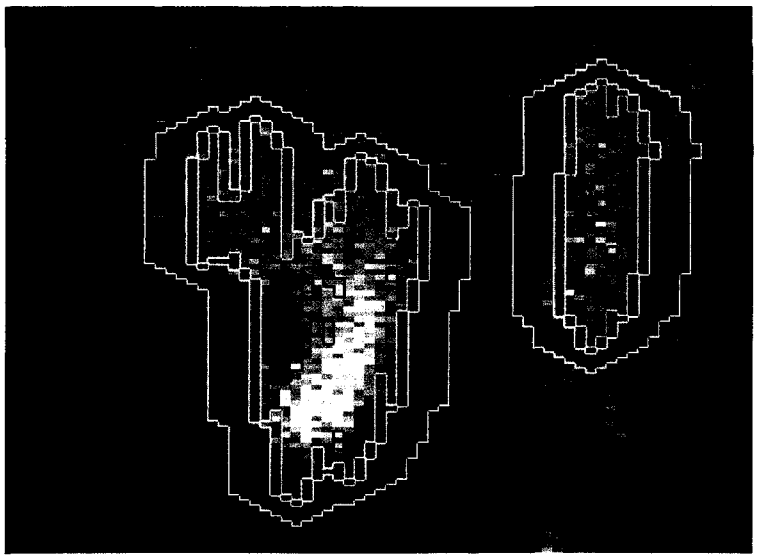

B

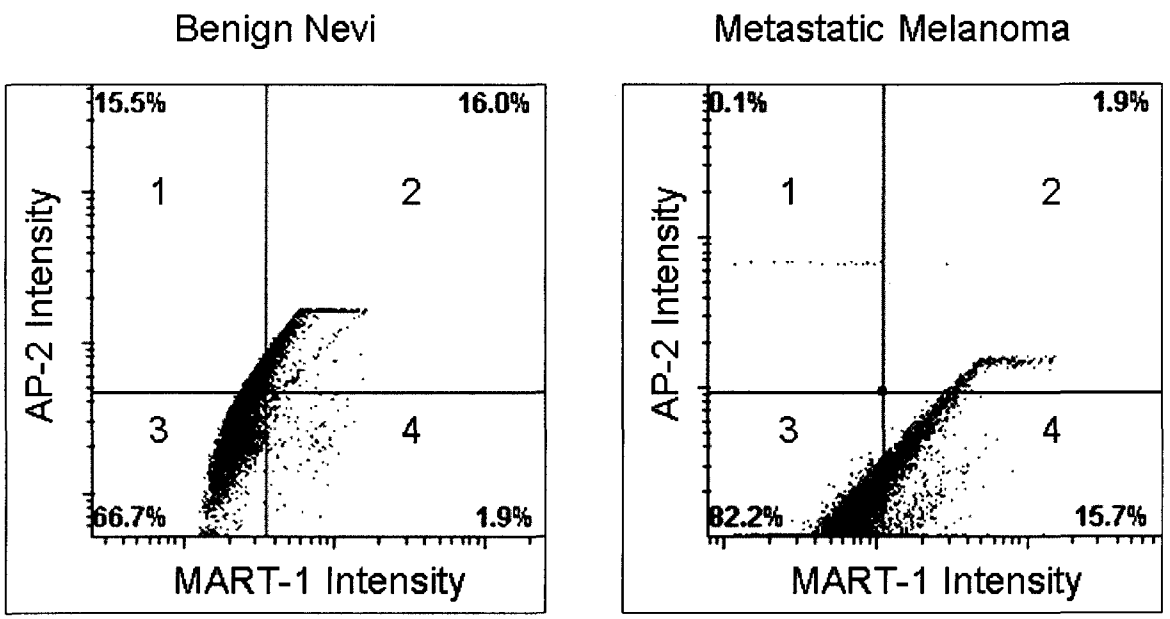

C

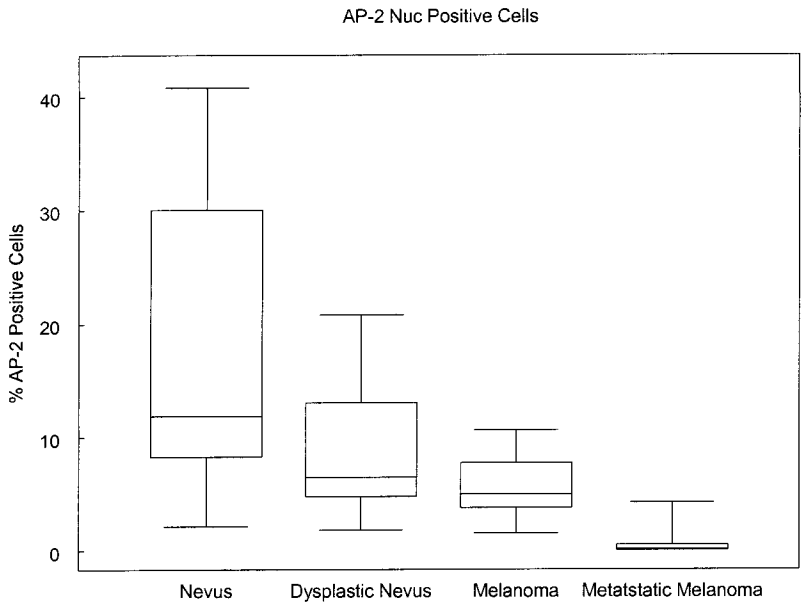

D

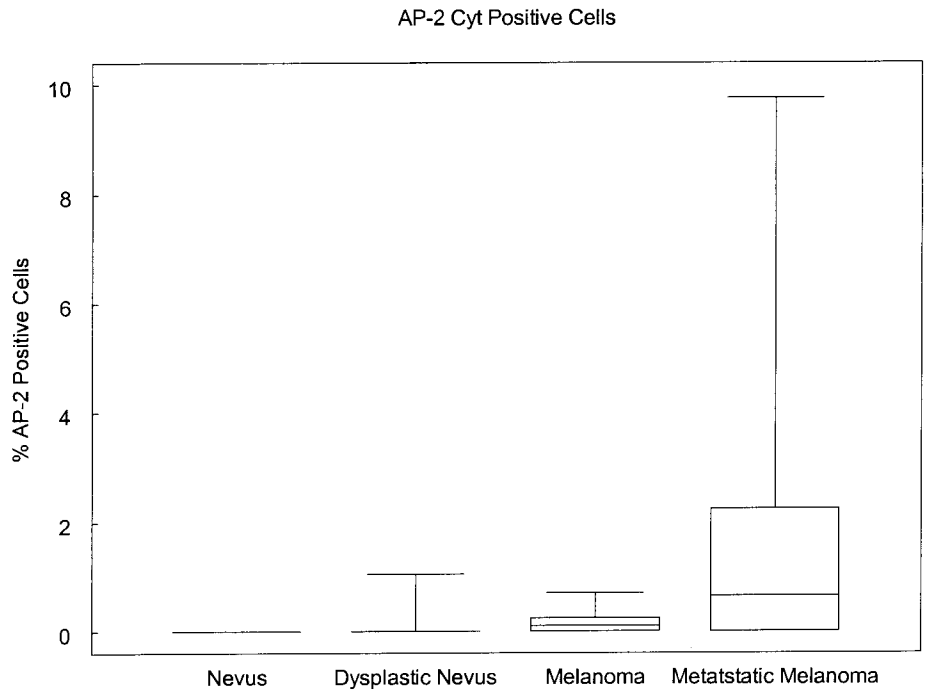

Figure 19. LSC-based quantitative analysis of subcellular AP-2 expression. *A*, LSC-mediated peripheral contour analysis. A representative LSC-scanned image of a single cell indicates the nuclear contour (red outline) and peripheral or cytoplasmic boundaries (two yellow lines). During laser scanning, quantitative information is acquired for each compartment (nuclear or cytoplasmic) based on the fluorescent intensity of each probe. Original magnification, x400, digital magnification 4X. *B*, Stained tissue microarrays were scanned by LSC and individual cases from each diagnostic group were selected from the tissue map to determine the number of MART-1 and AP-2 positive cells (quadrants 2). Representative scattergrams from a BN and MMM case reveal that the percentage of MART-1-positive cells (x-axis) and AP-2-positive cells (y-axis) decreased 8-fold, from 16% in the BN to 1.9% in the MMM group (quadrant 2) . Gates were set based on the negative staining controls. Note that the number of MART-1-positive cells (quadrants 2 and 4) was similar between the two groups (approximately 17%). *C*, Nuclear expression of AP-2 from each case were analyzed. A box plot displays the median (middle line) and the minimum and maximum range (outside lines) of MART-1/AP-2-positive cells by diagnosis group. *D*, Cytoplasmic expression of AP-2. Levels of AP-2 cytoplasmic expression from each case were analyzed using a Kruskal-Wallis test as described in Materials and Methods. A box plot displays the median (middle line) and the minimum and maximum range (outside lines) of MART-1/AP-2-positive cells by diagnosis group. Note that the median levels of AP-2 slightly increased with progression of melanoma.

Table 13. Characteristics of Tissue Cores Analyzed using LSC.

Group	n	No. of Cells Analyzed per Core	No. of MART-1 Cells[a]
Benign Nevi	18	287 ± 402	18% ± 3.53
Dysplastic Nevi	21	265 ± 196	17% ± 2.82
Melanoma	20	1450 ± 1082	14% ± 7.77
Metastatic Melanoma	27	420 ± 315	16% ± 2.82

[a]No significant difference between groups

A different section of the same TMA was analyzed by AQUA, in which S100 was used to detect the cells of melanocytic origin and DAPI was used to define the nuclear compartment. The melanoma-specific cytoplasmic compartment was defined by subtracting the DAPI image from the S100 image (after appropriate gating). Although overall expression of AP-2 tended to increase in the progression from benign nevi to malignant melanoma (Figure 20A & B), there were significant differences in the ratio of cytoplasmic to nuclear expression relative to lesion progression. Advanced lesions

demonstrated significantly more cytoplasmic over nuclear AP2 relative to benign nevi (Figure 20C and Table 14).

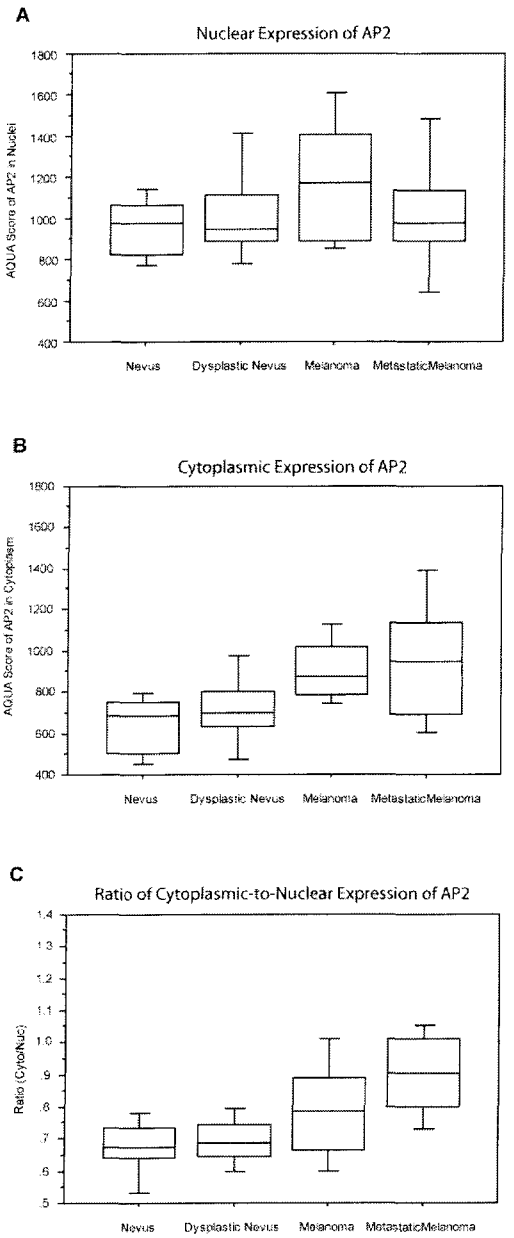

Figure 20. Box plots demonstrating the AQUA scores for compartment-specific (*A*, nuclear; *B*, cytoplasmic) expression of AP-2 measured on the *progression TMA,* as well as, *C*, the ratio of cytoplasmic/nuclear expression of AP-2.

Table 14. Subcellular Expression of AP-2 by Tissue Type

Group	*n*	Nucleus			Cytoplasm			Ratio		
		Mean (SE)	*P**	*P*‡	Mean (SE)	*P**	*P*‡	Mean (SE)	*P**	*P*‡
Benign nevi	15	942.39 (41.44)		0.1531	642.08 (38.28)		0.0007	0.68 (0.03)		<0.0001
Dysplastic nevi	13	1,032.23 (69.28)	0.2615		717.22 (50.95)	0.2419		0.70 (0.02)	0.6772	
Melanoma	16	1,185.96 (76.08)	0.1550		912.77 (42.09)	0.0059		0.80 (0.04)	0.0414	
Metastatic melanoma	23	1,041.62 (76.87)	0.2055		945.48 (69.80)	0.7213		0.91 (0.03)	0.0171	

*t test compared with group above.
‡ANOVA.

Survival Analysis and Clinicopathological Correlations.

The decrease in nuclear AP2 and increase in cytoplasmic AP2 with progression suggested that the differential expression pattern may be useful as a prognostic marker in melanoma. To assess this, we analyzed a cohort of nearly 600 cases of melanoma collected retrospectively at Yale University Department of Pathology. In order to assess this large cohort, a second fluorescence-based system of automated analysis was used. After image acquisition for each tissue core, AQUA was performed to establish the intensity of AP-2 expression per unit area within each core. Consistent with our LSC-generated results, strong nuclear AP-2 expression was noticeable in the primary melanoma cores whereas the metastatic cores displayed diffuse cytoplasmic staining (Figure 18B). Therefore, the cytoplasmic and nuclear AP-2 expression levels generated from the Yale University tissue microarray were used to determine their potential association with melanoma-specific survival. Statistical analysis of total AP-2 expression revealed no significant association with survival (data not shown). Hazard ratios determined by Cox univarate analysis of the AQUA scores for cytoplasmic and nuclear AP-2 expression were 1.000 (95% CI: 1.000-1.001, p=0.4846) and 1.000 (95% CI: 0.999-1.000, p=0.2969), respectively. When analyses were restricted to primary melanoma specimens, the HR's remained non-significant. In contrast,

analysis of the subcellular levels of AP-2 (ratio of cytoplasmic to nuclear expression) revealed a significant association with metastases ($p < 0.01$) and survival [HR: 2.795 (95% CI: 1.609-4.857, p=0.0003), Figure 21A and Table 15]. In the primary specimens, the AP-2 ratio maintained prediction of poor survival [Relative Risk 4.337 (95% CI:1.294-14.536, p = 0.0174), Figure 21B and Table 15]. Analysis of other clinicopathological factors revealed that the AP-2 ratio correlated with Breslow depth ($R=0.334$, $p < 0.001$, not shown), and was associated with microscopic satellitosis ($p = 0.0373$, not shown). Continuous AQUA scores were then divided into quartiles, based on the size of the cohort, reflecting the use of routine statistical divisions in the absence of an underlying justification for division of expression levels. Kaplan Meier analysis of the cohort is shown in figure 3. Using the ratio of cytoplasmic over nuclear AP-2 shows that the ratio is highly predictive of outcome, in both the total cohort (Figure 21A) and the subset of only primary lesions (Figure 21B). Log rank values for each are highly statistically significant ($p<0.0001$ and $p=0.0094$, respectively).

A

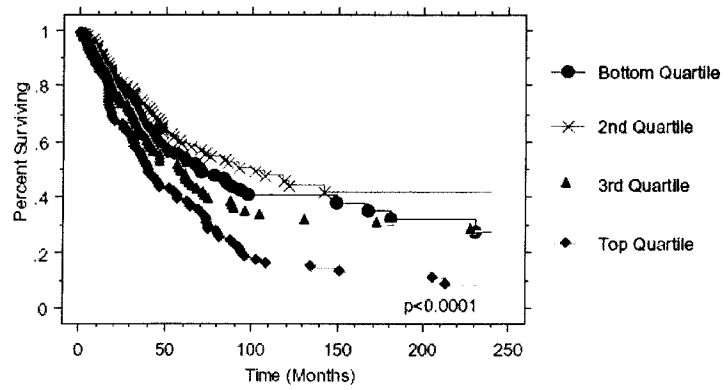

B

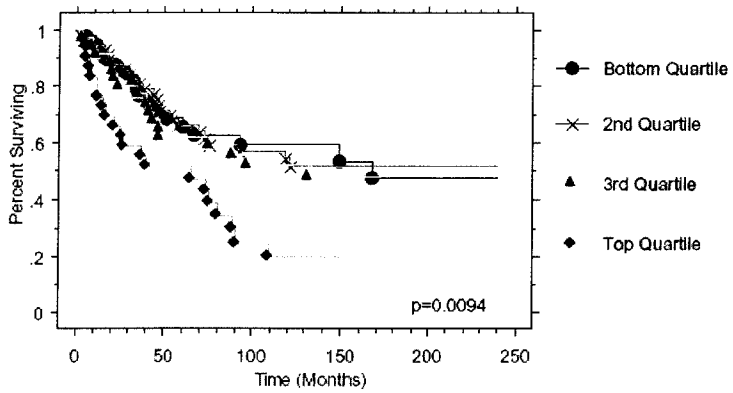

Figure 21. Melanoma tissue microarray analysis of subcellular AP-2 expression using AQUA. Kaplan-Meier survival curves were generated for AP-2 compartmental expression for the *A*, overall cohort and *B*, primary melanoma, with time given in months, showing the four quartiles of intensities of cytoplasmic to nuclear expression.

Table 15. Cox Univariate Survival Analysis of Continuous Variables.

Compartmentalized AQUA Score	All Specimens (HR (95% CI))	p value	Primary Specimens	p value
AP2 in Cytoplasm	1.000 (1.000-1.001)	0.4846	1.000 (0.999-1.001)	0.7540
AP2 in Nucleus	1.000 (0.999-1.000)	0.2969	1.000 (0.999-1.001)	0.4927
AP2 Ratio (Cytoplasmic AP2/Nuclear AP2)	2.795 (1.609-4.857)	0.0003	4.337 (1.294-14.536)	0.0174

To assess the independent predictive value of the AP-2 ratio, we performed a multivariate analysis on the primary cutaneous lesions. In addition to the AP-2 ratio, we included the following histopathologic variables in a Cox proportional hazards model: Breslow depth, Clark level, ulceration, microscopic satellites, tumor-infiltrating lymphocytes. The model (Table 16) demonstrates that the AP-2 ratio maintains prognostic significance ($p=0.0082$) after adjustment for the standard prognostic factors.

Table 16. Multivariate Suvival Analysis of AP2 Expression Pattern and Standard Histopathological Variables Among Primary Lesions

Variable	Hazard Ratio (95% CI)	p value
Tumor Infiltrating Lymphocytes (Absent vs. Present)	3.44 (1.52-7.76)	**0.003**
Breslow Depth (>2.00 mm vs. ≤2.00 mm)	2.18 (1.11-4.25)	**0.0229**
Clark Level (IV-V vs. I-III)	1.57 (0.79-3.13)	0.2022
Ulceration (Present vs. Absent)	1.29 (0.77-2.17)	0.3267
Microscopic Satellites (Present vs. Absent)	0.96 (0.55-1.70)	0.9003
Cytoplasmic by Nuclear AP2 Ratio (Top 25% vs. Bottom 75%)	2.14 (1.22-3.76)	**0.0082**

Discussion

Our goal in this study was to quantitatively assess the subcellular expression of AP-2 on a large cohort of melanoma specimens. Using two independent, automated quantitative systems to evaluate localization of AP-2 expression in two independent tissue microarrays from two separate institutions, we reached the same conclusion. Specifically, we demonstrate for the first time that the ratio of AP-2 cytoplasmic to nuclear expression pattern correlates with both progression of melanocytic lesions and survival.

Because AP-2 is a transcription factor, we hypothesized that AP-2 should be active in the nucleus, while cytoplasmic expression should be associated with loss of function. Analysis of the cohort from The University of Texas M. D. Anderson Cancer Center using LSC revealed almost a complete loss of AP-2 nuclear expression in the metastatic melanoma group. Our results are consistent with other studies demonstrating that AP-2 is lost in metastatic melanoma.[306, 309] However, most of these studies were based on categorical scoring of total cellular expression and were not able to distinguish subtle expression patterns between cellular compartments. Application of the LSC and AQUA automated quantitative

analysis revealed that the ratio between cytoplasmic to nuclear AP-2 expression changes with melanoma progression. Together, these data strongly suggest that translocation of AP-2 from the cytoplasm to the nucleus is disrupted during melanoma progression by an unknown mechanism. Our findings suggest that changes in subcellular AP-2 expression in melanocytes, particularly from benign nevi to dysplastic nevi (2-fold decrease), is a critical step in the genesis and progression of melanoma. Automated analysis of subcellular AP-2 expression in melanocytes may serve as a sensitive marker to monitor the progression of melanoma. It seems therefore, that the major deficiency in AP-2 activity in metastatic melanoma is the loss of nuclear translocation. We hypothesize that this deficiency may be due to changes in the nuclear translocation signal within the AP-2 protein itself or modifications in other chaperone or 'cargo' proteins. The precise mechanism is being investigated in the laboratory of our collaborator, Menashe Bar-Eli.

Both the LSC and AQUA systems offer advantages for quantitative analyses of tissue microarrays that are not practical using conventional methods. LSC-based quantification lies in its analytical power: tens of thousands of cells can be analyzed in a consistent manner between each tissue section, as opposed to hundreds of cells typically evaluated using conventional immunohistochemistry. Here, we demonstrate the peripheral contouring feature of the LSC which allows for accurate quantification of cytoplasmic and nuclear protein expression. In addition, the laser platform has the ability to simultaneously quantify up to five fluorescent probes and determination of positive and negative is accomplished objectively by gating against staining controls.[323] Together, these features permit investigators to evaluate levels of a protein in specific cell types, e.g., AP-2 in MART-1 or S100-positive cells, in a manner that is more reproducible between tissue cores and generates

consistent results in the hands of different investigators. The PM-1000 device and subsequent AQUA analysis is similarly quantitative. AQUA based quantitative analysis of AP-2 expression results in continuous scores that are directly proportional to the concentration, rather than subjective pathologist-based divisions of staining into categorical scores (0-3) or 'positive' and 'negative'. Both automated systems are excellent for analysis of subcellular localization, but the PM-1000 does not require laser illumination and has a much higher throughput which makes it ideal for analysis of large tissue microarrays as the one in this study. Thus, the ability to quantify subcellular localization of markers using automated, quantitative-based systems may be crucial in assessing their potential as prognostic indicators when analyzing tissue microarrays.

To further confirm whether the changes in AP-2 subcellular expression had any potential prognostic benefit, we used the AQUA system to analyze a separate tissue microarray containing a much larger cohort of melanoma specimens from Yale University. Statistical analyses of nuclear or cytoplasmic AP-2 expression levels alone were not significantly associated with survival, suggesting that there may be case to case variability that obscures the overall analysis. Intriguingly, the ratio of cytoplasmic to nuclear AP-2 expression levels correlated with survival, with high levels in the cytoplasm predicting an unfavorable outcome. These results illustrate the power of the ratio. Case to case variability, either real or artifact, is internally normalized by calculation of a ratio.

Heterogeneity is often an issue that is difficult to assess, but is generally addressed by repetition of the analysis with a second set of tissue cores (second fold redundancy). Indeed, these results were reproducible using a second melanoma tissue array containing different cores from the same patients suggesting that the levels of AP-2 are homogenously expressed

throughout the tumor. Furthermore, the subcellular expression patterns of AP-2 obtained using AQUA were further confirmed by their consistency using LSC to analyze a separate cohort.

This study demonstrates two powerful methods for automated, quantitative profiling of tissue microarrays. The automated nature of LSC and AQUA-based technology should facilitate high-throughput molecular profiling of tissue microarrays for use in a variety of applications such as target discovery and prognostic and diagnostic biomarker validation. When compared with conventional immunohistochemistry, these methods demonstrate the importance of quantifying expression based on fluorescence and subcellular localization. The ratio-based data would not be achievable using traditional DAB-based staining methods. Thus, the LSC and AQUA systems provide a useful tool for quantitative analysis of compartmental protein expression in a reproducible fashion, free of the subjectivity associated with pathologist-based scoring.

In summary, the data presented here add further support that the loss (or cytoplasmic translocation) of nuclear AP-2 is a crucial event in the progression of melanoma. Two quantitative methods, AQUA and LSC, were used successfully to demonstrate the importance of quantifying compartmental AP-2 expression and provide evidence that the loss of nuclear AP-2 correlates with progression in melanocytic lesions and also, when calculated as a ratio, predicts survival.

Chapter 5: Improvement of Outcome Prediction in Primary Cutaneous Melanoma by Multiplexed Quantitative (AQUA™) Analysis of Tissue Biomarkers

Abstract

OBJECTIVE: Breslow depth is currently the most reliable predictor of metastatic potential and clinical outcome in primary cutaneous melanoma. We hypothesize that multiplexed analysis of *in situ* protein expression in melanoma could augment the prognostic value of Breslow depth.

METHODS: A 521-case tissue microarray, including 214 primary melanomas, 293 metastases, and a series of controls was constructed with complete clinical annotation. Candidate biomarkers were selected from previous studies evaluating prognostic potential of markers, gene expression profiling studies (cDNA, oligonucleotide, etc.), and functional studies on individual genes and gene products. The AQUA™ (Automated Quantitative Analysis) technology was used to determine exact expression levels of protein biomarkers within nuclear, non-nuclear (i.e., cytoplasmic) and total melanocytic compartments. Several statistical methods were then used to build statistical models that improve, or exceed, the prognostic value of current methods. Briefly, Cox univariate analysis was used to select those markers most closely associated with melanoma-specific survival. Hierarchical clustering, multivariate regression models and genetic algorithms (GA) were then used to determine the optimal number of biomarkers and the optimal cut-points for each marker. Patients were classified by Breslow depth and GA score. Association with melanoma-specific death over 20 years was ultimately measured by Kaplan-Meier analysis.

RESULTS: Thirteen of the 66 variables (derived from 48 independent protein assays) analyzed were significantly ($p<0.1$) associated with outcome (N-cadherin, E-cadherin, p120, Beta-catenin, CD44, Tenascin C, p21, PCNA, Fibronectin, MDM2, ATF2, p16, AP2). GA software was run to convergence ($>20X10^6$ generations) multiple times and the runs repeatedly resulted in the same five-marker solution: ATF2_ratio of cytoplasm by nuclear; nuclear p21; p16_ratio of cytoplasm by nuclear; Beta catenin; and Fibronectin. In this training cohort, limited to 129 primary tumors for which all data points were available, Kaplan-Meier analyses show patients with Breslow depth <1.00 mm have a 78.1% 10-year survival compared to patients with depth ≥1.00 mm with a 45.4% 10-year survival($p<0.001$). Addition of the GA information further stratifies the patients. Patients with Breslow depth <1.00 mm are split into "low-risk" (86.4% survival) and "high-risk" groups (60% survival) while those with Breslow ≥1.00 mm split into "low-risk" (80.5%) and "high-risk" (19.6%) ($p<0.0001$).

CONCLUSION: These training set data suggest that it is possible to improve upon the best prognostic index in primary melanoma (i.e., Breslow depth) by using multiplexed *in situ* measurement of protein expression. We are in the process of validating our results on an independent cohort of patients with known sentinel lymph node outcomes to determine if this Breslow+GA assay is more accurate than sentinel node biopsy in the prediction of melanoma recurrence.

Introduction

Melanoma is the sixth most common cancer in the United States, and its yearly incidence is rising faster than that of any other cancer, with 47,700 new cases and 7,300 deaths in the year 2000; these numbers are estimated at 53,600 and 7,400 for the current year.[2] Initial management of the primary lesion is by surgery. The surgical treatment of melanoma can range from a marginal biopsy to wide local excision with regional lymphadenectomy, and advance in some cases to include extraction of distant metastases.

It has been suggested that metastatic melanoma will become a treatable disease in the coming years as specific inhibitors are being developed against most major targets.[148] Whether this does, in fact, occur remains to be seen. What is clear is that genome-wide screening approaches at the DNA, RNA and protein levels are yielding an increasing number of biomarker candidates that may serve as diagnostic, prognostic, selection of treatment and treatment follow-up markers.

Much success has been demonstrated in the genomic assessment of melanoma, with the majority of studies evaluating global mRNA expression. This has created a bottleneck in biomarker development. Hundreds to thousands of potential biomarkers can be discovered through genomic profiling studies. However, the verification and validation of initial selections from these screening studies requires demonstration on human tissue specimens. The use of tissue microarrays provides the next step in biomarker assessment and evaluation.

While the morphological biology of melanoma progression is well described, the genetic changes that take place as lesions invade deeper and ultimately become metastatic are not well understood. Work is under way in a number of laboratories to reveal these changes

and use them for their prognostic potential (to help predict aggressive potential) and ultimately develop therapies that target these changes.

A number of studies have been published, indicating the prognostic potential of various immunohistochemical markers in melanoma. Although some of the studies have already demonstrated that the levels of melanoma-associated proteins can serve as markers to predict disease outcome, there are a multitude of genes and gene products with prognostic potential in patients with localized melanoma. The expression of thousands of genes in melanoma tumors and cell lines can be surveyed using cDNA microarrays. It has been proposed for various cancers that a discrete and previously unrecognizable cancer taxonomy can be identified by assessing the systemized data acquired from gene expression experiments.[15] Most gene expression studies reported thus far have been based on cell lines, which may not be entirely representative of *in vivo* tumor biology. The data acquired must be validated on *in vivo* models and patient samples.

Melanoma is truly an unpredictable cancer. It is not clear what genetic changes take place in melanoma progression. As this cancer remains refractory to virtually every pharmacologic treatment, and has an incredible potential for aggressive growth, it is not surprising that many melanoma patients submit themselves to toxic and experimental therapies.[116] The products from cDNA microarray analyses not only provide validation of previously identified biomarkers, but also offer new genes that might be useful in molecular diagnosis, pathogenesis studies, and possible molecular targets for therapeutic interventions.

Prognosis in melanoma is currently determined by a number of factors unique to the primary lesion, as well as the presence of loco-regional (lymph node and in-transit metastases) and distant metastatic disease. This information is distilled into the recently

revised Melanoma Staging System of the American Joint Committee on Cancer (AJCC). The first published reports of variables to predict survival in primary melanoma came with publications from A Breslow[28, 29] and WH Clark[29] in the 1970s. The models they described have changed little and remain the most powerful and reliable predictors of survival based on characteristics of the primary cutaneous lesion. In addition to Breslow depth and Clark level, a number of other histopathological characteristics in melanoma have been observed to correlate with disease outcome. The strongest histological predictors of outcome are: tumor thickness (Breslow), anatomic depth of invasion (Clark)[324], presence of ulceration[35, 41-46], mitotic rate[47], presence of microscopic satellites (discrete nests of tumor cells separated from the main body of the tumor by normal subcutaneous tissue). Less powerful histopathological factors include: histologic subtype (i.e., superficial spreading, nodular, lentigo maligna, acral lentiginous, desmoplastic; acral and nodular melanomas may be more aggressive than other types[4]), angiogenesis[48], vascular invasion, regression, and tumor infiltrating lymphocytes. Of all clinical and pathological criteria, the majority of studies demonstrate that tumor thickness (Breslow) is the most reliable independent prognostic factor in cutaneous melanoma.[28, 35, 39, 40, 42, 43, 49-54]

In spite of the fact that these parameters represent the standard of care and the pillars of the AJCC staging system, these histopathologic characteristics of the primary tumor may not necessarily be indicative of tumor aggressiveness. There are a surprisingly large number of cases of melanoma in which tumor thickness does not predict outcome; cases in which thin melanoma turns out to be aggressive[36, 38, 44, 54-76] or thick melanoma indolent[77-80]. Significant efforts over the past 30 years have sought to discover molecular markers that could be used, but no marker has replaced or even matched the physical descriptors above.

Initially, markers were accrued and tested in a somewhat random fashion, based on success in other tumors or a defined role in tumorgenesis in a model system. A long list of these markers can be found in the literature and are reviewed by Li et al.[250] We have contributed to this list[282, 325-327], yet none have been broadly adopted, most likely due to the lack of standardization of these prognostic markers, or more significantly, the lack of a multi-center prospective clinical trial for molecular prognostic indicators.

Perhaps the most significant recent change in the management of melanoma is sentinel lymph node biopsy. This is a procedure initially developed in the treatment of penile cancer where a dye, and/or radiotracer, is injected into the tumor to identify the primary nodal drainage of a particular region, and then the identified nodes are removed for histologic analysis. This can determine if a patient has metastatic disease—regional or distant—and result in more accurate (or at least less morbid) initial staging and management. If the sentinel lymph node is negative for disease, it can be assumed that the rest of the regional nodes are also negative, and the patient will be spared an "unnecessary", invasive and debilitating procedure. The decision to perform a sentinel lymph node biopsy (in the absence of clinically apparent LN disease) is typically based upon the Breslow depth of the primary lesion. Generally, the threshold for performing a sentinel lymph node biopsy is a primary lesion around 1 mm thick[85], but the procedure is becoming the standard of care for patients with primary melanoma greater than 1 mm in thickness[86] or less[328]. Although this method is considered an accurate mechanism for predicting the pathologic status of regional lymph nodes, as well as in the prediction of patient outcome[83], it is far from faultless. However, it is now an essential component of the AJCC TNM classification of melanoma.

Sentinel node biopsies, while valuable, are not perfect. The false negative rate for the procedure is around 5-10%, but more significantly, nearly 25% of patients may be ultimately upstaged, especially if molecular tests are used.[329] Perhaps more importantly, as many as 90% of the sentinel nodes are negative, suggesting the test was unnecessary. Thus, management of melanoma could be improved if there were a method to determine metastasis without removing the nodes and without false negative tests.

Many groups have described promising single biomarkers for melanoma. While these biomarkers may have value, none have successfully transitioned to standard practice in melanoma management. There may be many reasons for this, including the subjective nature of assessment of these markers, the non-reproducibility of these assays, and the fact that assessment of a single marker has limited potential to describe specific biological disease classifications. Even with the addition of quantitative information, it is not clear that a single marker is the optimal way to define outcome classes.

Multiplexing of markers and definition of disease classifications has been a strength of the cDNA array technologies. The work of the Botstein and Brown group[330] and the group from the Netherlands Cancer Institute[234] in breast cancer or the Trent group in melanoma[15] has provided a model for this paradigm. In each case (and many others not referenced), a series of cDNA markers is used with a hierarchical clustering algorithm to produce a relatively small group of disease classifications that show significant differences in the disease outcomes. The classes are generally defined by groups of 70-200 or more markers. While these (and many other studies) show the power of multiplexing for classification, they also illustrate the weaknesses. Perhaps the most significant weakness is the difficulty of translating this technology to clinically useful tests. Not only is RNA

difficult to obtain for routine clinical testing, but the genes discovered by each group show relatively little overlap, suggesting that RNA may not be the most appropriate platform for multiplexing. Some efforts have been made to do multiplex analysis of protein expression, using tissue microarrays.[269] However, the non-quantitative and discontinuous nature of the scoring systems has resulted in results that are likely to lack reproducibility, and tend to be the subject to the same criticisms leveled at conventional immunohistochemistry. Use of a quantitative approach to tissue microarray analysis has the potential to solve this problem. In the present study, we assess numerous protein biomarkers on our large-cohort malignant melanoma tissue microarrays using our automated quantitative analysis (AQUA) system. After establishing biomarkers that are most closely associated with aggressive disease, we develop a prognostic model to predict patient outcome.

Materials and Methods

Tissue Microarray Construction and Cohort Descriptions.

Tissue microarrays were constructed as previously described, with 0.6mm diameter cores spaced 0.8mm apart. Representative tumor regions were selected for coring and placement in the tissue microarray using a Tissue Microarrayer (Beecher Instruments, Silver Spring, MD). The tissue microarrys were then cut to 5μm sections and placed onto slides using an adhesive tape-transfer system (Instrumedics, Inc., Hackensack, NJ) and UV crosslinking.

In collaboration with our laboratory, the Yale Cancer Center TMA Facility has constructed two melanoma tissue microarrays that were used for this study. Each of these is accompanied by a wealth of clinical and pathological data. Long-term follow-up data, including recurrence and survival, as well as cause of death, is available for the majority of the cases. These data have been acquired from YNHH medical records, the Yale University Department of Pathology, and the Connecticut Tumor Registry.

The first array (*Melanoma Discovery TMA;* YTMA 20 / 59) contains 553 melanoma specimens (with redundancy for some specimens), and 17 normal skin biopsies collected between 1959 and 1994, as well as nevi, melanoma cell line, and normal melanocyte controls. Regarding patient representation, there are 214 primary melanomas and 293 metastases. Median and mean age at the time of diagnosis were 56 and 55 years, respectively. The median follow-up time is 19 years. The value of this array lies in the exceptionally large cohort size and the availability of long-term survival data. When analyzed for outcome, the specimens collected on this tissue microarray are representative of

the overall melanoma population in the U.S., conforming to expected results based on current staging criteria (refer to Figure 16).

The second cohort (*Melanoma Validation TMA;* YTMA 76) contains 270 primary melanoma specimens with known SLN status, as well as 50 controls from YTMA 20/59, including 21 primary specimens, 38 metastatic specimens, 14 cell line controls. All of these patients underwent sentinel lymph node biopsy performed by the same surgeon (Dr. Stephan Ariyan). As most of these specimens were collected rather recently, the median follow-up time on the second cohort is approximately 12 months, with the last follow-up for many of the patients being the SLN post-operative visit. However, follow-up data collection on these patients occurs continuously and is a work-in-progress.

Biomarker Selection.

Through gene expression profiling studies, we[117], and others[15, 116, 120-123, 125, 146, 331, 332], have sought to identify molecular changes that take place in melanoma progression. Specific details of these studies can be found in Chapter 1. Table 17 displays the initial list of potential protein biomarkers for assessment of aggressive/metastatic potential in melanoma. Many of these markers were selected based on the potential they demonstrate in functional (cell biological) or small pre-clinical studies in melanoma. Others were selected from gene expression studies, and they were selected based on the significance of differential expression, as well as intersection on multiple studies with different experimental designs.

Table 17. INITIAL LIST OF MELANOMA BIOMARKERS

Selected by gene expression profiling, immunohistochemistry, and/or cell biology

Adhesion Molecules
- ALCAM (activated leukocyte adhesion molecule)/CD166
- CD44
- Cyr61
- E-cadherin (CDH1)
- Fascin (FSCN)
- Fibronectin (FN1)
- Hyaluronan
- ICAM
- ICAM2
- ILK
- Integrins
  - α2β1 (CD49B)
  - α4β1 (CD49D)
  - α6β1
  - αvβ1 (CD29)
  - αvβ3 (CD61)
  - αvβ6
- L1 (CD171)
- LECTINS
  - HPA
  - LPHA
- Muc1
- Muc18 (MCAM)
- N-cadherin (CDH2)
- P-cadherin (CDH3)
- Skeletrophin
- syndecan 4
- Tenascin C
- Thrombospondin 1
- Thrombospondin 2
- VCAM1
- VE-cadherin (CDH5)
- Versican
- α-catenin
- β-catenin
- γ-catenin

Apoptosis-related Factors
- ACS/TMS1
- APAF-1
- Bad
- Bax
- Bcl-X
- Bcl-2
- Bid
- DR4
- DR5
- FAS (CD95)
- FAS-ligand (CD95L)
- FLIP
- Survivin
- TRAIL

bHLH
- HEY1
- Twist

Growth Factors/Receptors
- CTGF
- EGF
- EGFR
- Endothelin receptor B
- EphA2 (Ephrin Receptor A2)
- Ephrin A1
- FGF2 (basic)
- FGFR-1 (Fig)
- IGFBP3
- IGFBP5
- IGFBP6
- IGFBP7
- KDR (VEGFR)

Immunoregulatory
- CD20
- CD26 (DPP4, ADCP2)
- CD40 (TNFRSF5, B cell receptor)
- CD59
- CXCR4
- HLA Class I
- HLA Class II

Melanoma-associated
- CD63
- MAGE-A1
- MAGE-A3
- MART-1
- MiTF

Motility
- Tropomyosin 1 (alpha)
- RhoC

Neural/Neural Crest
- Myelin basic protein
- GalNAc-T
- GFAP
- Growth associated protein 43
- Pax3
- Phosphoglycerate mutase 1 (brain)
- synuclein, alpha

Other
- Apolipoprotein C-II
- Apolipoprotein D
- HIF1α
- Hydroxyacyl-CoA Dehydrogenase; HADH
- Metallothionein
- MTAP (methylthioadenosin phosphorylase)
- Na/K ATPase, beta 1
- Osteonectin (SPARC)
- PFKL
- pirin
- Tropomodulin
- Desmoglein 2
- h-CD/CNh1
- RAB2
- RhoC
- UCHL1

Proliferation Molecules
- AXL receptor tyrosine kinase
- CDK2
- c-kit
- Cyclin D1
- GADD
- Ki67/MIB-1
- p16INK4a
- p21WAF1
- p27kip1
- PCNA
- SKI
- WNT5A

Proteases/-related Factors
- Cathepsin B
- Cathepsin D
- Cathepsin L
- EMMPRIN
- FAP (fibroblast activation protein)
- MMP1 (CLG, fibroblast collagenase)
- MMP13
- MMP2 (Type IV collagenase)
- MMP3
- MMP9
- MT1-MMP (MMP14)
- PA system (uPA, tPA, PAI's)
- PAI-1
- PAI-2
- TIMP1
- TIMP2
- TIMP3
- tPA
- uPA
- uPAR

Regulatory Molecules
- Annexin I (Lipocortin 1)
- Annexin II (Lipocortin 2)
- HDM2
- Melastatin
- MIA
- P53
- Rb

Signaling
- Akt/PKB
- PTEN

Transcription Factors
- AP-2
- ATF-1
- ATF-2

When possible, antibodies to the targets listed above were selected based on their publication record, or other data supporting their specificity and accuracy in immunohistochemisty. In some cases, however, we needed to engage our own antibody validation techniques; typically involving various methods (e.g., Western blots, IHC, peptide competition assays on positive- and negative- control cell lines). Table 18 demonstrates target molecules that have been successfully evaluated on our melanoma cohort, including clone and species information, as well as source and dilution information.

Immunohistochemistry.

Tissue microarray slides were deparaffinized in xylene, followed by rehydration through a graded ethanol series and washed with tris-buffered saline (TBS). The slides then underwent antigen retrieval, which involved 15-minute heat treatment in a pressure cooker containing 6.5 mmol/L citrate, pH 6.0 (except in the cases of ATF2 and HDM2, which were boiled in a pressure cooker containing 1 mM EDTA, pH 7.5). Endogenous peroxidase activity was blocked with 2.5% hydrogen peroxide in methanol for 30 minutes at room temperature. After washing with TBS, the slides were incubated at room temperature for 30 minutes in 0.3% bovine serum albumin in TBS to reduce non-specific background staining.

Immunohistochemical staining was performed on these slides using 50 different antibodies (source and concentration listed in Table 18). Antibodies used in this study were selected for their potential—or previously reported—role in the prediction of melanoma outcome, and/or for their role in key aspects of cell cycle, apoptosis, signal transduction, and melanoma differentiation. Prior to staining these antibodies on the

Discovery Melanoma TMA, each antibody was subjected to a series of dilution titrations on test TMAs to determine the optimal antibody concentration for detecting differences in expression levels. Depending on the species of the antibody, a cocktail was created with an anti-S100 protein antibody of a different species; rabbit polyclonal anti-S100 (1:6,000, DAKO Corporation, Carpinteria, CA) in the case of mouse antibodies or mouse monoclonal anti-S100, AM058 (Biogenex, San Ramon, CA) in the case of rabbit (or other nonmouse species). In all cases, the slides were incubated overnight at 4°C in a humidity chamber.

Secondary antibodies, an Alexa 546-conjugated goat antibody directed against the anti-S100 antibody (anti-mouse or anti-rabbit) (1:200, Molecular Probes, Eugene, OR) diluted in Envision—an HRP tagged polymer—directed against the 'target' antibody (neat; DAKO) were applied for 1 hour at room temperature. 4', 6-Diamidino-2-phenylindole (DAPI) was included with the secondary antibodies to visualize nuclei. Slides were then washed with BSA/TBS (three times for 5 minutes) and then incubated with Cy5-tyramide (Perkin-Elmer Life Science Products, Boston, MA) and activated by horseradish peroxidase, resulting in the deposition of numerous covalently associated Cy5 dyes immediately adjacent to the horseradish peroxidase-conjugated secondary antibody. Cy5 was used because its emission peak (red) is well outside of the green-orange spectrum of tissue autofluorescence. The slides were sealed with coverslips with an antifade-containing mounting medium (with 0.6% n-propyl gallate). Negative controls were obtained by omitting the primary antibody.

Table 18. Antibodies Examined in the Study, indicating Source, Clone, and Dilution

Protein	Clone (Cat No.)	Host Species	Source	Dilution
FN1 (Fibronectin)	ab299	Rabbit	Abcam	1:700
SPARC/ON (Osteonectin)	AON-5031	Mouse	Haematologic Technologies	1:8000
MMP1 (Matrix metalloproteinase 1)	IM35L	Mouse	Calbiochem	1:550
MMP3 (Matrix metalloproteinase 3)	AB810	Rabbit	Chemicon	1:3000
TIMP3 (Tissue inhibitor of MMP3)	136-13H4	Mouse	Oncogene Research Products	1:10
TIMP2 (Tissue Ihibitor of MMP2)	3A4 (18-7351)	Mouse	Zymed	1:75
MT (Metallothionein)	M0639	Mouse	DAKO	1:400
FSCN (Fascin)	55K-2 (M3567)	Mouse	DAKO	1:250
ANXA1 (Annexin A1)	29 (610066)	Mouse	Transduction Labs	1:1000
CDH1 (E-cadherin)	32 (610182)	Mouse	Transduction Labs	1:400
CDH2 (N-cadherin)	3B9 (18-0224)	Mouse	Zymed	1:150
CDH3 (P-cadherin)	56 (610228)	Mouse	Transduction Labs	1:250
L1CAM (L1 neural cell adhesion molecule)	L1-11A	Mouse	Gift of Paul Altevogt	Supernat
CTNNA1 (α-catenin)	αCAT-7A4 (18-0225)	Mouse	Zymed	1:150
CTNNB1 (β-Catenin)	14 (610154)	Mouse	Transduction Labs	1:2500
CTNND1 (p120-catenin)	98 (610133)	Mouse	Transduction Labs	1:400
CD44 (Hyaluronic acid receptor)	2C5	Mouse	R&D Systems	1:200
CD61/ITGB3 (integrin, beta 3)	SZ21 (0540)	Mouse	Beckman	1:50
ILK (Integrin-linked kinase)	KAP-ST203	Rabbit	Stressgen	1:300
APAF1 (apoptotic protease activating factor)	H-324 (SC8339)	Rabbit	Santa Cruz	1:100
Bad (Bcl-associated death promoter)	48 (610391)	Mouse	Transduction Labs	1:250
Bcl-2 (B-cell CLL/lymphoma 2)	124 (M0887)	Mouse	DAKO	1:30
Bcl-X (BCL2-like 1)	Poly (610211)	Rabbit	Transduction Labs	1:1600
Bid (BH3 interacting domain death agonist)		Rabbit	Gift from Gil Mor	1:100
cIAP (inhibitor of apoptosis)	A-13 (SC12410)	Goat	Santa Cruz	1:600
XIAP (X-linked inhibitor of apoptosis)		Mouse	Gift from Gil Mor	1:100
DR4/TRAILR1 (Death receptor 4)	69036 (MAB347)	Mouse	R&D Systems	1:80
DR5/TRAILR2/TNFRSF10B (Death receptor 5)	152415 (MAB6312)	Mouse	R&D Systems	1:350
Survivin	AF886	Rabbit	R&D Systems	1:800
Bax (Bcl-2 homology protein, pro-apoptotic)	A3533	Rabbit	DAKO	1:1500
CTGF (Connective tissue growth factor)	ab6992	Rabbit	Abcam	1:650
EFNA1 (EphrinA1)	I2203 (SC911)	Rabbit	Santa Cruz	1:250
EPHA2 (EPH receptor A2)	SC924	Rabbit	Santa Cruz	1:200
TWIST	H-81 (SC15393)	Rabbit	Santa Cruz	1:250
TNC (Tenascin C)	SC20932	Rabbit	Santa Cruz	1:600
MBP (Myelin Basic Protein)	(18-0038)	Rabbit	Zymed	1:300
HEY1 (hairy/enhancer-of-split related with YRPW motif 1)		Rabbit	Santa Cruz	1:200
LPHA (Leukoyte phytohemagglutinin—recognizes β1,6-branched oligosaccharides)	B-1115	N/A	Vector	1:10000
CD63 (Melanoma 1 antigen)	FC-5.01 (18-7300)	Mouse	Zymed	1:50
MAGEA1 (Melanoma antigen family A, 1)	MA454 (18-7353)	Mouse	Zymed	1:90
MITF (Micropthalmia transcription factor)	C5+D5 (08-8369)	Mouse	Zymed	Prediluted
HDM2 (Human homol. of murine double minute 2)	1B10	Mouse	Novocastra	1:100
ATF2 (Activating transcription factor 2)	C19 (SC187)	Rabbit	Santa Cruz	1:250
AP2α	K2403 (SC184)	Rabbit	Santa Cruz	1:1600
PCNA (Proliferating cell nuclear antigen)	PC10 (18-0110)	Mouse	Zymed	1:10000
Ki-67	B56 (556003)	Mouse	Transduction Labs	1:500
c-kit (kit oncogene)	2E4 (18-0384)	Mouse	Zymed	1:50
p16/CDKN2A/INK4a (cyclin-dependent kinase inhibitor 2A (melanoma, p16, inhibits CDK4)	G175-405 (554070)	Mouse	Transduction Labs	1:500
p21/Cip1/CDKN1A (cyclin-dependent kinase inhibitor 1A)	SX118 (556430)	Mouse	Transduction Labs	1:100
p27/Kip1/CDKN1B (cyclin-dependent kinase inhibitor 1B)	G173-524 (554069)	Mouse	Transduction Labs	1:300

Automated image acquisition and analysis.

The AQUA automated image acquisition and analysis was performed as described previously.[314] Briefly, images of the tissue microarray were captured through an Olympus BX51 microscope with automated x, y, and z stage movement with an Olympus Motorized Reflected Fluorescence System and software (IP lab v3.60, Scanalytics, Inc., Fairfax, VA) equipped with Cooke Sensicam QE High Performance camera. Low-power images of the microarray were stitched together with multiple low-resolution images of the microarray (64 X 64 pixels) at ~7-μm resolution.

Areas of tumor were distinguished from stroma and non-melanoma tissue by creating a mask with the S100 signal tagged with Alexa 546. Expression of S100 protein was used to identify the tumor mask and 4', 6-diamidino-2-phenylindole (DAPI) was used to identify the nuclear compartment. Areas of the tumor mask without DAPI were considered 'nonnuclear' or 'cytoplasmic'. The target markers were visualized with Cy5 (red). Rows and columns of the histospots were then identified, missing histospots filled in, allowing each histospot to be identified by its coordinates, and recorded based on its position in the grid. Subsequently, monochromatic, high-resolution (1024 X 1024 pixel, 0.5-μm resolution) images were obtained of each histospot, both in the plane of focus, and 8 μm below it, and recorded in an image stack as bitmaps. A resolution of 0.5 μm is suitable for distinguishing between large subcellular compartments such as the cell membrane/cytoplasm and nuclei. The 'target' signal from the cytoplasmic and nuclear compartment within the S100 tumor mask was measured on a scale of 0 to 255 and expressed as target signal intensity relative to the respective cytoplasmic or nuclear compartment area.

Data analysis.

Clinical data and immunohistochemistry scores were performed blind, and data were compiled only after all analyses were completed. Histospots containing <10% tumor, as assessed either subjectively (manual) or by mask area (automated), were usually excluded from further analysis. Our previous studies have demonstrated that scores from one to two histospots matches the score from an entire tissue section >95% of the time.

Hierarchical Clustering.

A general description of clustering methods can be found in Chapter 1. In order to perform clustering analyses, Z-score transformation[273] was utilized to normalize AQUA data between experiments. Z-score formula:

[(AQUA Score) – (mean of AQUA Scores on TMA) / standard deviation.]

The computer program CLUSTER[118] was used to perform unsupervised average linkage hierarchical clustering on unweighted z-score transformed AQUA data. The results were then visualized with TREEVIEW[118]. For the 50-marker clustering, cases shown include those with at least 75% of the marker values present.

Univariate logistic regression followed by Classification Error / ROC fitting for multivariate logistic regression models .

Tumor thickness (Breslow) has been repeatedly described as the best overall predictor of disease survival in melanoma patients. We aim to pair Breslow depth with protein expression patterns from tumor tissue microarrays in order to improve the prediction of disease outcome. The data consist of 71 tumor microarray variables—protein expression levels as well as combination variables—in 211 patients with primary

melanoma. The outcome variable is 5-year recurrence (binary). Missing values were imputed by using the column mean. We used a two-step variable selection approach to determine the optimal number of variables to be included in a model to best predict 5-year recurrence.

First, we performed univariate logistic regression to find the top scoring variables with a P value <0.05. This step resulted in a list of 15 variables.(Table 20)

Then, we then performed an *exhaustive search* over all variable combinations to find the best predictive set of variables using 10-fold cross-validation. We used two scoring functions: misclassification error and the area under ROC curve (AUC). The model was iteratively trained on 9/10 of the data, and then tested on the remaining 1/10 of the data. An attempt to build models based solely on traditional clinico-pathologic variables (e.g., Breslow depth, Clark level, ulceration, microscopic satellitosis, tumor infiltrating lymphocytes), in the absence of molecular marker information, was also attempted.

Cox Multivariate Analysis and Aiken Information Coefficient (AIC).

We used survival time as the only end point in this analysis. Firstly, we performed univariate Cox proportional hazard regression to assess the statistical significance of each candidate potential factor, and the factor was retained if a significance level of $p<0.05$ was attained. Factors showing statistical significance as a predictor were further analyzed using a multivariate Cox proportional hazard regression model with stepwise selection of variables based on the Akaike information criterion (AIC). AIC is a measure of the goodness of fit (log likelihood) with a "penalty score" for the complexity of the model (number of variables included), defined as: AIC = –2 x (maximum log likelihood)

+ 2 x (total number of parameters), and the optimum (that is, simplest effective) model gives the lowest AIC value.

Genetic Algorithm.

A general description of genetic algorithms can be found in Chapter 1. A genetic algorithm was used to develop a multiplex marker assay for separation of prognostic groups based on the expression of markers closely associated with outcome. First, those markers mostly closely associated with survival in the primary melanoma specimens were identified by Cox univariate survival analysis ($p<0.1$). (Table 21 & Table 22). These markers were then used as a starting point for the development of a genetic algorithm.

The genetic algorithm software (component of X-tile, written by Robert Camp) applies the elements of Darwinian evolution to optimization problems (e.g., mutation, recombination, selection) in order to the find the best combination of potential solutions to a problem. Each gene/algorithm represents an equation that is a true/false statement, such that the marker value is either 'greater than' (>) or 'less than or equal to' (≤) a particular AQUA score. Each patient is given one point for each 'true' statement and a zero for 'false' statements. A chromosome/solution then consists of the optimal number of if/then statements that can be calculated as true or false. Chromosomes/solutions were subjected to multiple iterations by mutation (i.e., randomly changing cutpoint) and/or cross-overs (i.e., mixing and matching elements of from one gene/algorithm with those of another) until the model converged on a maximum predictive value, measured as relative risk or chi-square. This process was repeated multiple times until the end-point (relative risk or chi-square) values converged. The genetic algorithm repeatedly resulted in a 5-

member model containing the same five variables: ATF2_ratio, Fibronectin, Beta Catenin, p16_ratio, p21_nuclear. Patients were then assigned to risk group based on the genetic algorithm score.

Survival analysis.

Complete follow-up survival data were available for the *Discovery* cohort. Overall survival analysis was assessed using Kaplan-Meier analysis and the Mantel-Cox log-rank score for assessment of statistical significance. Relative risk was assessed using univariate and multivariate Cox-proportional hazards model analyses. All statistical analyses were carried out using SPSS v. 13 (SPSS Inc., Chicago, IL).

Results

Protein Expression Profiling of Melanoma.

The results of expression profiling, in which primary cutaneous melanoma specimens were compared to metastatic melanoma specimens is demonstrated in Table 19. Significant differences ($p<0.05$) were observed for the following markers: Higher expression in primary specimens: Beta-catenin, MMP3, TIMP2, ATF2, HDM2, E-cadherin, P-cadherin, N-cadherin, CD61, HEY1, MAGE1, p16, Bcl-2; Higher expression in metastatic specimens: Fibronectin, CTGF, TIMP3, L1-CAM, alpha-catenin, Bad, Bax, Bcl-X, Bid, XIAP, Survivin, EphA2, Twist, Fascin, PCNA, Thioredoxin, LPHA, p21, Metallothionein.

Table 19. Comparison of Protein Expression Levels in Primary versus Metatstatic Specimens

	Primary Specimens	Metastatic Specimens			
Protein	**Mean ± SD**	**Mean ± SD**	**Mean Difference**	**t value**	**p value**
FN1	47.59±14.79	63.10±24.11	15.51	7.55	<.0001
CTGF	66.07±18.12	72.93±18.23	6.86	3.64	0.0003
SPARC/ON	20.53±15.33	21.38±17.40	0.85	0.5	0.6177
MMP1	37.41±19.88	37.28±22.80	-0.136	-0.06	0.9524
MMP3	20.44±11.52	13.78±6.89	-6.66	-6.474	<.0001
TIMP3	40.94±16.66	47.18±17.54	6.24	3.67	0.0003
TIMP2	56.40±16.07	50.67±12.35	-5.73	-3.39	0.0008
HDM2	52.38±18.06	43.26±16.84	-9.12	-5.25	<.0001
ATF2	69.21±40.24	60.36±39.78	-8.85	-2.52	0.0121
E-cad	37.46±19.51	29.85±18.05	-7.61	-3.43	0.0007
P-cad	35.68±7.23	32.70±5.74	-2.97	-4.38	<.0001
N-cad	19.00±14.77	13.38±12.96	-5.62	-3.92	0.0001
L1	6.52±3.35	8.17±4.29	1.65	3.71	0.0002
α-catenin	11.60±2.15	14.55±7.21	2.95	4.36	<.0001
β-Catenin	48.25±15.81	40.74±12.28	-7.50	-5.15	<.0001
p120	18.59±10.32	18.26±9.23	-0.327	-0.31	0.7569
APAF1	32.21±20.03	31.66±17.59	-0.544	-0.209	0.8344
Bad	40.89±15.35	48.71±22.82	7.83	2.97	0.0033
Bax	10.60±5.75	13.05±9.09	2.45	2.27	0.024
Bcl-2	19.61±20.19	15.43±17.16	-4.17	-1.98	0.0484
Bcl-X	17.50±8.10	21.23±12.32	3.73	2.84	0.0049
Bid	14.36±7.57	20.21±10.29	5.86	4.19	<.0001
cIAP	39.58±20.64	44.93±21.79	5.36	1.88	0.0608
XIAP	10.55±7.98	13.61±9.64	3.06	2.54	0.0116
DR4	35.80±11.83	34.01±11.03	-1.79	-1.11	0.2675
DR5	53.64±15.33	54.34±16.21	0.70	0.29	0.7706
Survivin	36.26±18.20	43.32±15.49	7.06	3.55	0.0005
CD61	30.52±11.18	26.25±7.54	-4.27	-4.01	<.0001
ILK	43.20±14.00	44.86±14.30	1.65	1.13	0.2612
EphrinA1	45.85±16.30	43.67±14.75	-2.18	-1.31	0.1897
EphA2	49.82±16.45	54.19±14.13	4.37	2.53	0.012
Twist	24.64±11.82	28.81±15.10	4.17	2.82	0.0051
Tenascin C	26.11±21.66	29.45±29.11	3.33	1.21	0.2275
MBP	45.24±17.32	43.27±15.75	-1.97	-1.04	0.3006
Annexin 1	40.43±20.80	40.04±25.85	-0.384	-0.16	0.8741
MITF	16.74±13.59	13.41±13.05	-3.33	-2.27	0.0241
Fascin	22.97±22.38	30.94±26.86	7.97	2.77	0.0059
HEY1	59.21±23.65	46.32±25.44	-12.89	-4.90	<.0001
PCNA	20.05±14.12	28.25±16.73	8.2	4.52	<.0001
Ki-67	18.89±6.80	20.35±8.17	1.46	1.91	0.0564
Thioredoxin	4.33±2.36	5.92±5.12	1.59	2.84	0.005
LPHA	21.40±21.65	27.94±16.10	6.54	2.9	0.004
MAGE1	14.45±13.08	11.11±7.16	-3.34	-2.87	0.0044
AP2	21.74±12.33	20.64±11.34	-1.1	-0.87	0.3842
CD63	15.16±17.07	15.58±14.67	0.421	0.23	0.815
c-kit	32.71±16.89	34.53±15.33	1.82	0.99	0.322
p16	29.44±23.11	23.88±19.22	-5.57	-2.65	0.0084
p21	13.01±4.90	13.85±5.46	1.84	3.578	0.0004
p27	38.89±19.55	40.64±21.33	1.75	0.86	0.3948
Metallothionein	31.00±25.65	37.21±30.86	6.21	2.00	0.0459
CD44	51.03±15.63	49.14±16.50	-1.89	-1.01	0.3113

Clustering Analysis.

Clustering models are a good preliminary method of analysis to potentially detect molecular subclasses of disease that may not be recognized otherwise. Although they may not necessarily produce prognostically relevant classifications, the analysis illustrates the strength of multiplexing of quantitative values of protein expression, and may provide some clues to melanoma biology.

We have performed AQUA analysis on 50 proteins using our 521 case *Discovery* Melanoma Tissue Microarray. When subsets of these proteins are clustered using unsupervised hierarchical clustering algorithms, the patient population can be divided into smaller subclasses (Figure 22A). However, these subclasses tend not to be prognostically relevant (Figure 22B & C). One method for improving our understanding of molecular subclasses, while using clinical information already available to us is semi-supervised clustering analysis. Semi-supervised clustering analysis involves the use of clinical data to identify a list of genes that correlate with a clinical variable of interest (melanoma-specific survival in this case) and then applying unsupervised clustering techniques to this subset of genes. After using Cox univariate survival data to identify those markers most closely associated with survival, unsupervised clustering analysis was used to identify groups of patients that have significantly different rates of melanoma-specific survival (Figure 23).

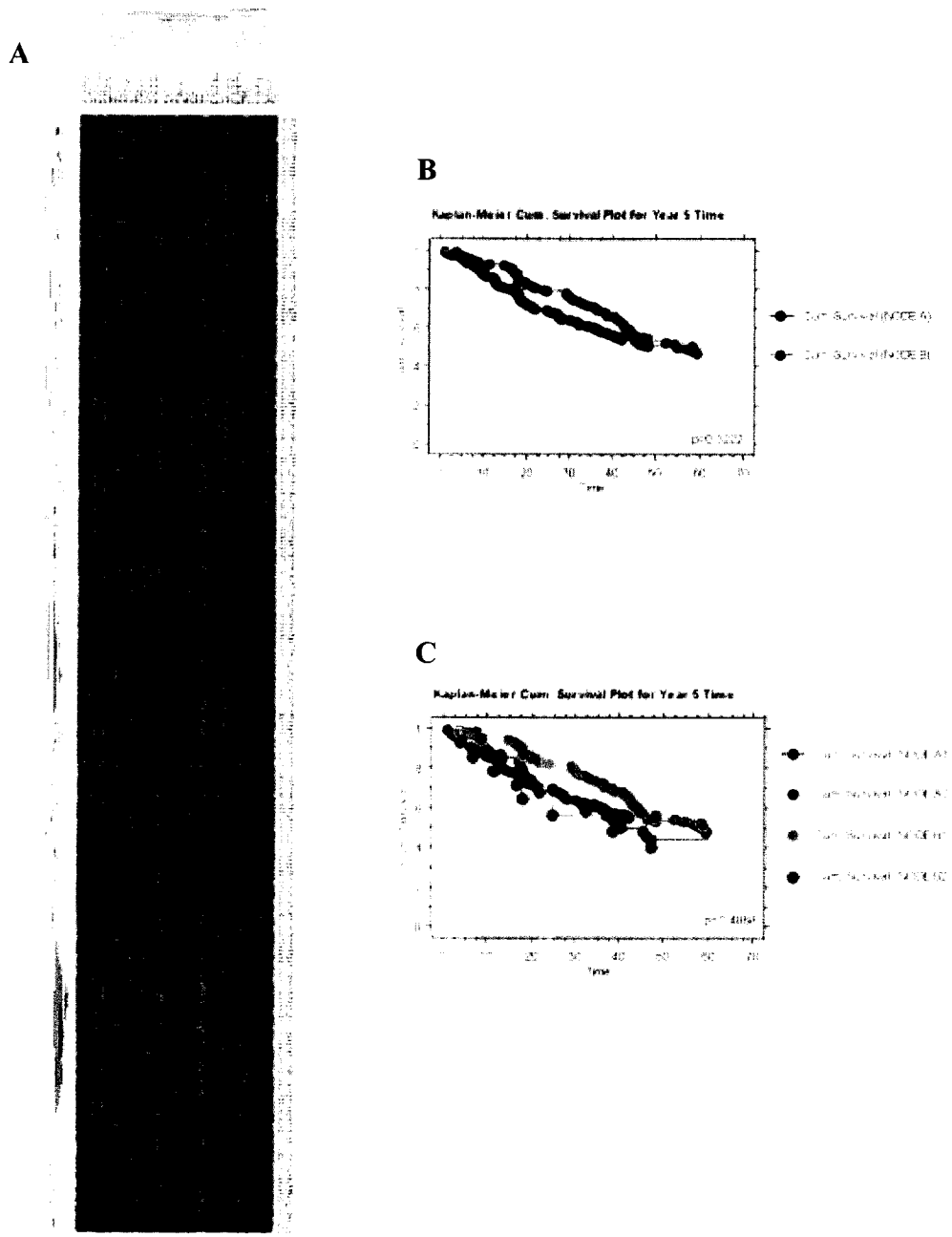

Figure 22. Unsupervised hierarchical clustering of protein expression. Average linkage cluster analysis of protein expression, measured by AQUA analysis, in melanoma patient specimens. A, Clustergram. The rows represent patients and the columns represent proteins. Scores were normalized to the mean by Z-score calculation. B, Kaplan-Meier plot demonstrating survival for the highest level of classification. C, Kaplan-Meier plot demonstrating survival for the second highest level of classification.

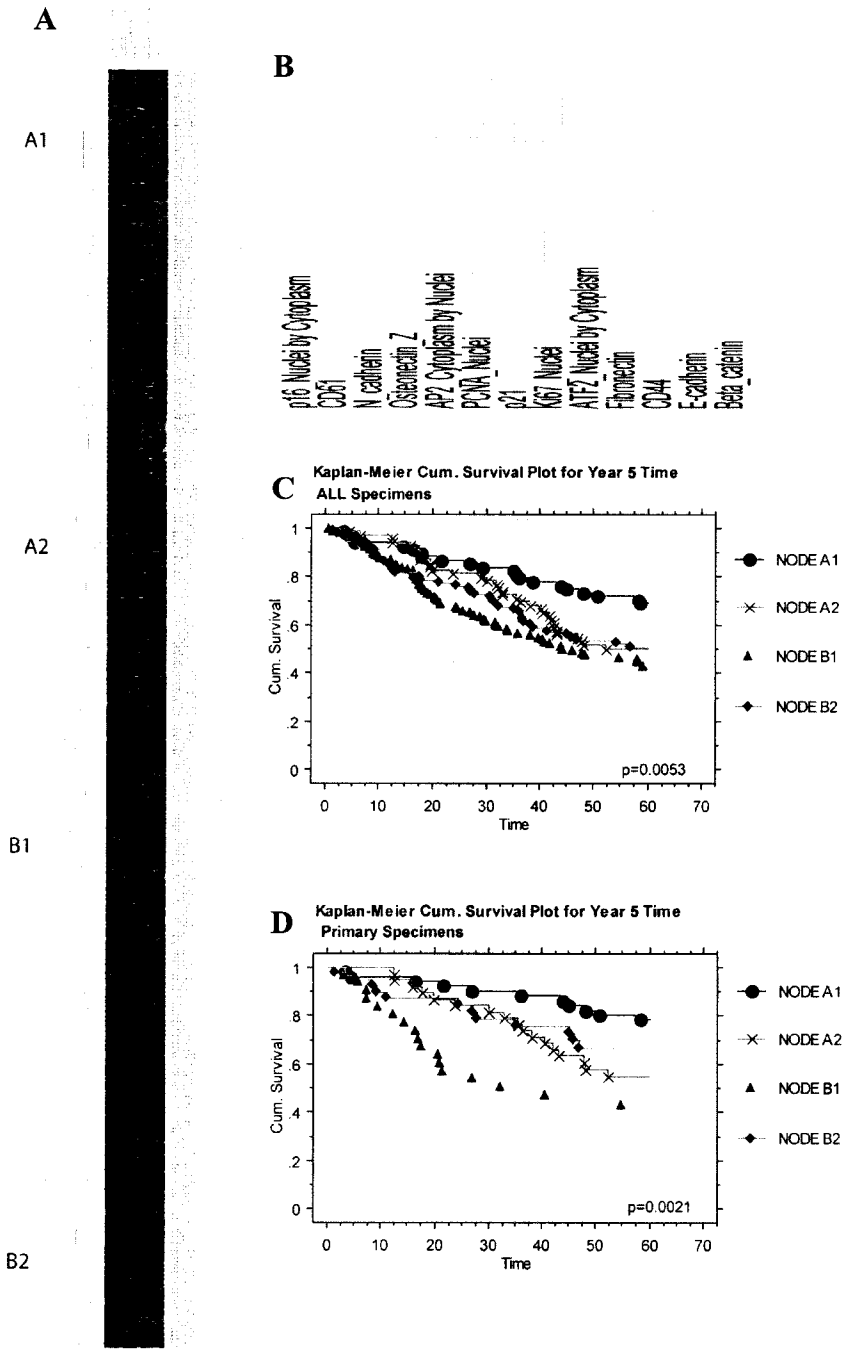

Figure 23. Semi-supervised hierarchical clustering. Molecular markers closely associated with survival by Cox regression analysis ($p<0.1$) were subjected to unsupervised hierarchical clustering. Clades were established and examined by Kaplan-Meier analysis. A, Clustergram. The rows represent patients and the columns represent proteins. Scores were normalized to the mean by Z-score calculation. B, Hierarchical clustering of proteins. C&D, Kaplan-Meier plots (C, all patients; D, primary specimens only) demonstrating survival for the clades identified in clustergram.

Univariate logistic regression followed by Classification Error Determination for multivariate logistic regression models.

We have found 15 variables that show prognostic value using univariate logistic regression analysis for death (as a surrogate marker of recurrence). These are listed in Table 20.

Table 20. Top scoring variables in univariate regression

Variable Name	coefficient	*P* value
BRESLOW	-0.823	1.38e-06
ATF2inCyto	0.549	0.00234
Ecadherin	0.499	0.0039
N_cadherin	0.601	0.00424
ATF2	0.501	0.00568
PCNA_Nuclei	-0.405	0.0086
CD44	0.438	0.00869
PCNA_Tumor_Mask	-0.373	0.0148
Fibronectin	-0.353	0.0205
ATF2_nucbycyto	-0.405	0.032
ATF2inNuc	0.348	0.038
Tenascin_C	-0.302	0.0415
Beta_catenin	0.314	0.0473
Bid	-0.327	0.0477
Survivin	0.325	0.049

Multivariate prognostic models were then constructed and tested through 10-fold cross-validation. Each possible model was trained on 9/10 of the population, followed by testing on the remaining 1/10 of the population; this process was then repeated 10 times. The results of these analyses (i.e., the ability of the model to correctly classify those patients who will 'recur' versus those who will not) can be measured as a classification error.

Model Including Clinicopathologic Factors Alone

- Input: 15 variables
  - BRESLOW
  - ATF2_Cytoplasm
  - E-cadherin
  - N-cadherin
  - ATF2
  - PCNA_Nuclei
  - CD44
  - PCNA_Tumor Mask
  - Fibronectin
  - ATF2_nucbycyto
  - ATF2_Nuclei
  - Tenascin C
  - Beta_catenin
  - Bid
  - Survivin

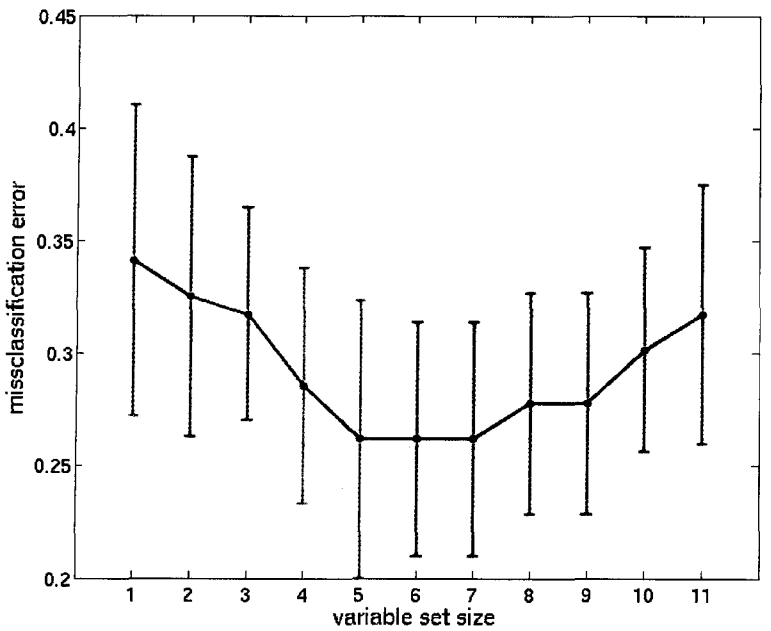

Figure 24. Missclassification error and 95% CI for Models including Molecular Markers + Breslow Depth

A plot of misclassification error (Figure 24) demonstrates the generalization/prediction error for models of different variable set sizes. As demonstrated in Figure 24, a prognostic model with 5-7 variables results in a misclassification error of about .26, down from .34 when using only one variable alone. This demonstrates that the addition of variables to Breslow depth improves the ability of the model to determine which patients will 'recur' up to a point, after which, the addition

of variables convolutes the picture. However, the direct utility of these markers is not entirely clear, or easy to apply to a prospective cohort, as they remain continuous variables in the constructed models.

Model Including Clinicopathologic Factors Alone

- Input: 11 variables
  - Breslow
  - Clark
  - Ulceration
  - TILs
  - Microscopic Satellites
  - Histologic subtype
  - Lesion site
  - Sex
  - Age

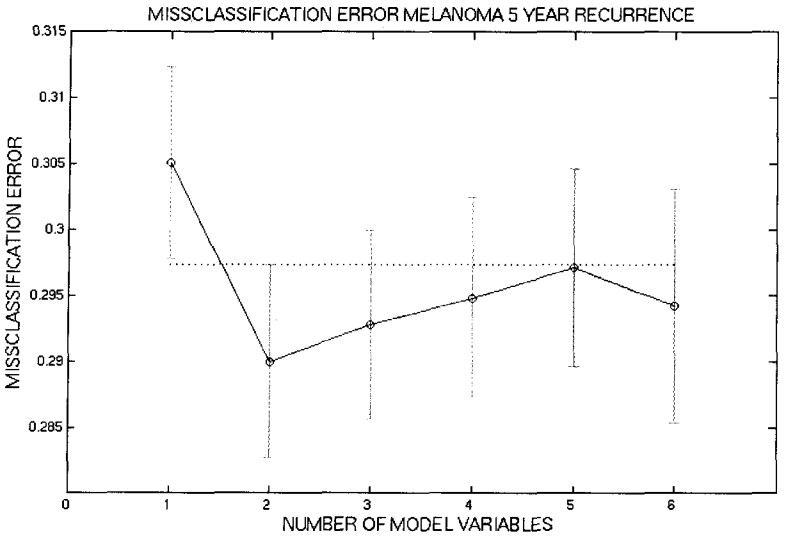

Figure 25. Missclassification error and 95% CI for Models including Clinicopathologic Variables

For a point of reference, and to determine the economic reality of the molecular assay, the same process was performed on the available standard clinicopathologic variables alone, in the absence of molecular markers.(Figure 25) The analyses

demonstrate that models constructed using only clinicopathologic variables do not dramatically improve the prediction of recurrence by Breslow alone.

Cox Proportional Hazard and AIC.

Univariate Cox proportional hazard analysis of the training data set revealed that 13 factors were significantly associated with prognosis of melanoma patients (Table 22). We included Breslow, which showed remarkable significance ($p<0.0001$), and performed multivariate analysis on the 14 factors with stepwise selection of variables using the AIC. Not surprisingly, a Cox multivariate modeling system produced similar results to those obtained with multivariate logistic regression, demonstrating that 5-8 markers provide the most reliable estimate of survival. (Figure 26)

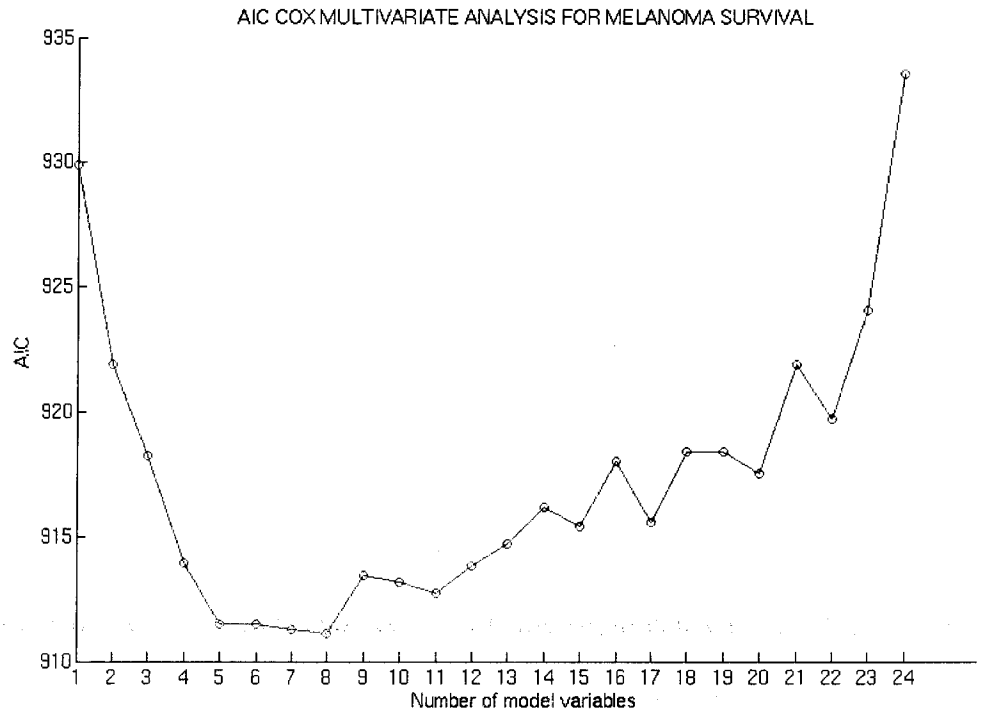

Figure 26. Plot of Akaike Information Coefficient (AIC) score by number of variables included in Cox multivariate models.

Table 21. Univariate Prediction of Melanoma-Specific Death at 20 year follow-up:

Associated with good outcome:

Marker	cont. p-value	Relative Risk 10% vs 90%	25% vs 75%	50% vs 50%
ATF2	0.00059	2.40	2.06	1.45
Beta_catenin	0.0007	3.49	1.68	1.43
N_cadherin	0.0013	1.97	1.95	1.61
CD44	0.0071	2.08	1.58	1.22
Ecadherin	0.0087	1.28	1.88	1.69
MDM2	0.01	2.41	1.79	1.27
ATF2_Nuclear	0.013	2.00	1.65	1.33
MDM2_Nuclear	0.018	2.52	1.57	1.22
CD61	0.023	2.15	1.39	1.29
p16_Nuclear by p16_Cytoplasm	0.026	1.33	1.63	1.49
p16_Nuclear	0.033	1.92	1.57	1.38
P_cadherin	0.067	1.41	1.04	1.22
p120catenin	0.083	1.75	1.43	1.18
MDM2_Cytoplasm	0.09	1.73	1.47	1.33
TIMP2	0.097	1.18	1.33	1.22
MMP3	0.1	2.05	1.47	1.22
EphA2	0.12	1.85	1.16	1.05
AP2_Nuclear	0.13	1.71	1.45	1.08
p16_Tumor_Mask	0.13	1.42	1.41	1.43
EphrinA1	0.15	1.11	1.45	1.24
ckit_Tumor_Mask	0.2	1.22	1.34	1.44
MBP	0.22	1.47	1.28	1.14
p16_Cytoplasm	0.26	1.31	1.29	1.32
LPHA	0.27	1.14	1.05	1.05
MITF_Nuclear	0.29	1.66	1.09	1.29
CD63	0.41	0.74	1.26	1.20
MAGE1	0.51	1.59	1.11	1.34
Hey1	0.54	1.60	1.23	1.00
p27_Nuclear	0.64	1.42	1.07	1.03
Apaf_1	0.69	1.60	1.31	1.06
AP2_Tumor_Mask	0.75	1.72	1.07	0.97
Bcl_x	0.77	0.80	1.08	1.33
ILK	0.83	0.81	1.14	1.11
Thioredoxin	0.88	1.10	0.98	0.85
L1	0.98	0.58	0.69	0.79

Associated with poor outcome:

Marker	cont. p-value	Relative Risk 10% vs 90%	25% vs 75%	50% vs 50%
BRESLOW	6.00E-13	11.95	7.33	4.10
ATF2_nuclear by ATF2_cytoplasm	3.20E-7	2.29	1.74	1.39
AP2_Cytoplasm by AP2_Nuclear	2.20E-5	1.62	2.09	1.83
Fibronectin	0.00071	1.62	2.13	1.57
PCNA_Nuclear	0.0095	2.43	1.51	1.36
Osteonectin	0.026	1.04	1.22	1.22
p16_Cytoplasm by p16_Nuclear	0.026	1.33	1.62	1.54
Metallothionein	0.048	1.12	1.49	1.34
p21_Nuclear	0.058	1.48	1.12	1.30
p21_Cytoplasm	0.066	1.20	1.73	1.27
Ki67_Nuclear	0.08	1.45	1.35	1.15
Fascin	0.091	1.29	0.97	1.08
p27_Cytoplasm by p27_Nuclear	0.1	1.09	1.37	1.31
p21_Tumor_Mask	0.11	0.97	1.34	1.29
MMP1	0.14	1.35	1.31	1.06
CTGF	0.14	1.88	1.10	1.29
Bax	0.23	1.88	1.28	1.32
Bid	0.29	1.66	1.29	1.06
p21_Nuclear by p21_Cytoplasm	0.3	0.99	1.01	0.99
TIMP3	0.34	1.14	1.40	1.05
XIAP	0.35	1.21	1.09	1.00
Twist	0.43	1.25	1.16	1.29
AP2_Cytoplasm	0.49	0.80	1.04	1.07
Bad	0.5	1.39	0.97	1.09
p27_Cytoplasm	0.52	1.04	1.02	1.06
Survivin	0.57	1.17	1.24	1.08
Tenascin_C	0.57	0.90	0.94	0.90
cIAP	0.62	0.89	1.06	1.07
DR4	0.88	1.05	1.07	0.88
p27_Tumor_Mask	0.94	0.91	0.95	0.99
alpha_catenin	0.98	1.01	0.98	0.90
TRAIL_DR5	0.98	1.03	0.95	0.90
Annexin_1	0.99	0.52	0.92	1.07

Table 22. Univariate Prediction of Melanoma-Specific Death at 20 year follow-up (Only Primary Specimens):

Associated with good outcome:

Marker	cont. p-value	Relative Risk 10% vs 90%	25% vs 75%	50% vs 50%
ATF2_Cytoplasm	0.00041	6.34	3.56	2.06
ATF2	0.0012	5.75	2.90	2.04
Ecadherin	0.0031	3.32	2.20	2.17
N_cadherin	0.0033	4.85	3.23	2.28
Beta_catenin	0.0048	5.89	2.89	1.61
CD44	0.0095	2.57	2.32	1.63
ATF2_Nuclear	0.019	2.55	2.24	1.82
MDM2	0.027	3.44	2.23	1.20
MDM2_Nuclear	0.033	3.08	2.04	1.15
p16_Nuclear by p16_Cytoplasm	0.033	0.81	1.55	1.82
MDM2_Cytoplasm	0.056	2.72	1.86	1.46
p120catenin	0.087	2.15	2.28	1.17
alpha_catenin	0.11	2.95	1.39	1.26
ckit_Tumor_Mask	0.13	1.43	2.20	1.96
EphrinA1	0.16	1.62	1.56	1.52
p16_Nuclear	0.21	1.81	1.61	1.27
P_cadherin	0.23	3.19	1.01	1.09
EphA2	0.28	1.91	0.97	1.08
MBP	0.38	1.63	1.26	1.13
MITF_Nuclear	0.42	1.04	1.56	1.27
MMP3	0.46	1.23	1.52	1.58
p16_Tumor_Mask	0.47	1.18	1.23	1.41
Survivin	0.5	1.26	1.41	0.87
LPHA	0.53	2.23	0.88	1.28
p27_Nuclear	0.53	1.76	0.96	1.01
CD61	0.58	1.65	1.04	1.01
Apaf_1	0.58	2.12	0.97	1.11
AP2_Nuclear	0.58	1.59	1.28	0.99
p16_Cytoplasm	0.6	1.31	1.38	1.32
ILK	0.72	0.77	1.43	1.36
Hey1	0.74	0.95	0.90	1.15
Thioredoxin	0.85	2.88	1.11	0.82
CD63	0.86	0.68	1.25	1.13
p27_Tumor_Mask	0.88	1.23	1.04	1.01
TIMP2	0.95	1.12	1.01	0.86
AP2_Tumor_Mask	0.96	1.64	0.95	0.97

Associated with poor outcome:

Marker	cont. p-value	Relative Risk 10% vs 90%	25% vs 75%	50% vs 50%
BRESLOW	9.00E-12	9.48	9.58	4.14
ATF2_nuclear by ATF2_cytoplasm	4.10E-05	1.91	2.06	1.43
PCNA_Nuclear	0.0012	4.24	2.74	1.28
Fibronectin	0.0087	2.88	1.65	1.17
AP2_Cytoplasm by AP2_Nuclear	0.018	1.66	2.00	1.63
Bid	0.065	5.11	1.27	1.09
p16_Cytoplasm by p16_Nuclear	0.088	0.99	1.63	1.85
Tenascin_C	0.093	1.29	1.18	0.89
p21_Nuclear	0.093	1.54	1.25	0.91
p27_Cytoplasm by p27_Nuclear	0.11	1.50	1.41	1.35
p21_Tumor_Mask	0.12	2.05	1.31	0.93
Osteonectin	0.18	1.44	1.65	1.14
p21_Cytoplasm	0.22	1.57	1.19	0.89
Metallothionein	0.24	0.78	1.20	1.43
MMP1	0.25	1.89	1.50	1.13
Fascin	0.31	0.91	0.90	0.78
Twist	0.32	1.71	1.26	1.36
Annexin_1	0.35	1.07	1.55	1.16
Ki67_Nuclear	0.35	1.29	1.29	1.20
L1	0.38	1.29	1.65	1.61
p21_Nuclear by p21_Cytoplasm	0.38	1.46	1.04	0.94
DR4	0.6	1.45	1.12	0.95
Bax	0.61	2.02	1.16	0.78
XIAP	0.67	0.47	0.50	0.81
TRAIL_DR5	0.68	1.23	1.01	0.89
AP2_Cytoplasm	0.68	0.69	1.06	1.13
CTGF	0.74	1.45	0.82	0.89
cIAP	0.79	1.40	1.08	0.85
MAGE1	0.81	1.10	0.76	0.78
p27_Cytoplasm	0.81	0.93	1.01	1.13
p21_Cytoplasm by p21_Nuclear	0.83	0.77	0.93	1.02
TIMP3	0.85	1.66	1.13	0.90
Bad	0.93	1.09	0.69	0.87
Bcl_x	0.95	1.54	0.60	0.72

Genetic Algorithm.

In order to develop a prognostic model with results that can be applied to future cohorts, or be used in a prospective trial, we applied genetic algorithm software to determine the optimal combination of markers, as well as optimal cutpoints for each marker. Thirteen of the 66 variables (derived from 50 independent protein assays) analyzed were significantly ($p<0.1$) associated with outcome (N-cadherin, E-cadherin, p120, Beta-catenin, CD44, Tenascin C, p21, PCNA, Fibronectin, MDM2, ATF2, p16, AP2) by Cox univariate analysis. GA software was run to convergence ($>20X10^6$ generations) multiple times (Figure 27A) and the runs repeatedly resulted in the same five-marker solution: ATF2_ratio of cytoplasm by nuclear; nuclear p21; p16_ratio of cytoplasm by nuclear; Beta catenin; and Fibronectin (Figure 27B).

It is interesting to note that the genetic algorithm resulted in a similar number of genes (five) in the 'optimal model' to optimal models derived from logistic and Cox multivariate regression models, which consider the variables in a linear fashion. The application of the GA model to the training set (*Discovery* cohort) is depicted in Figure 28. The groups were pooled 0-3 (high risk) and 4-5 (low risk) based on similar outcomes amongst the groups.

A

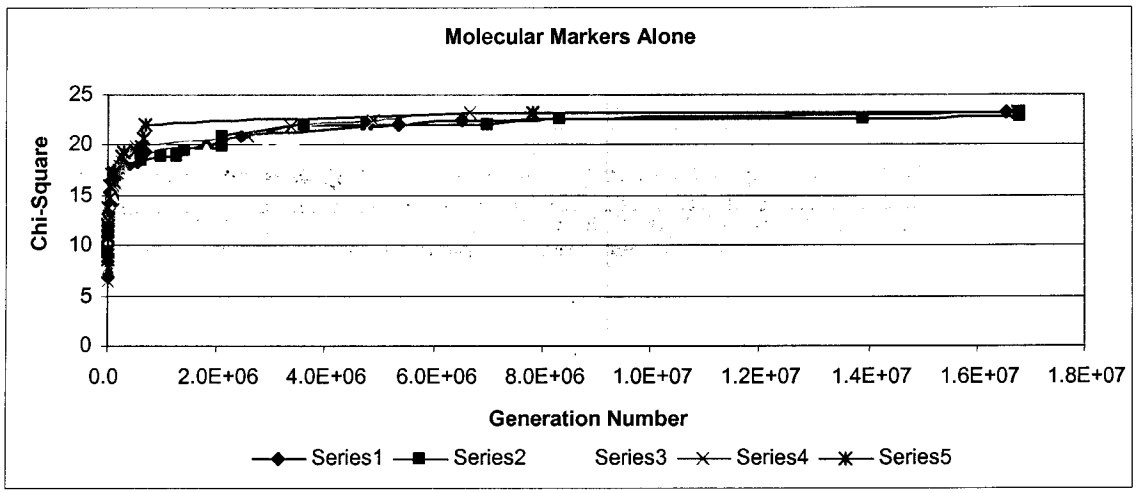

B

Gene 1: ATF2 (Cyto by Nuc) > -0.052

Gene 2: p21_Nuclei > 12.98

Gene 3: p16 (Cyto by Nuc) ≤ -0.083

Gene 4: Beta_catenin > 38.68

Gene 5: Fibronectin ≤ 57.93

Chi Square = 23.13

p-value = 1.54E-06

Figure 27. A, Plot of risk ratio by generation number amonst genetic algorithms, demonstrating progressive improvement of chi-square as generation number increases. B, Optimal gene set with optimal cut-points for each biomarker. The patient is assigned 1-point for each condition that is true, in an additive fashion.

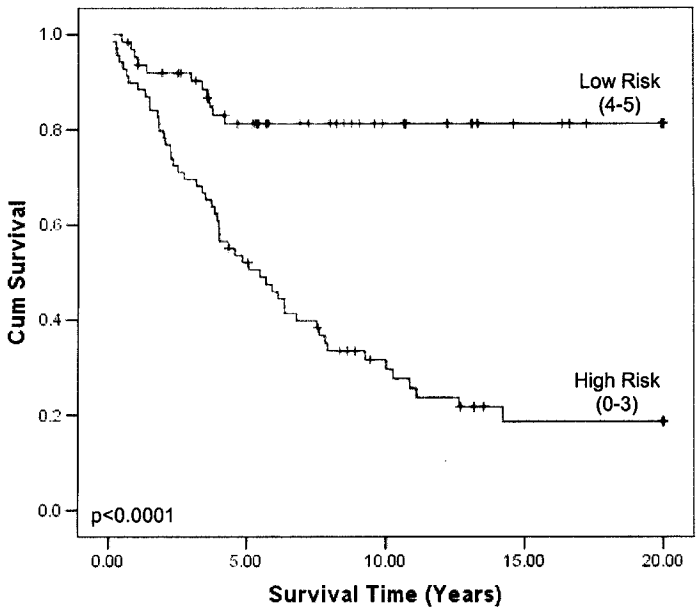

Figure 28. Kaplan-Meier plot of genetic algorithm applied to primary melanoma specimens. Risk groups were assigned based on stratification seen when plotting each individual score category.

In this training cohort, limited to 129 primary tumors for which all data points were available, Kaplan-Meier analyses show patients with Breslow depth <1.0 mm have a 78.1% 10-year survival compared to patients with depth ≥1.0 mm with a 45.4% 10-year survival ($p<0.001$). Addition of the GA information further stratifies the patients. Patients with Breslow depth <1.00mm are split into "low-risk" (86.4% survival) and "high-risk" groups (60% survival) while those with Breslow ≥1.00mm split into "low-risk" (80.5%) and "high-risk" (19.6%) ($p<0.0001$). This information is presented in Figure 29.

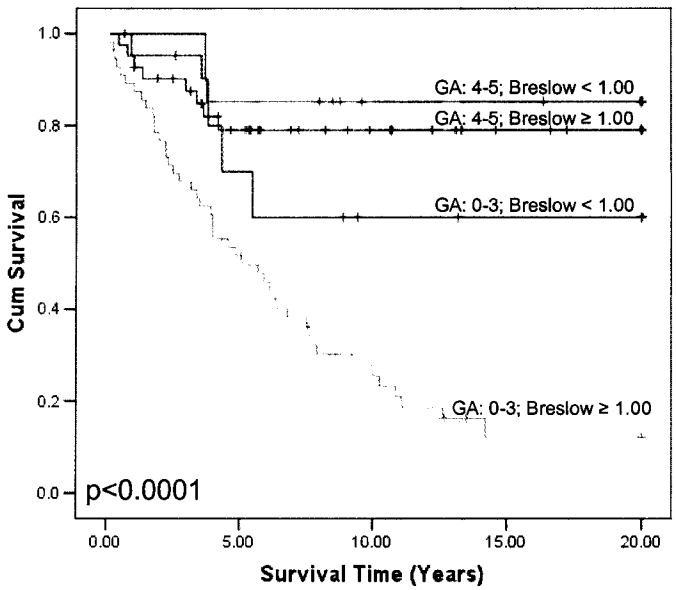

Figure 29. Kaplan-Meier plot demonstrating stratification of patients by Breslow depth (1.00 mm cut point; the 'standard' used by surgeons in determination of which patients receive sentinel lymph node biopsy) and genetic algorithm risk score.

This training set data suggests that it is possible to improve upon the best prognostic index in primary melanoma (i.e., Breslow depth) by using multiplexed *in situ* measurement of protein expression.

We are in the process of validating of our results on an independent cohort of patients with known sentinel lymph node outcomes to determine if the genetic algorithm (GA) assay is more accurate than sentinel node biopsy in predicting recurrence/metastasis. The preliminary data follow.

In the *Validation* cohort of 270 primary melanoma specimens, all patients underwent sentinel lymph node biopsy (SLNB). The mean time from wide local excision (WLE) to SLNB was 47 days. Patient and tumor characteristics include the following. There are 112 female and 158 male patients. The mean age at diagnosis is 58 years ± 17

years (range: 5 years – 98 years). The mean follow-up time is 23 months ± 18 months (range: 21 days – 74 months). The results of SLNB were positive in 33 cases (12.2%).

The majority of these patients received their SLNB within the last year and a half. As a result, recurrence/metastasis data on this cohort is somewhat limited. Using the restricted recurrence data available to us, we seek to examine the ability of Breslow depth, SLN status, and our GA risk test to predict metastasis. However, we first demonstrate the ability of Breslow depth to predict SLN status (Figure 30).

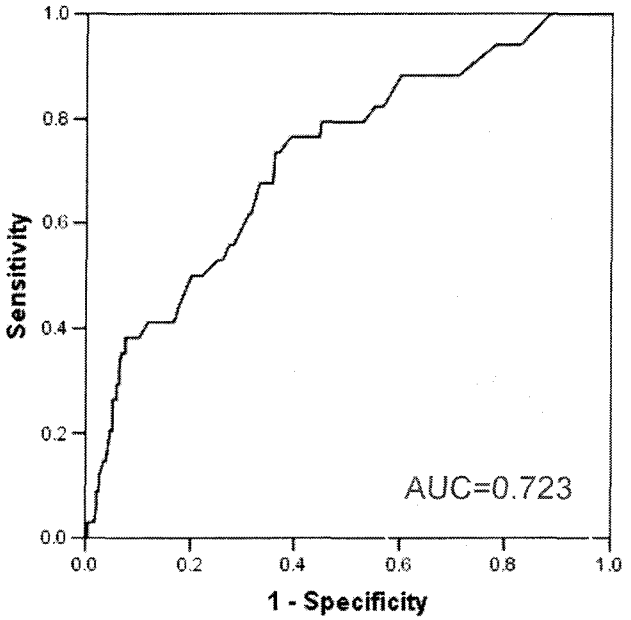

Figure 30. Receiver-operator characteristic curve for prediction of SLN status by Breslow depth.

Regarding recurrence, there are currently 30 patients (10.8%) who have developed metastases. Only seven of these patients had positive SLN results. In terms of prediction of recurrence, Kaplan-Meier plots demonstrate that Breslow depth (Figure 31), SLN status (Figure 32), and the GA risk test (Figure 33) are able to predict metastasis.

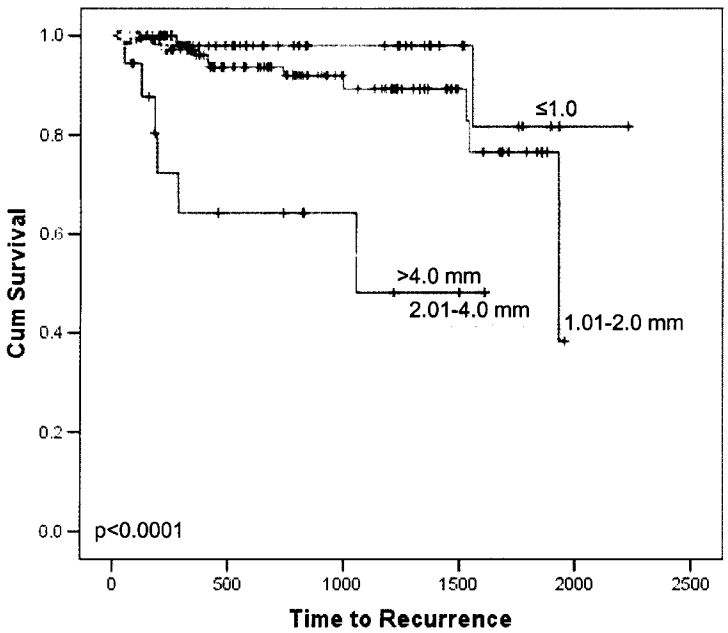

Figure 31. Prediction of metastasis by Breslow depth in SLN (YTMA 76) cohort. Time to recurrence is measured in days.

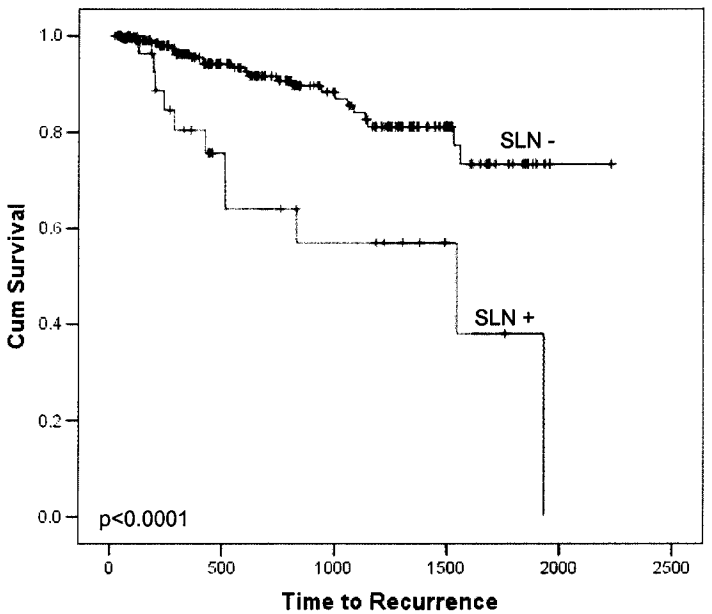

Figure 32. Prediction of metastasis by SLN status in SLN (YTMA 76) cohort. Time to recurrence is measured in days.

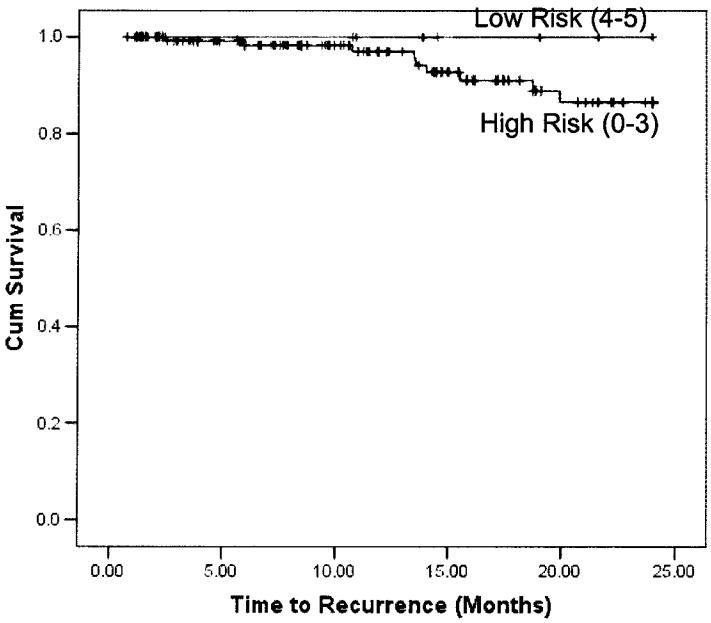

Figure 33. Prediction of metastasis by GA risk test on SLN (YTMA 76) cohort. Time to recurrence is measured in months.

Discussion

We have demonstrated a set of molecular markers that can be used as an independent predictor of survival, to potentially be used on a regular basis to aid in patient prognosis. It should be recognized, however, that these prognostic models should be tested on an independent validation set before being applied in a prospective clinical trial. We hope that these models will serve as an initial assessment to aid clinicians in the prognosis of their patient's disease, and possibly provide therapeutic guidance. Though the current aim of this project is to define aggressive melanoma from 'benign—less aggressive' melanoma, a number of molecular targets have been identified that may have therapeutic potential.

Tissue microarray technology, uniquely, provides the capacity for detecting multiple proteins in large series of patients. To our knowledge, only one study has demonstrated evidence of the feasibility of protein expression profiling for the prognosis of melanoma[269], and only a few papers based on the expression single proteins[109, 282, 325-327, 333] have been published. Born out of the unparalleled ability to control many of the ambiguities of immunohistochemistry, tissue microarray technology combined with automated quantitative analysis allows one to approximate molecular concentration measurements of a particular protein without loss of spatial information.

Many of the genes (i.e,. gene products) that demonstrate closest association with outcome in this study have an established role in melanoma progression. Others have a purported role that requires further investigation at the cellular and molecular biology level. All of them, however, are potential therapeutic targets in the treatment of melanoma.

Cyclins and cyclin-dependent kinases (CDKs) are evolutionarily conserved proteins that are essential for cell-cycle control in eukaryotes. Cyclins (regulatory subunits) bind to CDKs to form complexes that regulate the progression of the cell cycle. The activity of these complexes is modulated by activating and inhibitory phosphorylation events, as well as interactions with small regulatory proteins, including p16, p21, p27 and others. These proteins, referred to as inhibitors of CDK activity (CDKIs), bind to cyclins, CDKs, or their complexes.[334]

The $p16^{INK4a}$ gene, found at 9p21, is a tumor-suppressor gene that has long been known to be involved in familial and sporadic melanoma. The p16 protein has been identified as a specific inhibitor of CDK4, blocking CDK4 substrate phosphorylation.[335] Deletion of the INK4a/ARF (CDKN2a) locus is a common genetic lesion, detected in ~50% of primary tumors and nearly all melanoma cell lines.[336, 337] Work on mouse models has suggested that $p16^{INK4a}$ plays an important role in limiting inappropriate or aberrant cellular proliferation.[338] Previous studies have demonstrated that loss of nuclear p16 occurs more commonly in melanomas than benign nevi[339, 340], and that this occurrence in primary melanoma is also associated with increased proliferation (measured by Ki-67) and poor prognosis.[341]

Most papers approach the cytoplasmic localization of p16 as a nonspecific artifact. However, recent studies have suggested that cytoplasmic localization of p16 may represent prognostically-relevant subclasses of cancer. Emig et al. reported that in breast cancer, cytoplasmic accumulation of p16 identifies a subset of tumors with accelerated proliferation and other unfavorable parameters.[342] Another study demonstrated that nuclear and cytoplasmic p16 overexpression in breast cancer was

associated with a highly malignant tumor phenotype.[343] On the other hand, cytoplasmic p16 localization in colon cancers is associated with a good prognosis.[344] In an attempt to elucidate whether cytoplasmic p16 staining is specific or an artifact due to tissue fixation and/or nonspecific binding of the applied antibodies, Evangelou et al. used immunoelectronmicroscopy to demonstrate that p16 can, in fact, be present in the cytoplasm.[345]

An abundance of nuclear factors in the cytoplasm likely represents a defect in the cytoplasmic-nuclear shuttling system.[346] However, the mechanism is not fully understood. As p16 lacks Nuclear Location Signals (NLS) and Nuclear Export Signals (NES), the defect may lie in the nuclear chaperone group of proteins. The significance of these proteins has been shown in cases of APC and BRCA1 where destruction of NLS does not impede shuttling in the nucleus.[345] An alternative explanation is that cytoplasmic p16 may represent a protective response to over expression of CDK4. According to this scenario, a portion of p16 binds to CDK4 in the cytoplasm and inhibits its passage into the nucleus due to the large size of the complex, whereas the unbound protein enters the nucleus to exert its oncosuppressor activity.[344] In any event, based on our results, an aggressive phenotype is expected in melanoma when cytoplasmic concentrations of p16 exceed those in the nucleus.

The WAF1 gene, which encodes the $p21^{WAF1}$ protein, is located at 6p21. It is has been shown to be under the transcriptional control of p53, and the p21 protein is known to inhibit progression of the cell cycle at the G1to G2 phase.[347] The WAF1 gene is rarely mutated in metastatic melanoma, and expression is not always correlated with p53 expression.[348] Regarding melanocytic lesions, expression of p21 is found to be

low/undetectable in benign melanocytic lesions, while higher expression seen in malignant melanomas.[349] Additionally, increasing expression of p21 has been found to correlate with Clark level and Breslow thickness.[349, 350] However, the association of p21 with patient prognosis is not entirely clear or intuitive.[351]

Fibronectin is an extracellular glycoprotein that serves as a ligand for the integrin family of cell adhesion receptors and regulates cytoskeletal organization. Previous studies have demonstrated that fibronectin expression is associated with tumorigenesis[352] and metastasis[353]. Enhanced expression of extracellular matrix (ECM) proteins, such as fibronectin, may promote tumor cell survival or angiogenesis.[354] Experiments by Clark et al. demonstrate that metastatic transformation of relatively indolent cell lines is associated with upregulation of several genes that encode ECM proteins.[123] We have also previously demonstrated, through genomic analysis, that fibronectin expression is significantly increased in melanoma cell lines relative to normal melanocytes.[117] This is the first time, to our knowledge, that anyone has demonstrated that fibronectin expression by melanoma cells is associated with an invasive phenotype and poor prognosis.

The cadherin/catenin complex is critical for the formation and maintenance of cell-cell adhesion. E-cadherin, a calcium-dependent intercellular adhesion receptor, is the primary epithelial cell adhesion regulator.[355] Its functional role in melanocytes is to maintain melanocyte-keratinocyte adhesion.[356] The extracellular domain works like a molecular zipper, while the cytoplasmic tail is linked to the actin cytoskeleton via catenins.[357] Loss of E-cadherin expression has been implicated in tumor progression for a variety of tumor types, including malignant melanomas.[358-364] Recent studies show that E-cadherin is not only involved in cell-cell contact but multiple signaling pathways are

activated or repressed by E-cadherin. The most commonly discussed pathway is the β-catenin/LEF/TCF signaling cascade.[365, 366] However, E-cadherin is also involved in the regulation of other pathways as well, including MAP kinase[367] and NFκB[358] pathways.

N-cadherin, the neuronal equivalent of E-cadherin, is also expressed by melanoma and has been reported to be upregulated in melanoma cell lines when E-cadherin is downregulated.[359] Additionally, strong N-cadherin expression in single melanomas has been reported in the literature.[362] These observations suggest that this *shift* in cadherin profiles may endow melanocytic cells with new adhesive properties that favor uncontrolled proliferation, migration, and invasion. However, examination of a larger cohort of tumor specimens demonstrates that only a minor percentage of invasive melanomas demonstrate N-cadherin expression.[368] Based on previous data and our results, it is unlikely that the E- to N-cadherin "switch" actually takes place *in vivo*. The role of cadherins as causative factors in melanoma tumor progression remains to be proven. It is likely, however, that overall cadherin expression, in general, is indicative of the differentiation status of a tumor. Based on our results, it is clear that maintenance of E- and/or N-cadherin expression is an excellent predictor of outcome in melanoma.

Regarding the cadherins, our results indicate that it does not matter which cadherin is present at the cell surface. Both E- and N-cadherin are significantly associated with survival in a positive fashion. That is, it is unlikely that the E- to N-cadherin shift is an actual *in vivo* phenomenon. The mere presence of one of these cadherins at the cell surface is probably sufficient to stabilize melanoma cells and retard their invasion.

Catenins are the cytoplasmic proteins that regulate and effect cadherin function. β- and γ-catenin bind directly to the cytoplasmic carboxy-terminal domain of E-cadherin, forming mutually exclusive complexes, while α-catenin links the bound β- and γ-catenin to actin microfilaments of the cellular cytoskeleton.[369] The catenins are thought to have a signaling role through the cytoplasmic adenomatous polyposis coli (APC) protein, which is the product of a tumor suppressor gene mutated in colorectal and other cancers. They are also known to interact with the epidermal growth factor (EGF) and hepatocyte growth factor (HGF) receptors, becoming tyrosine phosphorylated upon activation by these growth factors.[370, 371] A fourth member of the catenin family is p120-catenin (p120). Although it was originally identified as a Src substrate, p120 regulates cell-cell adhesion through its interaction with the cytoplasmic tail of cadherins. It is purported to regulate cadherin turnover at the cell surface, thereby controlling the amount of cadherin available for cell-cell adhesion. p120 also modulates the activities of RhoA, Rac, and Cdc42, suggesting that along with other Src substrates, p120 regulates actin dynamics.[372] Thus, p120, a regulator of cadherin abundance and activity, likely participates in regulating the balance between adhesive and motile cellular phenotypes.

Very little data is available regarding expression of the catenins in melanoma. A relatively small study performed by Zhang et al. demonstrated that there is no correlation between the expression of α-, β-, γ-catenins. However, β- and p120-catenin showed coordinated expression levels. α-catenin exhibited an inverse correlation with tumor thickness, as well as lower expression levels in advanced primary melanoma and metastases.[373] Studies also show that expression of β-catenin is reduced in metastatic

compared with primary melanoma lesions,[100, 362, 374] and reduced β-catenin expression in superficial spreading melanomas is associated with a poor prognosis[375].

Based on our results, all members of the catenin family are associated with improved disease-specific survival. However, expression of β-catenin is most closely associated with outcome. This likely corresponds to the presence of functional cadherin-catenin complexes, representing 'stable' melanoma cells. However, it has also been suggested that β-catenin participates in induction of apoptosis in early lesions and that the expression is lost or down-regulated in the more advanced tumors.[375]

Transcriptional regulation of the genes that are critical in melanoma progression is beginning to be elucidated. Transcription factors that have been implicated in melanoma progression include AP-2, ATF-2, SNAIL, MITF, and NFκB.[376] As demonstrated in chapters two and four, the transcription factors ATF-2 and AP-2 are closely associated with outcome in melanoma.[282, 377] These are likely master regulators in the development of melanoma, with AP-2 inhibiting tumorigenicity and metastasis and ATF-2 promoting these qualities. In fact, AP-2 has been shown to directly affect transcription of c-KIT, MCAM/MUC18, MMP-2, and PAR-1,[378-380] and also influence expression of E-cadherin, p21, HER2, PAI-1, Bcl-2, VEGF, and IGFR-1.[376] ATF-2 has been shown to be associated with tumor growth and metastasis[251, 252] in cell culture and animal models, and its prognostic role in melanoma is demonstrated in this dissertation. MITF, the microophthalmia transcription factor, plays an important role in the differentiation of melanocytes and other neural crest-derived cells. Although its role in this process is still poorly understood, MITF has multiple functions.[381] In the Appendix (Garraway et al. publication in *Nature*[382]) , we show that although protein levels of MITF

are not significantly associated with patient outcome, genetic aberrations (i.e., gains in DNA copy number of the MITF gene detected by fluorescence *in situ* hybridization) predict a poor outcome in metastatic malignant melanoma.

Many factors influence tumor initiation, proliferation, invasion, and metastasis, including alterations in multiple genes affecting cell cycle regulation, cell-cell interaction, adhesion to extracellular matrix, and vascularization. Using an objective measurement of expression levels in a large cohort of melanoma specimens, we have demonstrated some of the most promising prognostic biomarkers in malignant melanoma.

These preliminary analyses demonstrate great promise for predicting metastasis based on molecular information. Sentinel lymph node biopsy only identifies those melanomas that metastasize through the lymphatic system. Melanoma, however, can metastasize through other routes, including direct extension and hematogenous dissemination. In the era before sentinel lymph node biopsy, initial presentation of melanoma metastases occurred in the lymph nodes only 50% of the time, with satellite/in-transit metastases (15-20%) and distant metastases (30-35%) representing the remaining patients who develop metastatic disease.[383, 384] It is likely that the development of metastatic disease through these different pathways represents different biological classes of melanoma; a reasonable explanation for the low sensitivity and high "false negative" rate (up to 25%)[92] of SLNB for melanoma. The goal of our test is to identify those patients who are likely to have (or develop) a metastasis, regardless of their Breslow depth and despite the presence of negative lymph nodes.

Further studies are needed to validate the current models we have constructed and are in the process of constructing. Although the risk test we have developed through

genetic algorithms is intuitive, and easy to apply to future patients (in a prospective fashion), it may be too simple in its current form. Plans are in place to develop more complex models that will impart weightings to the score given to markers, as their contribution to outcome prediction is probably not equal (as the current model assumes). Additionally, patient follow-up on our validation cohort is a work in progress.

References:

1. Rigel DS, Friedman RJ, Kopf AW. The incidence of malignant melanoma in the United States: issues as we approach the 21st century. J Am Acad Dermatol 1996; 34:839-47.
2. Jemal A, Murray T, Ward E, et al. Cancer Statistics, 2005. CA Cancer J Clin 2005; 55:10-30.
3. Weinstock MA. Do sunscreens increase or decrease melanoma risk: an epidemiologic evaluation. J Investig Dermatol Symp Proc 1999; 4:97-100.
4. Slominski A, Wortsman J, Carlson AJ, Matsuoka LY, Balch CM, Mihm MC. Malignant melanoma. Arch Pathol Lab Med 2001; 125:1295-306.
5. Shaw JC. Overview of Melanoma: UptoDate Online, 2003.
6. Bale SJ, Dracopoli NC, Tucker MA, et al. Mapping the gene for hereditary cutaneous malignant melanoma-dysplastic nevus to chromosome 1p. N Engl J Med 1989; 320:1367-72.
7. Cannon-Albright LA, Goldgar DE, Meyer LJ, et al. Assignment of a locus for familial melanoma, MLM, to chromosome 9p13-p22. Science 1992; 258:1148-52.
8. Goldstein AM, Dracopoli NC, Engelstein M, Fraser MC, Clark WH, Jr., Tucker MA. Linkage of cutaneous malignant melanoma/dysplastic nevi to chromosome 9p, and evidence for genetic heterogeneity. Am J Hum Genet 1994; 54:489-96.
9. Soufir N, Avril MF, Chompret A, et al. Prevalence of p16 and CDK4 germline mutations in 48 melanoma-prone families in France. The French Familial Melanoma Study Group. Hum Mol Genet 1998; 7:209-16.
10. Goldstein AM, Struewing JP, Chidambaram A, Fraser MC, Tucker MA. Genotype-phenotype relationships in U.S. melanoma-prone families with CDKN2A and CDK4 mutations. J Natl Cancer Inst 2000; 92:1006-10.
11. Monzon J, Liu L, Brill H, et al. CDKN2A mutations in multiple primary melanomas. N Engl J Med 1998; 338:879-87.
12. Bataille V. Genetics of familial and sporadic melanoma. Clin Exp Dermatol 2000; 25:464-70.
13. Funk JO, Schiller PI, Barrett MT, Wong DJ, Kind P, Sander CA. p16INK4a expression is frequently decreased and associated with 9p21 loss of heterozygosity in sporadic melanoma. J Cutan Pathol 1998; 25:291-6.
14. Cachia AR, Indsto JO, McLaren KM, Mann GJ, Arends MJ. CDKN2A mutation and deletion status in thin and thick primary melanoma. Clin Cancer Res 2000; 6:3511-5.
15. Bittner M, Meltzer P, Chen Y, et al. Molecular classification of cutaneous malignant melanoma by gene expression profiling. Nature 2000; 406:536-40.
16. Rigel DS, Carucci JA. Malignant melanoma: prevention, early detection, and treatment in the 21st century. CA Cancer J Clin 2000; 50:215-36; quiz 237-40.
17. McMasters KM, Sondak VK, Lotze MT, Ross MI. Recent advances in melanoma staging and therapy. Ann Surg Oncol 1999; 6:467-75.
18. Lawson DH. Choices in adjuvant therapy of melanoma. Cancer Control 2005; 12:236-41.

19. Balch CM, Buzaid AC, Soong SJ, et al. Final version of the American Joint Committee on Cancer staging system for cutaneous melanoma. J Clin Oncol 2001; 19:3635-48.
20. Kim SH, Garcia C, Rodriguez J, Coit DG. Prognosis of thick cutaneous melanoma. J Am Coll Surg 1999; 188:241-7.
21. Schubert B, Rudolph P. Basal cell carcinoma: a natural milieu for melanocytes? Am J Dermatopathol 2001; 23:558-60.
22. Chin L, Merlino G, DePinho RA. Malignant melanoma: modern black plague and genetic black box. Genes Dev 1998; 12:3467-81.
23. Bedrosian I, Gershenwald JE. Surgical clinical trials in melanoma. Surg Clin North Am 2003; 83:385-403.
24. Khayat D, Rixe O, Martin G, et al. Surgical margins in cutaneous melanoma (2 cm versus 5 cm for lesions measuring less than 2.1-mm thick). Cancer 2003; 97:1941-6.
25. Pawlik TM, Sondak VK. Malignant melanoma: current state of primary and adjuvant treatment. Crit Rev Oncol Hematol 2003; 45:245-64.
26. Kirkwood JM, Strawderman MH, Ernstoff MS, Smith TJ, Borden EC, Blum RH. Interferon alfa-2b adjuvant therapy of high-risk resected cutaneous melanoma: the Eastern Cooperative Oncology Group Trial EST 1684. J Clin Oncol 1996; 14:7-17.
27. Schuchter LM. Adjuvant interferon therapy for melanoma: high-dose, low-dose, no dose, which dose? J Clin Oncol 2004; 22:7-10.
28. Breslow A. Thickness, cross-sectional areas and depth of invasion in the prognosis of cutaneous melanoma. Ann Surg 1970; 172:902-8.
29. Clark WH, Jr., Ainsworth AM, Bernardino EA, Yang CH, Mihm CM, Jr., Reed RJ. The developmental biology of primary human malignant melanomas. Semin Oncol 1975; 2:83-103.
30. Breslow A. Prognostic factors in the treatment of cutaneous melanoma. J Cutan Pathol 1979; 6:208-12.
31. Zettersten E, Shaikh L, Ramirez R, Kashani-Sabet M. Prognostic factors in primary cutaneous melanoma. Surg Clin North Am 2003; 83:61-75.
32. Austin PF, Cruse CW, Lyman G, Schroer K, Glass F, Reintgen DS. Age as a prognostic factor in the malignant melanoma population. Ann Surg Oncol 1994; 1:487-94.
33. Balch CM, Soong SJ, Bartolucci AA, et al. Efficacy of an elective regional lymph node dissection of 1 to 4 mm thick melanomas for patients 60 years of age and younger. Ann Surg 1996; 224:255-63; discussion 263-6.
34. Schuchter L, Schultz DJ, Synnestvedt M, et al. A prognostic model for predicting 10-year survival in patients with primary melanoma. The Pigmented Lesion Group. Ann Intern Med 1996; 125:369-75.
35. Masback A, Olsson H, Westerdahl J, Ingvar C, Jonsson N. Prognostic factors in invasive cutaneous malignant melanoma: a population-based study and review. Melanoma Res 2001; 11:435-45.
36. Kalady MF, White RR, Johnson JL, Tyler DS, Seigler HF. Thin melanomas: predictive lethal characteristics from a 30-year clinical experience. Ann Surg 2003; 238:528-37.

37. Unger JM, Flaherty LE, Liu PY, Albain KS, Sondak VK. Gender and other survival predictors in patients with metastatic melanoma on Southwest Oncology Group trials. Cancer 2001; 91:1148-55.
38. Slingluff CL, Jr., Vollmer RT, Reintgen DS, Seigler HF. Lethal "thin" malignant melanoma. Identifying patients at risk. Ann Surg 1988; 208:150-61.
39. Clark WH, Jr., Elder DE, Guerry Dt, et al. Model predicting survival in stage I melanoma based on tumor progression. J Natl Cancer Inst 1989; 81:1893-904.
40. Garbe C, Buttner P, Bertz J, et al. Primary cutaneous melanoma. Prognostic classification of anatomic location. Cancer 1995; 75:2492-8.
41. Balch CM, Wilkerson JA, Murad TM, Soong SJ, Ingalls AL, Maddox WA. The prognostic significance of ulceration of cutaneous melanoma. Cancer 1980; 45:3012-7.
42. Balch CM, Soong SJ, Gershenwald JE, et al. Prognostic factors analysis of 17,600 melanoma patients: validation of the American Joint Committee on Cancer melanoma staging system. J Clin Oncol 2001; 19:3622-34.
43. Buzaid AC, Ross MI, Balch CM, et al. Critical analysis of the current American Joint Committee on Cancer staging system for cutaneous melanoma and proposal of a new staging system. J Clin Oncol 1997; 15:1039-51.
44. Finley JW, Gibbs JF, Rodriguez LM, Letourneau R, Driscoll D, Kraybill W. Pathologic and clinical features influencing outcome of thin cutaneous melanoma: correlation with newly proposed staging system. Am Surg 2000; 66:527-31; discussion 531-2.
45. McGovern VJ, Shaw HM, Milton GW, McCarthy WH. Ulceration and prognosis in cutaneous malignant melanoma. Histopathology 1982; 6:399-407.
46. Tompkins VN. Cutaneous melanoma: ulceration as a prognostic sign. Cancer 1953; 6:1215-8.
47. Azzola MF, Shaw HM, Thompson JF, et al. Tumor mitotic rate is a more powerful prognostic indicator than ulceration in patients with primary cutaneous melanoma: an analysis of 3661 patients from a single center. Cancer 2003; 97:1488-98.
48. Massi D, Franchi A, Borgognoni L, Paglierani M, Reali UM, Santucci M. Tumor angiogenesis as a prognostic factor in thick cutaneous malignant melanoma. A quantitative morphologic analysis. Virchows Arch 2002; 440:22-8.
49. Soong SJ, Shaw HM, Balch CM, McCarthy WH, Urist MM, Lee JY. Predicting survival and recurrence in localized melanoma: a multivariate approach. World J Surg 1992; 16:191-5.
50. Buttner P, Garbe C, Bertz J, et al. Primary cutaneous melanoma. Optimized cutoff points of tumor thickness and importance of Clark's level for prognostic classification. Cancer 1995; 75:2499-2506.
51. Balch CM, Soong SJ, Milton GW, et al. A comparison of prognostic factors and surgical results in 1,786 patients with localized (stage I) melanoma treated in Alabama, USA, and New South Wales, Australia. Ann Surg 1982; 196:677-84.
52. Barnhill RL, Fine JA, Roush GC, Berwick M. Predicting five-year outcome for patients with cutaneous melanoma in a population-based study. Cancer 1996; 78:427-32.

53. Breslow A. Tumor thickness, level of invasion and node dissection in stage I cutaneous melanoma. Ann Surg 1975; 182:572-5.
54. Owen SA, Sanders LL, Edwards LJ, Seigler HF, Tyler DS, Grichnik JM. Identification of higher risk thin melanomas should be based on Breslow depth not Clark level IV. Cancer 2001; 91:983-91.
55. Gromet MA, Epstein WL, Blois MS. The regressing thin malignant melanoma: a distinctive lesion with metastatic potential. Cancer 1978; 42:2282-92.
56. Day CL, Jr., Mihm MC, Jr., Sober AJ, et al. Prognostic factors for melanoma patients with lesions 0.76 - 1.69 mm in thickness. An appraisal of "thin" level IV lesions. Ann Surg 1982; 195:30-4.
57. Cooper PH, Wanebo HJ, Hagar RW. Regression in thin malignant melanoma. Microscopic diagnosis and prognostic importance. Arch Dermatol 1985; 121:1127-31.
58. Kelly JW, Sagebiel RW, Clyman S, Blois MS. Thin level IV malignant melanoma. A subset in which level is the major prognostic indicator. Ann Surg 1985; 202:98-103.
59. Jones SK, Pocock PV, Briggs JC. Tumor thickness is not a prognostic factor in thin melanoma. Arch Dermatol Res 1989; 281:81-2.
60. Kuehnl-Petzoldt C, Fischer S. Tumor thickness is not a prognostic factor in thin melanoma. Arch Dermatol Res 1987; 279:487-8.
61. Shaw HM, McCarthy SW, McCarthy WH, Thompson JF, Milton GW. Thin regressing malignant melanoma: significance of concurrent regional lymph node metastases. Histopathology 1989; 15:257-65.
62. Salman SM, Rogers GS. Prognostic factors in thin cutaneous malignant melanoma. J Dermatol Surg Oncol 1990; 16:413-8.
63. Slingluff CL, Jr., Seigler HF. "Thin" malignant melanoma: risk factors and clinical management. Ann Plast Surg 1992; 28:89-94.
64. Moloney DM, Gordon DJ, Briggs JC, Rigby HS. Recurrence of thin melanoma: how effective is follow-up? Br J Plast Surg 1996; 49:409-13.
65. Cook MG, Clarke TJ, Humphreys S, et al. The evaluation of diagnostic and prognostic criteria and the terminology of thin cutaneous malignant melanoma by the CRC Melanoma Pathology Panel. Histopathology 1996; 28:497-512.
66. Vilmer C, Bailly C, Le Doussal V, et al. Thin melanomas with unusual aggressive behavior: a report on nine cases. Melanoma Group of French Federation of Cancer Centers. J Am Acad Dermatol 1996; 34:439-44.
67. Johnson RC, Fenn NJ, Horgan K, Mansel RE. Follow-up of patients with a thin melanoma. Br J Surg 1999; 86:619-21.
68. Fearfield LA, Rowe A, Francis N, Fisher C, Gore ME, Bunker CB. Clinico-pathological features of relapsing very thin melanoma. Clin Exp Dermatol 2001; 26:686-95.
69. Heenan PJ, Taran JM. Re: Cook et al. Identification of histological features associated with metastatic potential in thin (<1.0 mm) cutaneous melanoma with metastases. A study on behalf of the EORTC Melanoma Group. J Pathol 2002; 197: 188-193. J Pathol 2003; 199:132; author reply 132-3.
70. Cook MG, Spatz A, Brocker EB, Ruiter DJ. Identification of histological features associated with metastatic potential in thin (<1.0 mm) cutaneous melanoma with

metastases. A study on behalf of the EORTC Melanoma Group. J Pathol 2002; 197:188-93.
71. Massi D, Franchi A, Santucci M. [Prognostic factors in thin cutaneous malignant melanoma]. Pathologica 2002; 94:282-9.
72. Heenan PJ, Taran JM. Metastasizing thin melanoma or multiple primary melanomas? Arch Dermatol 2003; 139:388; author reply 388-9.
73. Nahabedian MY, Tufaro AP, Manson PN. Sentinel lymph node biopsy for the T1 (thin) melanoma: is it necessary? Ann Plast Surg 2003; 50:601-6.
74. Jacobs IA, Chang CK, DasGupta TK, Salti GI. Role of sentinel lymph node biopsy in patients with thin (<1 mm) primary melanoma. Ann Surg Oncol 2003; 10:558-61.
75. McGovern VJ, Shaw HM, Milton GW. Prognosis in patients with thin malignant melanoma: influence of regression. Histopathology 1983; 7:673-80.
76. McKinnon JG, Yu XQ, McCarthy WH, Thompson JF. Prognosis for patients with thin cutaneous melanoma: long-term survival data from New South Wales Central Cancer Registry and the Sydney Melanoma Unit. Cancer 2003; 98:1223-31.
77. Schneebaum S, Briele HA, Walker MJ, et al. Cutaneous thick melanoma. Prognosis and treatment. Arch Surg 1987; 122:707-11.
78. Zettersten E, Sagebiel RW, Miller JR, 3rd, Tallapureddy S, Leong SP, Kashani-Sabet M. Prognostic factors in patients with thick cutaneous melanoma (> 4 mm). Cancer 2002; 94:1049-56.
79. Salti GI, Kansagra A, Warso MA, Ronan SG, Das Gupta TK. Clinical node-negative thick melanoma. Arch Surg 2002; 137:291-5.
80. Massi D, Borgognoni L, Franchi A, Martini L, Reali UM, Santucci M. Thick cutaneous malignant melanoma: a reappraisal of prognostic factors. Melanoma Res 2000; 10:153-64.
81. Cabanas RM. An approach for the treatment of penile carcinoma. Cancer 1977; 39:456-66.
82. Cook MG, Green MA, Anderson B, et al. The development of optimal pathological assessment of sentinel lymph nodes for melanoma. J Pathol 2003; 200:314-9.
83. Ferrone CR, Panageas KS, Busam K, Brady MS, Coit DG. Multivariate prognostic model for patients with thick cutaneous melanoma: importance of sentinel lymph node status. Ann Surg Oncol 2002; 9:637-45.
84. Cody HS. Sentinel lymph node biopsy. London; Florence, KY: Martin Dunitz; Distributed in the USA by Taylor & Francis, 2002:xiii, 370.
85. Zapas JL, Coley HC, Beam SL, Brown SD, Jablonski KA, Elias EG. The risk of regional lymph node metastases in patients with melanoma less than 1.0 mm thick: recommendations for sentinel lymph node biopsy. J Am Coll Surg 2003; 197:403-7.
86. McMasters KM, Reintgen DS, Ross MI, et al. Sentinel lymph node biopsy for melanoma: controversy despite widespread agreement. J Clin Oncol 2001; 19:2851-5.
87. Messina JL, Glass LF, Cruse CW, Berman C, Ku NK, Reintgen DS. Pathologic examination of the sentinel lymph node in malignant melanoma. Am J Surg Pathol 1999; 23:686-90.

88. Brocker EB, Suter L, Sorg C. HLA-DR antigen expression in primary melanomas of the skin. J Invest Dermatol 1984; 82:244-7.
89. Bruggen J, Brocker EB, Suter L, Redmann K, Sorg C. The expression of tumor-associated antigens in primary and metastatic human malignant melanoma. Behring Inst Mitt 1984:19-23.
90. Balch CM, Buzaid AC, Soong SJ, et al. New TNM melanoma staging system: linking biology and natural history to clinical outcomes. Semin Surg Oncol 2003; 21:43-52.
91. Morton DL, Hoon DS, Cochran AJ, et al. Lymphatic mapping and sentinel lymphadenectomy for early-stage melanoma: therapeutic utility and implications of nodal microanatomy and molecular staging for improving the accuracy of detection of nodal micrometastases. Ann Surg 2003; 238:538-49; discussion 549-50.
92. Leong SP. Paradigm of metastasis for melanoma and breast cancer based on the sentinel lymph node experience. Ann Surg Oncol 2004; 11:192S-7S.
93. Eliopoulos P, Mohammed MQ, Henry K, Retsas S. Overexpression of HER-2 in thick melanoma. Melanoma Res 2002; 12:139-45.
94. Ferrier CM, Suciu S, van Geloof WL, et al. High tPA-expression in primary melanoma of the limb correlates with good prognosis. Br J Cancer 2000; 83:1351-9.
95. Florenes VA, Maelandsmo GM, Faye R, Nesland JM, Holm R. Cyclin A expression in superficial spreading malignant melanomas correlates with clinical outcome. J Pathol 2001; 195:530-6.
96. Florenes VA, Faye RS, Maelandsmo GM, Nesland JM, Holm R. Levels of cyclin D1 and D3 in malignant melanoma: deregulated cyclin D3 expression is associated with poor clinical outcome in superficial melanoma. Clin Cancer Res 2000; 6:3614-20.
97. Florenes VA, Maelandsmo GM, Kerbel RS, Slingerland JM, Nesland JM, Holm R. Protein expression of the cell-cycle inhibitor p27Kip1 in malignant melanoma: inverse correlation with disease-free survival. Am J Pathol 1998; 153:305-12.
98. Gradilone A, Gazzaniga P, Ribuffo D, et al. Survivin, bcl-2, bax, and bcl-X gene expression in sentinel lymph nodes from melanoma patients. J Clin Oncol 2003; 21:306-12.
99. Hieken TJ, Ronan SG, Farolan M, Shilkaitis AL, Das Gupta TK. Molecular prognostic markers in intermediate-thickness cutaneous malignant melanoma. Cancer 1999; 85:375-82.
100. Kageshita T, Hamby CV, Ishihara T, Matsumoto K, Saida T, Ono T. Loss of beta-catenin expression associated with disease progression in malignant melanoma. Br J Dermatol 2001; 145:210-6.
101. Karjalainen JM, Tammi RH, Tammi MI, et al. Reduced level of CD44 and hyaluronan associated with unfavorable prognosis in clinical stage I cutaneous melanoma. Am J Pathol 2000; 157:957-65.
102. Kunz M, Koczan D, Ibrahim SM, Gillitzer R, Gross G, Thiesen HJ. Differential expression of thrombospondin 2 in primary and metastatic malignant melanoma. Acta Derm Venereol 2002; 82:163-9.

103. Massi D, Franchi A, Borgognoni L, Reali UM, Santucci M. Osteonectin expression correlates with clinical outcome in thin cutaneous malignant melanomas. Hum Pathol 1999; 30:339-44.
104. Miranda E, Vizoso F, Martin A, et al. Apolipoprotein D expression in cutaneous malignant melanoma. J Surg Oncol 2003; 83:99-105.
105. Morgan MB, Cowper SE. Expression of p-27 (kip1) in nevi and melanomas. Am J Dermatopathol 1999; 21:121-4.
106. Niezabitowski A, Czajecki K, Rys J, et al. Prognostic evaluation of cutaneous malignant melanoma: a clinicopathologic and immunohistochemical study. J Surg Oncol 1999; 70:150-60.
107. Ostmeier H, Fuchs B, Otto F, et al. Can immunohistochemical markers and mitotic rate improve prognostic precision in patients with primary melanoma? Cancer 1999; 85:2391-9.
108. Ostmeier H, Fuchs B, Otto F, et al. Prognostic immunohistochemical markers of primary human melanomas. Br J Dermatol 2001; 145:203-9.
109. Polsky D, Melzer K, Hazan C, et al. HDM2 protein overexpression and prognosis in primary malignant melanoma. J Natl Cancer Inst 2002; 94:1803-6.
110. Salti GI, Manougian T, Farolan M, Shilkaitis A, Majumdar D, Das Gupta TK. Micropthalmia transcription factor: a new prognostic marker in intermediate-thickness cutaneous malignant melanoma. Cancer Res 2000; 60:5012-6.
111. Sparrow LE, English DR, Taran JM, Heenan PJ. Prognostic significance of MIB-1 proliferative activity in thin melanomas and immunohistochemical analysis of MIB-1 proliferative activity in melanocytic tumors. Am J Dermatopathol 1998; 20:12-6.
112. Straume O, Akslen LA. Importance of vascular phenotype by basic fibroblast growth factor, and influence of the angiogenic factors basic fibroblast growth factor/fibroblast growth factor receptor-1 and ephrin-A1/EphA2 on melanoma progression. Am J Pathol 2002; 160:1009-19.
113. Straume O, Akslen LA. Expresson of vascular endothelial growth factor, its receptors (FLT-1, KDR) and TSP-1 related to microvessel density and patient outcome in vertical growth phase melanomas. Am J Pathol 2001; 159:223-35.
114. Straume O, Akslen LA. Alterations and prognostic significance of p16 and p53 protein expression in subgroups of cutaneous melanoma. Int J Cancer 1997; 74:535-9.
115. Vaisanen A, Kallioinen M, Taskinen PJ, Turpeenniemi-Hujanen T. Prognostic value of MMP-2 immunoreactive protein (72 kD type IV collagenase) in primary skin melanoma. J Pathol 1998; 186:51-8.
116. Carr KM, Bittner M, Trent JM. Gene-expression profiling in human cutaneous melanoma. Oncogene 2003; 22:3076-80.
117. Hoek K, Rimm DL, Williams KR, et al. Expression Profiling Reveals Novel Pathways in the Transformation of Melanocytes to Melanomas. Cancer Res 2004; *accepted, in press (6/22/04).*
118. Eisen MB, Spellman PT, Brown PO, Botstein D. Cluster analysis and display of genome-wide expression patterns. Proc Natl Acad Sci U S A 1998; 95:14863-8.
119. Weeraratna AT, Jiang Y, Hostetter G, et al. Wnt5a signaling directly affects cell motility and invasion of metastatic melanoma. Cancer Cell 2002; 1:279-88.

120. Valery C, Grob JJ, Verrando P. Identification by cDNA microarray technology of genes modulated by artificial ultraviolet radiation in normal human melanocytes: relation to melanocarcinogenesis. J Invest Dermatol 2001; 117:1471-82.
121. Seykora JT, Jih D, Elenitsas R, Horng WH, Elder DE. Gene expression profiling of melanocytic lesions. Am J Dermatopathol 2003; 25:6-11.
122. Dooley TP, Curto EV, Davis RL, Grammatico P, Robinson ES, Wilborn TW. DNA microarrays and likelihood ratio bioinformatic methods: discovery of human melanocyte biomarkers. Pigment Cell Res 2003; 16:245-53.
123. Clark EA, Golub TR, Lander ES, Hynes RO. Genomic analysis of metastasis reveals an essential role for RhoC. Nature 2000; 406:532-5.
124. Ridley A. Molecular switches in metastasis. Nature 2000; 406:466-7.
125. McGill GG, Horstmann M, Widlund HR, et al. Bcl2 regulation by the melanocyte master regulator Mitf modulates lineage survival and melanoma cell viability. Cell 2002; 109:707-18.
126. King R, Weilbaecher KN, McGill G, Cooley E, Mihm M, Fisher DE. Microphthalmia transcription factor. A sensitive and specific melanocyte marker for MelanomaDiagnosis. Am J Pathol 1999; 155:731-8.
127. Dorvault CC, Weilbaecher KN, Yee H, et al. Microphthalmia transcription factor: a sensitive and specific marker for malignant melanoma in cytologic specimens. Cancer 2001; 93:337-43.
128. Cerroni L, Soyer HP, Kerl H. bcl-2 protein expression in cutaneous malignant melanoma and benign melanocytic nevi. Am J Dermatopathol 1995; 17:7-11.
129. Collins KA, White WL. Intercellular adhesion molecule 1 (ICAM-1) and bcl-2 are differentially expressed in early evolving malignant melanoma. Am J Dermatopathol 1995; 17:429-38.
130. Plettenberg A, Ballaun C, Pammer J, et al. Human melanocytes and melanoma cells constitutively express the Bcl-2 proto-oncogene in situ and in cell culture. Am J Pathol 1995; 146:651-9.
131. Rodriguez-Villanueva J, Colome MI, Brisbay S, McDonnell TJ. The expression and localization of bcl-2 protein in normal skin and in non-melanoma skin cancers. Pathol Res Pract 1995; 191:391-8.
132. Tron VA, Krajewski S, Klein-Parker H, Li G, Ho VC, Reed JC. Immunohistochemical analysis of Bcl-2 protein regulation in cutaneous melanoma. Am J Pathol 1995; 146:643-50.
133. Verhaegh ME, Sanders CJ, Arends JW, Neumann HA. Expression of the apoptosis-suppressing protein Bcl-2 in non-melanoma skin cancer. Br J Dermatol 1995; 132:740-4.
134. Grover R, Wilson GD. Bcl-2 expression in malignant melanoma and its prognostic significance. Eur J Surg Oncol 1996; 22:347-9.
135. Jay V, Yi Q, Hunter WS, Zielenska M. Expression of bcl-2 in uveal malignant melanoma. Arch Pathol Lab Med 1996; 120:497-8.
136. Selzer E, Schlagbauer-Wadl H, Okamoto I, Pehamberger H, Potter R, Jansen B. Expression of Bcl-2 family members in human melanocytes, in melanoma metastases and in melanoma cell lines. Melanoma Res 1998; 8:197-203.

137. Radhi JM. Malignant melanoma arising from nevi, p53, p16, and Bcl-2: expression in benign versus malignant components. J Cutan Med Surg 1999; 3:293-7.
138. Leiter U, Schmid RM, Kaskel P, Peter RU, Krahn G. Antiapoptotic bcl-2 and bcl-xL in advanced malignant melanoma. Arch Dermatol Res 2000; 292:225-32.
139. Iervolino A, Trisciuoglio D, Ribatti D, et al. Bcl-2 overexpression in human melanoma cells increases angiogenesis through VEGF mRNA stabilization and HIF-1-mediated transcriptional activity. Faseb J 2002; 16:1453-5.
140. Sviatoha V, Rundgren A, Tani E, Hansson J, Kleina R, Skoog L. Expression of CD40, CD44, bcl-2 antigens and rate of cell proliferation on fine needle aspirates from metastatic melanoma. Cytopathology 2002; 13:11-21.
141. Utikal J, Leiter U, Udart M, Kaskel P, Peter RU, Krahn GM. Expression of c-myc and bcl-2 in primary and advanced cutaneous melanoma. Cancer Invest 2002; 20:914-21.
142. Vlaykova T, Talve L, Hahka-Kemppinen M, et al. Immunohistochemically detectable bcl-2 expression in metastatic melanoma: association with survival and treatment response. Oncology 2002; 62:259-68.
143. Hakansson A, Gustafsson B, Abdiu A, Krysander L, Hakansson L. Bcl-2 expression in metastatic malignant melanoma. Importance for the therapeutic efficacy of biochemotherapy. Cancer Immunol Immunother 2003; 52:249-54.
144. Jansen B, Wacheck V, Heere-Ress E, et al. Chemosensitisation of malignant melanoma by BCL2 antisense therapy. Lancet 2000; 356:1728-33.
145. de Wit NJ, Burtscher HJ, Weidle UH, Ruiter DJ, van Muijen GN. Differentially expressed genes identified in human melanoma cell lines with different metastatic behaviour using high density oligonucleotide arrays. Melanoma Res 2002; 12:57-69.
146. Brem R, Hildebrandt T, Jarsch M, Van Muijen GN, Weidle UH. Identification of metastasis-associated genes by transcriptional profiling of a metastasizing versus a non-metastasizing human melanoma cell line. Anticancer Res 2001; 21:1731-40.
147. Wang E, Miller LD, Ohnmacht GA, et al. Prospective molecular profiling of melanoma metastases suggests classifiers of immune responsiveness. Cancer Res 2002; 62:3581-6.
148. Herlyn M. Molecular targets in melanoma: Strategies and challenges for diagnosis and therapy. Int J Cancer 2005.
149. Kononen J, Bubendorf L, Kallioniemi A, et al. Tissue microarrays for high-throughput molecular profiling of tumor specimens. Nat Med 1998; 4:844-7.
150. Rimm DL, Camp RL, Charette LA, Costa J, Olsen DA, Reiss M. Tissue microarray: a new technology for amplification of tissue resources. Cancer J 2001; 7:24-31.
151. Rimm DL, Camp RL, Charette LA, Olsen DA, Provost E. Amplification of tissue by construction of tissue microarrays. Exp Mol Pathol 2001; 70:255-64.
152. DeVita VT, Hellman S, Rosenberg SA. Cancer, principles & practice of oncology. Philadelphia, PA: Lippincott Williams & Wilkins, 2005:lxxv, 2898.

153. Garcia JF, Camacho FI, Morente M, et al. Hodgkin and Reed-Sternberg cells harbor alterations in the major tumor suppressor pathways and cell-cycle checkpoints: analyses using tissue microarrays. Blood. Vol. 101, 2003:681-9.
154. Hedvat CV, Hegde A, Chaganti RS, et al. Application of tissue microarray technology to the study of non-Hodgkin's and Hodgkin's lymphoma. Hum Pathol. Vol. 33, 2002:968-74.
155. Tzankov A, Zimpfer A, Lugli A, et al. High-throughput tissue microarray analysis of G1-cyclin alterations in classical Hodgkin's lymphoma indicates overexpression of cyclin E1. J Pathol. Vol. 199, 2003:201-7.
156. Ginestier C, Charafe-Jauffret E, Bertucci F, et al. Distinct and complementary information provided by use of tissue and DNA microarrays in the study of breast tumor markers. Am J Pathol. Vol. 161, 2002:1223-33.
157. Torhorst J, Bucher C, Kononen J, et al. Tissue microarrays for rapid linking of molecular changes to clinical endpoints. Am J Pathol. Vol. 159, 2001:2249-56.
158. Sallinen SL, Sallinen PK, Haapasalo HK, et al. Identification of differentially expressed genes in human gliomas by DNA microarray and tissue chip techniques. Cancer Res. Vol. 60, 2000:6617-22.
159. Moch H, Schraml P, Bubendorf L, et al. High-throughput tissue microarray analysis to evaluate genes uncovered by cDNA microarray screening in renal cell carcinoma. Am J Pathol. Vol. 154, 1999:981-6.
160. Nocito A, Bubendorf L, Maria Tinner E, et al. Microarrays of bladder cancer tissue are highly representative of proliferation index and histological grade. J Pathol. Vol. 194, 2001:349-57.
161. Camp RL, Charette LA, Rimm DL. Validation of tissue microarray technology in breast carcinoma. Lab Invest. Vol. 80, 2000:1943-9.
162. Hoos A, Urist MJ, Stojadinovic A, et al. Validation of tissue microarrays for immunohistochemical profiling of cancer specimens using the example of human fibroblastic tumors. Am J Pathol. Vol. 158, 2001:1245-51.
163. Yosepovich A, Kopolovic J. [Tissue microarray technology--a new and powerful tool for the molecular profiling of tumors]. Harefuah. Vol. 141, 2002:1039-41, 1090.
164. Hendriks Y, Franken P, Dierssen JW, et al. Conventional and tissue microarray immunohistochemical expression analysis of mismatch repair in hereditary colorectal tumors. Am J Pathol. Vol. 162, 2003:469-77.
165. Rassidakis GZ, Jones D, Thomaides A, et al. Apoptotic rate in peripheral T-cell lymphomas. A study using a tissue microarray with validation on full tissue sections. Am J Clin Pathol. Vol. 118, 2002:328-34.
166. Mucci NR, Akdas G, Manely S, Rubin MA. Neuroendocrine expression in metastatic prostate cancer: evaluation of high throughput tissue microarrays to detect heterogeneous protein expression. Hum Pathol. Vol. 31, 2000:406-14.
167. Natkunam Y, Warnke RA, Montgomery K, Falini B, van De Rijn M. Analysis of MUM1/IRF4 protein expression using tissue microarrays and immunohistochemistry. Mod Pathol. Vol. 14, 2001:686-94.
168. Rubin MA, Dunn R, Strawderman M, Pienta KJ. Tissue microarray sampling strategy for prostate cancer biomarker analysis. Am J Surg Pathol. Vol. 26, 2002:312-9.

169. Engellau J, Akerman M, Anderson H, et al. Tissue microarray technique in soft tissue sarcoma: immunohistochemical Ki-67 expression in malignant fibrous histiocytoma. Appl Immunohistochem Mol Morphol. Vol. 9, 2001:358-63.
170. Gulmann C, Butler D, Kay E, Grace A, Leader M. Biopsy of a biopsy: validation of immunoprofiling in gastric cancer biopsy tissue microarrays. Histopathology. Vol. 42, 2003:70-6.
171. Fernebro E, Dictor M, Bendahl PO, Ferno M, Nilbert M. Evaluation of the tissue microarray technique for immunohistochemical analysis in rectal cancer. Arch Pathol Lab Med. Vol. 126, 2002:702-5.
172. Merseburger AS, Kuczyk MA, Serth J, et al. Limitations of tissue microarrays in the evaluation of focal alterations of bcl-2 and p53 in whole mount derived prostate tissues. Oncol Rep. Vol. 10, 2003:223-8.
173. Simon R, Mirlacher M, Sauter G. Tissue microarrays in cancer diagnosis. Expert Rev Mol Diagn. Vol. 3, 2003:421-30.
174. Bertheau P, Cazals-Hatem D, Meignin V, et al. Variability of immunohistochemical reactivity on stored paraffin slides. J Clin Pathol. Vol. 51, 1998:370-4.
175. Henson DE. Loss of p53-immunostaining intensity in breast cancer. J Natl Cancer Inst. Vol. 88, 1996:1015-6.
176. Jacobs TW, Prioleau JE, Stillman IE, Schnitt SJ. Loss of tumor marker-immunostaining intensity on stored paraffin slides of breast cancer. J Natl Cancer Inst. Vol. 88, 1996:1054-9.
177. van den Broek LJ, van de Vijver MJ. Assessment of problems in diagnostic and research immunohistochemistry associated with epitope instability in stored paraffin sections. Appl Immunohistochem Mol Morphol. Vol. 8, 2000:316-21.
178. Fergenbaum JH, Garcia-Closas M, Hewitt SM, Lissowska J, Sakoda LC, Sherman ME. Loss of antigenicity in stored sections of breast cancer tissue microarrays. Cancer Epidemiol Biomarkers Prev. Vol. 13, 2004:667-72.
179. DiVito KA, Charette LA, Rimm DL, Camp RL. Long-term preservation of antigenicity on tissue microarrays. Lab Invest, 2004.
180. Sen Gupta R, Hillemann D, Kubica T, et al. HOPE-fixation enables improved PCR-based detection and differentiation of Mycobacterium tuberculosis complex in paraffin-embedded tissues. Pathol Res Pract. Vol. 199, 2003:619-23.
181. Wester K, Asplund A, Backvall H, et al. Zinc-based fixative improves preservation of genomic DNA and proteins in histoprocessing of human tissues. Lab Invest. Vol. 83, 2003:889-99.
182. Beckstead JH. A simple technique for preservation of fixation-sensitive antigens in paraffin-embedded tissues. J Histochem Cytochem. Vol. 42, 1994:1127-34.
183. Gillespie JW, Best CJ, Bichsel VE, et al. Evaluation of non-formalin tissue fixation for molecular profiling studies. Am J Pathol. Vol. 160, 2002:449-57.
184. Ahram M, Flaig MJ, Gillespie JW, et al. Evaluation of ethanol-fixed, paraffin-embedded tissues for proteomic applications. Proteomics. Vol. 3, 2003:413-21.
185. Vincek V, Nassiri M, Nadji M, Morales AR. A tissue fixative that protects macromolecules (DNA, RNA, and protein) and histomorphology in clinical samples. Lab Invest. Vol. 83, 2003:1427-35.

186. DiVito KA, Charette LA, Rimm DL, Camp RL. Long-term preservation of antigenicity on tissue microarrays. Lab Invest 2004; 84:1071-8.
187. Gown AM. Unmasking the mysteries of antigen or epitope retrieval and formalin fixation. Am J Clin Pathol. Vol. 121, 2004:172-4.
188. Fraenkel-Conrat H, Brandon B, Olcott H. The reaction of formaldehyde with proteins, IV: participation of indole groups: gramicidin. J Biol Chem. Vol. 168, 1947:99-118.
189. Fox CH, Johnson FB, Whiting J, Roller PP. Formaldehyde fixation. J Histochem Cytochem. Vol. 33, 1985:845-53.
190. Sompuram SR, Vani K, Messana E, Bogen SA. A molecular mechanism of formalin fixation and antigen retrieval. Am J Clin Pathol. Vol. 121, 2004:190-9.
191. Shi S-R, Gu J, Turrens J. Development of the antigen retrieval technique: philosophical and theoretical bases. In: Taylor C, ed. Antigen Retrieval Techniques: Immunohistochemistry & Molecular Morphology. Natick, MA: Eaton Publishing, 2000:17-40.
192. Shi S-R, Cote RJ, Taylor CR. Antigen Retrieval Techniques: Current Perspectives. J. Histochem. Cytochem. Vol. 49, 2001:931-938.
193. Larsson L-I. Immunocytochemistry : theory and practice. Boca Raton, Fla.: CRC Press, 1988:272 p., [2] p. of plates.
194. Huang SN, Minassian H, More JD. Application of immunofluorescent staining on paraffin sections improved by trypsin digestion. Lab Invest. Vol. 35, 1976:383-90.
195. Key M. Antigen Retrieval. Vol. 2004: Dakocytomation.
196. Shi SR, Key ME, Kalra KL. Antigen retrieval in formalin-fixed, paraffin-embedded tissues: an enhancement method for immunohistochemical staining based on microwave oven heating of tissue sections. J Histochem Cytochem. Vol. 39, 1991:741-8.
197. Shi SR, Cote RJ, Taylor CR. Antigen retrieval techniques: current perspectives. J Histochem Cytochem. Vol. 49, 2001:931-7.
198. Shi SR, Cote C, Kalra KL, Taylor CR, Tandon AK. A technique for retrieving antigens in formalin-fixed, routinely acid-decalcified, celloidin-embedded human temporal bone sections for immunohistochemistry. J Histochem Cytochem. Vol. 40, 1992:787-92.
199. Shi SR, Cote RJ, Taylor CR. Antigen retrieval immunohistochemistry: past, present, and future. J Histochem Cytochem. Vol. 45, 1997:327-43.
200. Cattoretti G, Pileri S, Parravicini C, et al. Antigen unmasking on formalin-fixed, paraffin-embedded tissue sections. J Pathol. Vol. 171, 1993:83-98.
201. Shiurba RA, Spooner ET, Ishiguro K, et al. Immunocytochemistry of formalin-fixed human brain tissues: microwave irradiation of free-floating sections. Brain Res Brain Res Protoc. Vol. 2, 1998:109-19.
202. Morgan JM, Navabi H, Jasani B. Role of calcium chelation in high-temperature antigen retrieval at different pH values. J Pathol. Vol. 182, 1997:233-7.
203. Morgan JM, Navabi H, Schmid KW, Jasani B. Possible role of tissue-bound calcium ions in citrate-mediated high-temperature antigen retrieval. J Pathol. Vol. 174, 1994:301-7.

204. Rait VK, Xu L, O'Leary TJ, Mason JT. Modeling formalin fixation and antigen retrieval with bovine pancreatic RNase A II. Interrelationship of cross-linking, immunoreactivity, and heat treatment. Lab Invest. Vol. 84, 2004:300-6.
205. Rait VK, O'Leary TJ, Mason JT. Modeling formalin fixation and antigen retrieval with bovine pancreatic ribonuclease A: I-structural and functional alterations. Lab Invest. Vol. 84, 2004:292-9.
206. Boenisch T. Formalin-fixed and heat-retrieved tissue antigens: a comparison of their immunoreactivity in experimental antibody diluents. Appl Immunohistochem Mol Morphol. Vol. 9, 2001:176-9.
207. Mowry RW. Report from the president. The biological stain commission: its goals, its past and its present status. Stain Technol. Vol. 55, 1980:1-7.
208. Coons AH, Creech HJ, Jones RN. Immunological propterties of an antibody containing a fluorescent group. Proc. Soc. Exp. Biol. Med. Vol. 47, 1941:200-202.
209. DeLellis RA, Sternberger LA, Mann RB, Banks PM, Nakane PK. Immunoperoxidase technics in diagnostic pathology. Report of a workshop sponsored by the National Cancer Institute. Am J Clin Pathol. Vol. 71, 1979:483-8.
210. Shi S-R, Gu J, Cote C, Taylor C. Standardization of Routine Immunohistochemistry: Where to begin? In: Taylor C, ed. Antigen Retrieval Techniques: Immunohistochemistry & Molecular Morphology. Natick, MA: Eaton Publishing, 2000:255-272.
211. Taylor CR. Immunomicroscopy: A Diagnostic Tool for the Surgical Pathologist. Philadelphia: WB Saunders Co, 1986.
212. Taylor CR. Immunohistologic studies of lymphoma: past, present, and future. J Histochem Cytochem. Vol. 28, 1980:777-87.
213. Taylor CR. The total test approach to standardization of immunohistochemistry. Arch Pathol Lab Med. Vol. 124, 2000:945-51.
214. Yaziji H, Goldstein LC, Barry TS, et al. HER-2 testing in breast cancer using parallel tissue-based methods. Jama. Vol. 291, 2004:1972-7.
215. Taylor CR. An exaltation of experts: concerted efforts in the standardization of immunohistochemistry. Hum Pathol. Vol. 25, 1994:2-11.
216. McCarty KS, Jr., Szabo E, Flowers JL, et al. Use of a monoclonal anti-estrogen receptor antibody in the immunohistochemical evaluation of human tumors. Cancer Res. Vol. 46, 1986:4244s-4248s.
217. Harvey JM, Clark GM, Osborne CK, Allred DC. Estrogen receptor status by immunohistochemistry is superior to the ligand-binding assay for predicting response to adjuvant endocrine therapy in breast cancer. J Clin Oncol. Vol. 17, 1999:1474-81.
218. Kay EW, Walsh CJ, Cassidy M, Curran B, Leader M. C-erbB-2 immunostaining: problems with interpretation. J Clin Pathol. Vol. 47, 1994:816-22.
219. Thomson TA, Hayes MM, Spinelli JJ, et al. HER-2/neu in breast cancer: interobserver variability and performance of immunohistochemistry with 4 antibodies compared with fluorescent in situ hybridization. Mod Pathol. Vol. 14, 2001:1079-86.

220. Oberholzer M, Ostreicher M, Christen H, Bruhlmann M. Methods in quantitative image analysis. Histochemistry & Cell Biology. Vol. 105, 1996:333-55.
221. Bacus S, Flowers JL, Press MF, Bacus JW, McCarty KS, Jr. The evaluation of estrogen receptor in primary breast carcinoma by computer-assisted image analysis. Am J Clin Pathol. Vol. 90, 1988:233-9.
222. Liu CL, Prapong W, Natkunam Y, et al. Software Tools for High-Throughput Analysis and Archiving of Immunohistochemistry Staining Data Obtained with Tissue Microarrays. Am J Pathol. Vol. 161, 2002:1557-1565.
223. Vrolijk H, Sloos W, Mesker W, et al. Automated Acquisition of Stained Tissue Microarrays for High-Throughput Evaluation of Molecular Targets. J Mol Diagn. Vol. 5, 2003:160-167.
224. Matkowskyj KA, Cox R, Jensen RT, Benya RV. Quantitative Immunohistochemistry by Measuring Cumulative Signal Strength Accurately Measures Receptor Number. J. Histochem. Cytochem. Vol. 51, 2003:205-214.
225. Matkowskyj KA, Schonfeld D, Benya RV. Quantitative Immunohistochemistry by Measuring Cumulative Signal Strength Using Commercially Available Software Photoshop and Matlab. J. Histochem. Cytochem. Vol. 48, 2000:303-312.
226. Camp RL, Chung GG, Rimm DL. Automated subcellular localization and quantification of protein expression in tissue microarrays. Nat Med. Vol. 8, 2002:1323-7.
227. Matthews DE, Farewell VT. Using and understanding medical statistics. Basel ; New York: Karger, 1996:xiii, 246.
228. Kaplan EL, Meier, P. Nonparametric estimation from incomplete observations. J Am Stat Assoc 1958; 53:457-481.
229. Alizadeh AA, Eisen MB, Davis RE, et al. Distinct types of diffuse large B-cell lymphoma identified by gene expression profiling. Nature 2000; 403:503-11.
230. Bhattacharjee A, Richards WG, Staunton J, et al. Classification of human lung carcinomas by mRNA expression profiling reveals distinct adenocarcinoma subclasses. Proc Natl Acad Sci U S A 2001; 98:13790-5.
231. Sorlie T, Perou CM, Tibshirani R, et al. Gene expression patterns of breast carcinomas distinguish tumor subclasses with clinical implications. Proc Natl Acad Sci U S A 2001; 98:10869-74.
232. Beer DG, Kardia SL, Huang CC, et al. Gene-expression profiles predict survival of patients with lung adenocarcinoma. Nat Med 2002; 8:816-24.
233. Lapointe J, Li C, Higgins JP, et al. Gene expression profiling identifies clinically relevant subtypes of prostate cancer. Proc Natl Acad Sci U S A 2004; 101:811-6.
234. van de Vijver MJ, He YD, van't Veer LJ, et al. A gene-expression signature as a predictor of survival in breast cancer. N Engl J Med 2002; 347:1999-2009.
235. Shipp MA, Ross KN, Tamayo P, et al. Diffuse large B-cell lymphoma outcome prediction by gene-expression profiling and supervised machine learning. Nat Med 2002; 8:68-74.
236. van 't Veer LJ, Dai H, van de Vijver MJ, et al. Expression profiling predicts outcome in breast cancer. Breast Cancer Res 2003; 5:57-8.
237. van 't Veer LJ, Dai H, van de Vijver MJ, et al. Gene expression profiling predicts clinical outcome of breast cancer. Nature 2002; 415:530-6.

238. Bair E, Tibshirani R. Semi-supervised methods to predict patient survival from gene expression data. PLoS Biol 2004; 2:E108.
239. Zhang DH, Salto-Tellez M, Chiu LL, Shen L, Koay ES. Tissue microarray study for classification of breast tumors. Life Sci 2003; 73:3189-99.
240. Makretsov N, Gilks CB, Coldman AJ, Hayes M, Huntsman D. Tissue microarray analysis of neuroendocrine differentiation and its prognostic significance in breast cancer. Hum Pathol 2003; 34:1001-8.
241. Korsching E, Packeisen J, Agelopoulos K, et al. Cytogenetic alterations and cytokeratin expression patterns in breast cancer: integrating a new model of breast differentiation into cytogenetic pathways of breast carcinogenesis. Lab Invest 2002; 82:1525-33.
242. Jacquemier J, Ginestier C, Rougemont J, et al. Protein expression profiling identifies subclasses of breast cancer and predicts prognosis. Cancer Res 2005; 65:767-79.
243. Makretsov NA, Huntsman DG, Nielsen TO, et al. Hierarchical clustering analysis of tissue microarray immunostaining data identifies prognostically significant groups of breast carcinoma. Clin Cancer Res 2004; 10:6143-51.
244. Holland JH. Adaptation in natural and artificial systems : an introductory analysis with applications to biology, control, and artificial intelligence. Ann Arbor: University of Michigan Press, 1975:viii, 183.
245. Mitchell M. An Introduction to Genetic Algorithms. Cambridge, Massachusetts: MIT Press, 1998.
246. Reeves CR, Rowe JE. Genetic algorithms : principles and perspectives : a guide to GA theory. Operations research/computer science interfaces series ; ORCS 20. Boston: Kluwer Academic Publishers, 2003:vii, 332.
247. Vose MD. The simple genetic algorithm : foundations and theory. Complex adaptive systems. Cambridge, Mass.: MIT Press, 1999:ix, 251.
248. Camp RL, Dolled-Filhart M, Rimm DL. X-Tile: A New Bio-Informatics Tool for Biomarker Assessment and Outcome-Based Cut-Point Optimization. Clin Cancer Res 2004; 10:7252-7259.
249. Hastie T, Tibshirani R, Friedman JH. The elements of statistical learning : data mining, inference, and prediction : with 200 full-color illustrations. Springer series in statistics. New York: Springer, 2001:xvi, 533.
250. Li N, Mangini J, Bhawan J. New prognostic factors of cutaneous melanoma: a review of the literature. J Cutan Pathol 2002; 29:324-40.
251. Jean D, Harbison M, McConkey DJ, Ronai Z, Bar-Eli M. CREB and its associated proteins act as survival factors for human melanoma cells. J Biol Chem 1998; 273:24884-90.
252. Xie S, Price JE, Luca M, Jean D, Ronai Z, Bar-Eli M. Dominant-negative CREB inhibits tumor growth and metastasis of human melanoma cells. Oncogene 1997; 15:2069-75.
253. van Dam H, Duyndam M, Rottier R, et al. Heterodimer formation of cJun and ATF-2 is responsible for induction of c-jun by the 243 amino acid adenovirus E1A protein. Embo J 1993; 12:479-87.
254. Galcheva-Gargova Z, Derijard B, Wu IH, Davis RJ. An osmosensing signal transduction pathway in mammalian cells. Science 1994; 265:806-8.

255. Fuchs SY, Tappin I, Ronai Z. Stability of the ATF2 transcription factor is regulated by phosphorylation and dephosphorylation. J Biol Chem 2000; 275:12560-4.
256. Kaszubska W, Hooft van Huijsduijnen R, Ghersa P, et al. Cyclic AMP-independent ATF family members interact with NF-kappa B and function in the activation of the E-selectin promoter in response to cytokines. Mol Cell Biol 1993; 13:7180-90.
257. Kim SJ, Wagner S, Liu F, O'Reilly MA, Robbins PD, Green MR. Retinoblastoma gene product activates expression of the human TGF-beta 2 gene through transcription factor ATF-2. Nature 1992; 358:331-4.
258. Fuchs SY, Ronai Z. Ubiquitination and degradation of ATF2 are dimerization dependent. Mol Cell Biol 1999; 19:3289-98.
259. Ronai Z, Yang YM, Fuchs SY, Adler V, Sardana M, Herlyn M. ATF2 confers radiation resistance to human melanoma cells. Oncogene 1998; 16:523-31.
260. Yang YM, Dolan LR, Ronai Z. Expression of dominant negative CREB reduces resistance to radiation of human melanoma cells. Oncogene 1996; 12:2223-33.
261. Ivanov VN, Ronai Z. p38 protects human melanoma cells from UV-induced apoptosis through down-regulation of NF-kappaB activity and Fas expression. Oncogene 2000; 19:3003-12.
262. Bhoumik A, Ivanov V, Ronai Z. Activating transcription factor 2-derived peptides alter resistance of human tumor cell lines to ultraviolet irradiation and chemical treatment. Clin Cancer Res 2001; 7:331-42.
263. Bhoumik A, Huang TG, Ivanov V, et al. An ATF2-derived peptide sensitizes melanomas to apoptosis and inhibits their growth and metastasis. J Clin Invest 2002; 110:643-50.
264. van Dam H, Castellazzi M. Distinct roles of Jun : Fos and Jun : ATF dimers in oncogenesis. Oncogene 2001; 20:2453-64.
265. Ivanov VN, Krasilnikov M, Ronai Z. Regulation of Fas expression by STAT3 and c-Jun is mediated by phosphatidylinositol 3-kinase-AKT signaling. J Biol Chem 2002; 277:4932-44.
266. Davies H, Bignell GR, Cox C, et al. Mutations of the BRAF gene in human cancer. Nature 2002; 417:949-54.
267. Ries LAG, Eisner MP, Kosary CL, et al. SEER Cancer Statistics Review, 1975-2001. Vol. 2004. Bethdesda, MD: National Cancer Institute, 2004.
268. Jemal A, Thomas A, Murray T, Thun M. Cancer statistics, 2002. CA Cancer J Clin 2002; 52:23-47.
269. Alonso SR, Ortiz P, Pollan M, et al. Progression in cutaneous malignant melanoma is associated with distinct expression profiles: a tissue microarray-based study. Am J Pathol 2004; 164:193-203.
270. Korabiowska M, Bauer H, Quentin T, Stachura J, Cordon-Cardo C, Brinck U. Application of new in situ hybridization probes for Ku70 and Ku80 in tissue microarrays of paraffin-embedded malignant melanomas: correlation with immunohistochemical analysis. Hum Pathol 2004; 35:210-6.
271. Camp RL, Chung GG, Rimm DL. Automated subcellular localization and quantification of protein expression in tissue microarrays. Nat Med 2002; 8:1323-7.

272. Camp RL, Dolled-Filhart M, King BL, Rimm DL. Quantitative analysis of breast cancer tissue microarrays shows that both high and normal levels of HER2 expression are associated with poor outcome. Cancer Res 2003; 63:1445-8.
273. Rubin MA, Zerkowski, M.P., Camp, R.L., Kuefer, R., Hofer, M.D., Chinnaiyan, A.M., Rimm, D.L. Quantitative determination of expression of the prostate alpha-methylacyl-CoA racemase using automated quantitative analysis (AQUA): a novel paradigm for automated and continuous biomarker measurements. Am J Pathol 2004; 164:831-40.
274. Smoller BR. Immunohistochemistry in the diagnosis of melanocytic neoplasms. Pathology (Phila) 1994; 2:371-83.
275. Dabbs DJ. Diagnostic Immunohistochemistry. Philadelphia: Churchill Livingstone, 2002.
276. Vogelstein B, Lane D, Levine AJ. Surfing the p53 network. Nature 2000; 408:307-10.
277. Michael D, Oren M. The p53-Mdm2 module and the ubiquitin system. Semin Cancer Biol 2003; 13:49-58.
278. Piette J, Neel H, Marechal V. Mdm2: keeping p53 under control. Oncogene 1997; 15:1001-10.
279. Onel K, Cordon-Cardo C. MDM2 and prognosis. Mol Cancer Res 2004; 2:1-8.
280. Hernberg M, Turunen JP, von Boguslawsky K, Muhonen T, Pyrhonen S. Prognostic value of biomarkers in malignant melanoma. Melanoma Res 1998; 8:283-91.
281. Sauroja I, Smeds J, Vlaykova T, et al. Analysis of G(1)/S checkpoint regulators in metastatic melanoma. Genes Chromosomes Cancer 2000; 28:404-14.
282. Berger AJ, Kluger HM, Li N, et al. Subcellular localization of activating transcription factor 2 in melanoma specimens predicts patient survival. Cancer Res 2003; 63:8103-7.
283. Matsumura T, Yoshihama Y, Kimura T, Shintani S, Alcalde RE. p53 and MDM2 expression in oral squamous cell carcinoma. Oncology 1996; 53:308-12.
284. Pilotti S, Della Torre G, Lavarino C, et al. Distinct mdm2/p53 expression patterns in liposarcoma subgroups: implications for different pathogenetic mechanisms. J Pathol 1997; 181:14-24.
285. Higashiyama M, Doi O, Kodama K, et al. MDM2 gene amplification and expression in non-small-cell lung cancer: immunohistochemical expression of its protein is a favourable prognostic marker in patients without p53 protein accumulation. Br J Cancer 1997; 75:1302-8.
286. Camp RL, Charette LA, Rimm DL. Validation of tissue microarray technology in breast carcinoma. Lab Invest 2000; 80:1943-9.
287. Torhorst J, Bucher C, Kononen J, et al. Tissue microarrays for rapid linking of molecular changes to clinical endpoints. Am J Pathol 2001; 159:2249-56.
288. Lahav G, Rosenfeld N, Sigal A, et al. Dynamics of the p53-Mdm2 feedback loop in individual cells. Nat Genet 2004; 36:147-50.
289. Ganguli G, Wasylyk B. p53-independent functions of MDM2. Mol Cancer Res 2003; 1:1027-35.
290. Iwakuma T, Lozano G. MDM2, an introduction. Mol Cancer Res 2003; 1:993-1000.

291. Moll UM, Zaika A. Nuclear and mitochondrial apoptotic pathways of p53. FEBS Lett 2001; 493:65-9.
292. Ferbeyre G, de Stanchina E, Lin AW, et al. Oncogenic ras and p53 cooperate to induce cellular senescence. Mol Cell Biol 2002; 22:3497-508.
293. Serrano M, Lin AW, McCurrach ME, Beach D, Lowe SW. Oncogenic ras provokes premature cell senescence associated with accumulation of p53 and p16INK4a. Cell 1997; 88:593-602.
294. Olsen CL, Gardie B, Yaswen P, Stampfer MR. Raf-1-induced growth arrest in human mammary epithelial cells is p16-independent and is overcome in immortal cells during conversion. Oncogene 2002; 21:6328-39.
295. O'Reilly LA, Huang DC, Strasser A. The cell death inhibitor Bcl-2 and its homologues influence control of cell cycle entry. Embo J 1996; 15:6979-90.
296. Deb SP. Cell cycle regulatory functions of the human oncoprotein MDM2. Mol Cancer Res 2003; 1:1009-16.
297. Jemal A, Murray T, Ward E, et al. Cancer statistics, 2005. CA Cancer J Clin. Vol. 55, 2005:10-30.
298. Breslow A. Thickness, cross-sectional areas and depth of invasion in the prognosis of cutaneous melanoma. Ann Surg. Vol. 172, 1970:902-8.
299. Clark WH, Jr., Ainsworth AM, Bernardino EA, Yang CH, Mihm CM, Jr., Reed RJ. The developmental biology of primary human malignant melanomas. Semin Oncol. Vol. 2, 1975:83-103.
300. Tellez C, McCarty M, Ruiz M, Bar-Eli M. Loss of activator protein-2alpha results in overexpression of protease-activated receptor-1 and correlates with the malignant phenotype of human melanoma. J Biol Chem. Vol. 278, 2003:46632-42.
301. Bar-Eli M. Gene regulation in melanoma progression by the AP-2 transcription factor. Pigment Cell Res. Vol. 14, 2001:78-85.
302. Gershenwald JE, Sumner W, Calderone T, Wang Z, Huang S, Bar-Eli M. Dominant-negative transcription factor AP-2 augments SB-2 melanoma tumor growth in vivo. Oncogene. Vol. 20, 2001:3363-75.
303. Jean D, Gershenwald JE, Huang S, et al. Loss of AP-2 results in up-regulation of MCAM/MUC18 and an increase in tumor growth and metastasis of human melanoma cells. J Biol Chem. Vol. 273, 1998:16501-8.
304. Huang S, Luca M, Gutman M, et al. Enforced c-KIT expression renders highly metastatic human melanoma cells susceptible to stem cell factor-induced apoptosis and inhibits their tumorigenic and metastatic potential. Oncogene. Vol. 13, 1996:2339-47.
305. Huang S, Jean D, Luca M, Tainsky MA, Bar-Eli M. Loss of AP-2 results in downregulation of c-KIT and enhancement of melanoma tumorigenicity and metastasis. Embo J. Vol. 17, 1998:4358-69.
306. Baldi A, Santini D, Battista T, et al. Expression of AP-2 transcription factor and of its downstream target genes c-kit, E-cadherin and p21 in human cutaneous melanoma. J Cell Biochem. Vol. 83, 2001:364-72.
307. Nyormoi O, Wang Z, Doan D, Ruiz M, McConkey D, Bar-Eli M. Transcription factor AP-2alpha is preferentially cleaved by caspase 6 and degraded by

proteasome during tumor necrosis factor alpha-induced apoptosis in breast cancer cells. Mol Cell Biol. Vol. 21, 2001:4856-67.
308. Bar-Eli M. Molecular mechanisms of melanoma metastasis. J Cell Physiol. Vol. 173, 1997:275-8.
309. Karjalainen JM, Kellokoski JK, Eskelinen MJ, Alhava EM, Kosma VM. Downregulation of transcription factor AP-2 predicts poor survival in stage I cutaneous malignant melanoma. J Clin Oncol. Vol. 16, 1998:3584-91.
310. Kononen J, Bubendorf L, Kallioniemi A, et al. Tissue microarrays for high-throughput molecular profiling of tumor specimens. Nat Med. Vol. 4, 1998:844-7.
311. Rimm DL, Camp RL, Charette LA, Costa J, Olsen DA, Reiss M. Tissue microarray: a new technology for amplification of tissue resources. Cancer J. Vol. 7, 2001:24-31.
312. Cordon-Cardo C. Mutations of cell cycle regulators. Biological and clinical implications for human neoplasia. Am J Pathol. Vol. 147, 1995:545-60.
313. Schraml P, Kononen J, Bubendorf L, et al. Tissue microarrays for gene amplification surveys in many different tumor types. Clin Cancer Res. Vol. 5, 1999:1966-75.
314. Camp RL, Chung GG, Rimm DL. Automated subcellular localization and quantification of protein expression in tissue microarrays. Nat Med. Vol. 8, 2002:1323-7.
315. Berger AJ, Camp RL, Divito KA, Kluger HM, Halaban R, Rimm DL. Automated quantitative analysis of HDM2 expression in malignant melanoma shows association with early-stage disease and improved outcome. Cancer Res. Vol. 64, 2004:8767-72.
316. Shen SS, Zhang PS, Eton O, Prieto VG. Analysis of protein tyrosine kinase expression in melanocytic lesions by tissue array. J Cutan Pathol. Vol. 30, 2003:539-47.
317. Davis DW, Shen Y, Mullani NA, et al. Quantitative analysis of biomarkers defines an optimal biological dose for recombinant human endostatin in primary human tumors. Clin Cancer Res 2004; 10:33-42.
318. Kawakami Y, Battles JK, Kobayashi T, et al. Production of recombinant MART-1 proteins and specific antiMART-1 polyclonal and monoclonal antibodies: use in the characterization of the human melanoma antigen MART-1. J Immunol Methods. Vol. 202, 1997:13-25.
319. Coulie PG, Brichard V, Van Pel A, et al. A new gene coding for a differentiation antigen recognized by autologous cytolytic T lymphocytes on HLA-A2 melanomas. J Exp Med. Vol. 180, 1994:35-42.
320. Smoller BR. Immunohistochemistry in the diagnosis of melanocytic neoplasms. Pathology (Phila). Vol. 2, 1994:371-83.
321. Divito KA, Berger AJ, Camp RL, Dolled-Filhart M, Rimm DL, Kluger HM. Automated quantitative analysis of tissue microarrays reveals an association between high Bcl-2 expression and improved outcome in melanoma. Cancer Res. Vol. 64, 2004:8773-7.
322. Berset M, Cerottini JP, Guggisberg D, et al. Expression of Melan-A/MART-1 antigen as a prognostic factor in primary cutaneous melanoma. Int J Cancer. Vol. 95, 2001:73-7.

323. Davis DW, McConkey DJ, Zhang W, Herbst RS. Antiangiogenic tumor therapy. Biotechniques. Vol. 34, 2003:1048-50, 1052, 1054 passim.
324. Clark WH, Jr., From L, Bernardino EA, Mihm MC. The histogenesis and biologic behavior of primary human malignant melanomas of the skin. Cancer Res 1969; 29:705-27.
325. Kielhorn E, Provost E, Olsen D, et al. Tissue microarray-based analysis shows phospho-beta-catenin expression in malignant melanoma is associated with poor outcome. Int J Cancer 2003; 103:652-6.
326. DiVito KA, A.J. B, Camp RL, Dolled-Filhart M, Rimm DL, Kluger HM. Automated Quantitative Analysis (AQUA) of Tissue Microarrays Reveals an Association between High Bcl-2 Expression and Improved Outcome in Melanoma. Cancer Res 2004; *submitted July 12, 2004.*
327. Berger AJ, Camp RL, Di Vito KA, Kluger HM, Halaban R, Rimm DL. Automated Quantitative Analysis (AQUA) of HDM2 Expression in Malignant Melanoma Shows Association with Metastasis and Poor Outcome. Cancer Res 2004; *submitted July 12, 2004.*
328. Bleicher RJ, Essner R, Foshag LJ, Wanek LA, Morton DL. Role of sentinel lymphadenectomy in thin invasive cutaneous melanomas. J Clin Oncol 2003; 21:1326-31.
329. Leong SP. Sentinel lymph node mapping and selective lymphadenectomy: the standard of care for melanoma. Curr Treat Options Oncol 2004; 5:185-94.
330. Perou CM, Sorlie T, Eisen MB, et al. Molecular portraits of human breast tumours. Nature 2000; 406:747-52.
331. Loftus SK, Chen Y, Gooden G, et al. Informatic selection of a neural crest-melanocyte cDNA set for microarray analysis. Proc Natl Acad Sci U S A 1999; 96:9277-80.
332. Weeraratna AT, Becker D, Carr KM, et al. Generation and analysis of melanoma SAGE libraries: SAGE advice on the melanoma transcriptome. Oncogene 2004; 23:2264-74.
333. Sauter ER, Yeo UC, von Stemm A, et al. Cyclin D1 is a candidate oncogene in cutaneous melanoma. Cancer Res 2002; 62:3200-6.
334. Grana X, Reddy EP. Cell cycle control in mammalian cells: role of cyclins, cyclin dependent kinases (CDKs), growth suppressor genes and cyclin-dependent kinase inhibitors (CKIs). Oncogene 1995; 11:211-9.
335. Serrano M, Hannon GJ, Beach D. A new regulatory motif in cell-cycle control causing specific inhibition of cyclin D/CDK4. Nature 1993; 366:704-7.
336. Flores JF, Walker GJ, Glendening JM, et al. Loss of the p16INK4a and p15INK4b genes, as well as neighboring 9p21 markers, in sporadic melanoma. Cancer Res 1996; 56:5023-32.
337. Walker GJ, Flores JF, Glendening JM, Lin AH, Markl ID, Fountain JW. Virtually 100% of melanoma cell lines harbor alterations at the DNA level within CDKN2A, CDKN2B, or one of their downstream targets. Genes Chromosomes Cancer 1998; 22:157-63.
338. Sharpless E, Chin L. The INK4a/ARF locus and melanoma. Oncogene 2003; 22:3092-8.

339. Mihic-Probst D, Saremaslani P, Komminoth P, Heitz PU. Immunostaining for the tumour suppressor gene p16 product is a useful marker to differentiate melanoma metastasis from lymph-node nevus. Virchows Arch 2003; 443:745-51.
340. Wang YL, Uhara H, Yamazaki Y, Nikaido T, Saida T. Immunohistochemical detection of CDK4 and p16INK4 proteins in cutaneous malignant melanoma. Br J Dermatol 1996; 134:269-75.
341. Straume O, Sviland L, Akslen LA. Loss of nuclear p16 protein expression correlates with increased tumor cell proliferation (Ki-67) and poor prognosis in patients with vertical growth phase melanoma. Clin Cancer Res 2000; 6:1845-53.
342. Emig R, Magener A, Ehemann V, et al. Aberrant cytoplasmic expression of the p16 protein in breast cancer is associated with accelerated tumour proliferation. Br J Cancer 1998; 78:1661-8.
343. Milde-Langosch K, Bamberger AM, Rieck G, Kelp B, Loning T. Overexpression of the p16 cell cycle inhibitor in breast cancer is associated with a more malignant phenotype. Breast Cancer Res Treat 2001; 67:61-70.
344. Zhao P, Hu YC, Talbot IC. Expressing patterns of p16 and CDK4 correlated to prognosis in colorectal carcinoma. World J Gastroenterol 2003; 9:2202-6.
345. Evangelou K, Bramis J, Peros I, et al. Electron microscopy evidence that cytoplasmic localization of the p16(INK4A) "nuclear" cyclin-dependent kinase inhibitor (CKI) in tumor cells is specific and not an artifact. A study in non-small cell lung carcinomas. Biotech Histochem 2004; 79:5-10.
346. Fabbro M, Henderson BR. Regulation of tumor suppressors by nuclear-cytoplasmic shuttling. Exp Cell Res 2003; 282:59-69.
347. el-Deiry WS, Tokino T, Velculescu VE, et al. WAF1, a potential mediator of p53 tumor suppression. Cell 1993; 75:817-25.
348. Vidal MJ, Loganzo F, Jr., de Oliveira AR, Hayward NK, Albino AP. Mutations and defective expression of the WAF1 p21 tumour-suppressor gene in malignant melanomas. Melanoma Res 1995; 5:243-50.
349. Sparrow LE, Eldon MJ, English DR, Heenan PJ. p16 and p21WAF1 protein expression in melanocytic tumors by immunohistochemistry. Am J Dermatopathol 1998; 20:255-61.
350. Trotter MJ, Tang L, Tron VA. Overexpression of the cyclin-dependent kinase inhibitor p21(WAF1/CIP1) in human cutaneous malignant melanoma. J Cutan Pathol 1997; 24:265-71.
351. Karjalainen JM, Eskelinen MJ, Kellokoski JK, Reinikainen M, Alhava EM, Kosma VM. p21(WAF1/CIP1) expression in stage I cutaneous malignant melanoma: its relationship with p53, cell proliferation and survival. Br J Cancer 1999; 79:895-902.
352. Zhang L, Zhou W, Velculescu VE, et al. Gene expression profiles in normal and cancer cells. Science. Vol. 276, 1997:1268-72.
353. Maniotis AJ, Folberg R, Hess A, et al. Vascular channel formation by human melanoma cells in vivo and in vitro: vasculogenic mimicry. Am J Pathol. Vol. 155, 1999:739-52.
354. Ruoslahti E. Fibronectin and its integrin receptors in cancer. Adv Cancer Res. Vol. 76, 1999:1-20.

355. Takeichi M. Cadherin cell adhesion receptors as a morphogenetic regulator. Science 1991; 251:1451-5.
356. Tang A, Eller MS, Hara M, Yaar M, Hirohashi S, Gilchrest BA. E-cadherin is the major mediator of human melanocyte adhesion to keratinocytes in vitro. J Cell Sci 1994; 107 (Pt 4):983-92.
357. Cowin P. Unraveling the cytoplasmic interactions of the cadherin superfamily. Proc Natl Acad Sci U S A 1994; 91:10759-61.
358. Kuphal S, Poser I, Jobin C, Hellerbrand C, Bosserhoff AK. Loss of E-cadherin leads to upregulation of NFkappaB activity in malignant melanoma. Oncogene 2004; 23:8509-19.
359. Hsu MY, Wheelock MJ, Johnson KR, Herlyn M. Shifts in cadherin profiles between human normal melanocytes and melanomas. J Investig Dermatol Symp Proc 1996; 1:188-94.
360. Tamura S, Shiozaki H, Miyata M, et al. Decreased E-cadherin expression is associated with haematogenous recurrence and poor prognosis in patients with squamous cell carcinoma of the oesophagus. Br J Surg 1996; 83:1608-14.
361. Silye R, Karayiannakis AJ, Syrigos KN, et al. E-cadherin/catenin complex in benign and malignant melanocytic lesions. J Pathol 1998; 186:350-5.
362. Sanders DS, Blessing K, Hassan GA, Bruton R, Marsden JR, Jankowski J. Alterations in cadherin and catenin expression during the biological progression of melanocytic tumours. Mol Pathol 1999; 52:151-7.
363. Melki JR, Vincent PC, Brown RD, Clark SJ. Hypermethylation of E-cadherin in leukemia. Blood 2000; 95:3208-13.
364. Poser I, Dominguez D, de Herreros AG, Varnai A, Buettner R, Bosserhoff AK. Loss of E-cadherin expression in melanoma cells involves up-regulation of the transcriptional repressor Snail. J Biol Chem 2001; 276:24661-6.
365. Nollet F, Berx G, van Roy F. The role of the E-cadherin/catenin adhesion complex in the development and progression of cancer. Mol Cell Biol Res Commun 1999; 2:77-85.
366. Novak A, Dedhar S. Signaling through beta-catenin and Lef/Tcf. Cell Mol Life Sci 1999; 56:523-37.
367. Pece S, Gutkind JS. Signaling from E-cadherins to the MAPK pathway by the recruitment and activation of epidermal growth factor receptors upon cell-cell contact formation. J Biol Chem 2000; 275:41227-33.
368. Krengel S, Groteluschen F, Bartsch S, Tronnier M. Cadherin expression pattern in melanocytic tumors more likely depends on the melanocyte environment than on tumor cell progression. J Cutan Pathol 2004; 31:1-7.
369. Aberle H, Schwartz H, Kemler R. Cadherin-catenin complex: protein interactions and their implications for cadherin function. J Cell Biochem 1996; 61:514-23.
370. Hoschuetzky H, Aberle H, Kemler R. Beta-catenin mediates the interaction of the cadherin-catenin complex with epidermal growth factor receptor. J Cell Biol 1994; 127:1375-80.
371. Shibamoto S, Hayakawa M, Takeuchi K, et al. Tyrosine phosphorylation of beta-catenin and plakoglobin enhanced by hepatocyte growth factor and epidermal growth factor in human carcinoma cells. Cell Adhes Commun 1994; 1:295-305.

372. Reynolds AB, Roczniak-Ferguson A. Emerging roles for p120-catenin in cell adhesion and cancer. Oncogene 2004; 23:7947-56.
373. Zhang XD, Hersey P. Expression of catenins and p120cas in melanocytic nevi and cutaneous melanoma: deficient alpha-catenin expression is associated with melanoma progression. Pathology 1999; 31:239-46.
374. Demunter A, Libbrecht L, Degreef H, De Wolf-Peeters C, van den Oord JJ. Loss of membranous expression of beta-catenin is associated with tumor progression in cutaneous melanoma and rarely caused by exon 3 mutations. Mod Pathol 2002; 15:454-61.
375. Maelandsmo GM, Holm R, Nesland JM, Fodstad O, Florenes VA. Reduced beta-catenin expression in the cytoplasm of advanced-stage superficial spreading malignant melanoma. Clin Cancer Res 2003; 9:3383-8.
376. Nyormoi O, Bar-Eli M. Transcriptional regulation of metastasis-related genes in human melanoma. Clin Exp Metastasis 2003; 20:251-63.
377. Berger AJ, Davis DW, Tellez C, et al. Automated Quantitative Analysis of Activator Protein-2{alpha} Subcellular Expression in Melanoma Tissue Microarrays Correlates with Survival Prediction. Cancer Res 2005; 65:11185-92.
378. Luca M, Hunt B, Bucana CD, Johnson JP, Fidler IJ, Bar-Eli M. Direct correlation between MUC18 expression and metastatic potential of human melanoma cells. Melanoma Res 1993; 3:35-41.
379. Jean D, Gershenwald JE, Huang S, et al. Loss of AP-2 results in up-regulation of MCAM/MUC18 and an increase in tumor growth and metastasis of human melanoma cells. J Biol Chem 1998; 273:16501-8.
380. Huang S, Jean D, Luca M, Tainsky MA, Bar-Eli M. Loss of AP-2 results in downregulation of c-KIT and enhancement of melanoma tumorigenicity and metastasis. Embo J 1998; 17:4358-69.
381. Shibahara S, Takeda K, Yasumoto K, et al. Microphthalmia-associated transcription factor (MITF): multiplicity in structure, function, and regulation. J Investig Dermatol Symp Proc 2001; 6:99-104.
382. Garraway LA, Widlund HR, Rubin MA, et al. Integrative genomic analyses identify MITF as a lineage survival oncogene amplified in malignant melanoma. Nature 2005; 436:117-22.
383. Leiter U, Meier F, Schittek B, Garbe C. The natural course of cutaneous melanoma. J Surg Oncol 2004; 86:172-8.
384. Meier F, Will S, Ellwanger U, et al. Metastatic pathways and time courses in the orderly progression of cutaneous melanoma. Br J Dermatol 2002; 147:62-70.